





Universitat Autònoma de Barcelona

ADVERTIMENT. L'accés als continguts d'aquesta tesi queda condicionat a l'acceptació de les condicions d'ús establertes per la següent llicència Creative Commons:  http://cat.creativecommons.org/?page_id=184

ADVERTENCIA. El acceso a los contenidos de esta tesis queda condicionado a la aceptación de las condiciones de uso establecidas por la siguiente licencia Creative Commons:  <http://es.creativecommons.org/blog/licencias/>

WARNING. The access to the contents of this doctoral thesis it is limited to the acceptance of the use conditions set by the following Creative Commons license:  <https://creativecommons.org/licenses/?lang=en>



Contributions to Array Processing: Beamforming, Synchronization and Localization

MARTÍ MAÑOSAS CABALLÚ

Department of Telecommunications and Systems Engineering
Universitat Autònoma de Barcelona
Bellaterra, Spain 2022

THESIS FOR THE DEGREE OF DOCTOR OF PHILOSOPHY IN ELECTRONIC AND
TELECOMMUNICATION ENGINEERING

CONTRIBUTIONS TO ARRAY PROCESSING:
BEAMFORMING, SYNCHRONIZATION
AND LOCALIZATION

Author:

Martí Mañosas Caballú

Supervisor:

Gonzalo Seco Granados



Department of Telecommunications and Systems Engineering
Universitat Autònoma de Barcelona
Bellaterra, Spain 2022

Contributions to Array Processing: Beamforming, Synchronization and Localization

© MARTÍ MAÑOSAS CABALLÚ, 2022

Department of Telecommunications and Systems Engineering
Universitat Autònoma de Barcelona
08193 Bellaterra, Spain
Telephone +34 93 581 40 30

Cover: *Columnes de Bellaterra*, a sculptural work located in the Bellaterra campus and owned by Universitat Autònoma de Barcelona. It represents the desire for knowledge, freedom of expression, cultural identity, and solidarity.

Typeset by the author using L^AT_EX.

Printed by Centre de Reprografia UAB
Bellaterra, Spain 2022

To my parents

Abstract

This thesis addresses several problems within the field of array signal processing. Its main part focuses on what is purely understood as array processing, that is, the manipulation of the data obtained from an antenna array to estimate certain inherent information. The rest of the work discusses applicative aspects of the field, often decoupled from the processing techniques to be used but also essential for their final implementation. As a result, the contribution of the thesis can be divided into three distinct topics: beamforming, synchronization, and localization.

Beamforming is an array processing technique designed to emulate a given antenna pattern, and thus to receive signals radiating from specific locations and attenuate signals from other locations. Deterministic and data-dependent approaches exist that are highly useful while still presenting limitations. In deterministic beamforming, the design metrics are significantly decoupled from standard system requirements. In data-dependent beamforming, most techniques do not work well in the presence of multipath reflections that are very correlated with the desired signal. To solve these issues, an analysis of deterministic beamformers is provided that considers other practical design metrics, a power-based data-dependent beamformer is proposed that attenuates the effects of correlated multipaths, and a new approach for multipath mitigation is presented that exploits additional temporal filtering.

Synchronization is the coordination of events to operate a system in unison. It can be found in many field and disciplines, for instance, in multi-user wireless communication systems. In these systems, the need for synchronization occurs when users with common information aim to cooperate and focus their transmissions towards an intended destination, thus emulating an antenna array. Since users have independent and imperfect oscillators, proper synchronization becomes essential. To cope with this, a novel time-slotted round-trip protocol for carrier and timing synchronization is proposed, which presents important robustness in the sense that users can disappear from the network without severely affecting performance.

Finally, localization is the determination of the location of a given physical body by means of electromagnetic or mechanical waves. More particularly, it refers to passively finding a distant object rather than actively one's own position. Among all possible applications, avalanche victim detection is very valuable, but the techniques used are anachronistic and the localization often becomes slow and complicated. In this regard, a novel localization device and protocol are proposed that exploit the use of antenna arrays, allowing a more efficient and convenient search than traditional devices, and with great potential for industrial development.

Keywords: Array gain, array processing, attenuation, AVD, beamforming, Capon, carrier-phase, coherent, correlated, FIR, GNSS, localization, multipath, synchronization, time-delay, WSN.

Acknowledgments

This work wouldn't have been possible without the unconditional and selfless support of my immediate family. Hence, this thesis is especially dedicated to all of them: to my mother, for persistently being willing to make things very easy for me; to my father, for always being open to help in my mathematical vicissitudes; to my sister Laia, for believing me so capable every time; and to my sister Maria, for her constant interest in my progressions.

Apart from these special people, many others have contributed to this thesis, and first of all, professor Gonzalo Seco Granados, as director and supervisor of my doctoral studies. My most sincere gratitude for the many given opportunities, for the valuable facilities that he provided, and above all, for letting me explore and work on the problems that have interested me the most with enormous flexibility.

Another person who deserves special emphasis is professor A. Lee Swindlehurst, who received me in Irvine and made my two stays at the University of California very pleasant and rewarding. I will always keep in mind the lighthearted appointments and the motivating feedback from our discussions. Many clever ideas emerged or were reaffirmed there, and some of them are now fundamental to this work.

On the more psychological and emotional side, there are also some people that I would like to name. First and foremost, Leo Vegué, Ramon Blasi, and Marta Valero, who gave me immense confidence, great support and invaluable help in exceptional situations, and made the completion of this thesis possible. Furthermore, the people from Farrera, who gave me love and company in the most difficult moments of my life — especially Cesca Gelabert, Lluís Llobet and Arnau Llobet, the family in charge of the Centre d'Art i Natura (CAN), for their kindness, generosity and respect.

Finally, I want to thank my lovely friends Marc García, Luis Hidalgo, Andreu Turró, Adrià Navarro, and Alejandro Álvarez, for the much-needed laughs, for always being there when I needed them, and for helping prevent me from becoming a true hermit. And impossible to forget are my climbing mates Marc Pons and Jordi Tusell, for the countless times spent together talking and climbing in the crags, which were fundamental for my physical and emotional well-being, and therefore essential for the development of this thesis.

Martí Mañosas Caballú
Bellaterra, November 2021

Acronyms

AVD	–	Avalanche Victim Detector
BS	–	Base Station
CAP	–	CAPon
DAS	–	Delay-And-Sum
DLL	–	Delay-Locked Loop
DOA	–	Direction Of Arrival
DS-SS	–	Direct-Sequence Spread-Spectrum
FBC	–	Forward/Backward Capon
FIR	–	Finite Impulse Response
GLONASS	–	GLObalnaya NAVigazionnaya Sputnikovaya Sistema
GNSS	–	Global Navigation Satellite System
GPS	–	Global Positioning System
LCMV	–	Linearly Constrained Minimum Variance
LOSS	–	Line-Of-Sight Signal
MAP	–	Maximum A Posteriori
MEG	–	MagnetoEncephaloGraphy
MIMO	–	Multiple-Input Multiple-Output
ML	–	Maximum Likelihood
MMSE	–	Minimum Mean Squared Error
MSC	–	Multiple Sidelobe Canceller
MSE	–	Mean Squared Error
MSNR	–	Maximum Signal-to-Noise Ratio
MUSIC	–	MUltiple Signal Classification
MVDR	–	Minimum Variance Distortionless Response
OPC	–	Optimal Performance Curve
PBC	–	Power-Based Capon
PI	–	Power Inversion
PLL	–	Phase-Locked Loop
SIR	–	Signal-to-Interference Ratio
SNR	–	Signal-to-Noise Ratio
SSC	–	Spatial Smoothing Capon
SW	–	Spectral Weighting
WSN	–	Wireless Sensor Network

Contents

Abstract	v
Acknowledgments	vii
Acronyms	ix
I Thesis Overview	1
1 Introduction	3
1.1 Array Signal Processing	3
1.2 Global Navigation Satellite Systems	5
1.3 Wireless Sensor Networks	7
1.4 Avalanche Victim Detectors	8
2 Main Results	11
2.1 Deterministic Beamforming	11
2.2 Data-Dependent Beamforming	12
2.3 Distributed Synchronization	17
2.4 Magnetic Source Localization	18
3 General Conclusion	21
Bibliography	23
II Primary Publications	31
A Performance of Deterministic Beamformers	33
A.1 Introduction	35
A.2 Problem Statement	36
A.3 Array Gain versus Attenuation Trade-Off	36
A.4 Optimal Performance Curve	38
A.5 Conclusion	39
References	39

B	Power-Based Capon Beamforming	41
B.1	Introduction	43
B.2	Problem Model	44
B.3	Capon Beamforming Review	45
B.4	Power-Based Capon Beamforming	45
B.5	Simulation Results	47
B.6	Conclusion	50
	References	50
C	Power-Based Capon Implementations	53
C.1	Introduction	55
C.2	Problem Statement	55
C.3	Equivalent Approach	56
C.4	Simulation Results	57
C.5	Conclusion	58
	References	59
III	Supplementary Publications	61
D	Beamforming via FIR Filtering	63
D.1	Introduction	65
D.2	Modeling Assumptions	65
D.3	GNSS Multipath Mitigation	66
D.4	Numerical Results	68
D.5	Conclusion	68
	References	69
E	Carrier and Timing Synchronization	71
E.1	Introduction	73
E.2	System Model	74
E.3	Robust Round-Trip Synchronization Protocol	74
E.4	Simulation Results	76
E.5	Conclusion	77
	References	77
F	Avalanche Victim Localization	79
F.1	Field of the Art	81
F.2	Prior State of the Art	81
F.3	Description of the Invention	84
F.4	Brief Description of the Drawings	88
F.5	Detailed Description of Several Embodiments	89
F.6	Claims	93
	Abstract	99

Part I

Thesis Overview

Chapter 1

Introduction

This thesis aims to provide solutions to various specific problems appearing in the world of telecommunications through the use of antenna arrays. The considered applications include, but are not limited to, satellite-based navigation, physical condition monitoring and avalanche victim search. All of them are strongly motivated by the author's interest in the natural environment, and more specifically, by the need to explore and better know wilderness.

Since this work is presented in the form of a compendium of publications, its content is divided into three parts. This first part is an overview of the thesis, and it includes three chapters: a concise introduction to array processing and the covered applications, a summary of the obtained results, and the overall conclusions. Part II appends the articles published in scientific journals. Part III appends the contributions in scientific conferences and patents.

1.1 Array Signal Processing

The IEEE Antennas and Propagation Society published its first special issue on active and adaptive antennas in March 1964 [1]. At the time, array signal processing emerged as an active area of research, and it was centered on the ability to fuse data captured by spatially separated sensors in order to perform a given estimation task. The main motivation was to exploit the spatial diversity of the signals present, that is, the fact that they usually take different values at separate space positions. Figure 1.1 shows this idea, where a set of L spatially distributed sensors captures the different values of a given analog signal $s(t)$ at a particular time instant t .

Today, array signal processing is a wide area of research, and it extends from the simplest form of a linear array of sensors to planar and volumetric geometries. The type of sensors typically used are electromagnetic antennas, but other examples can be found such as microphones, geophones, hydrophones and optical telescopes for interferometry. The amount of existing techniques is extensive and well-documented in the literature [2], and they basically differ on how the data is processed after its collection. Three types of processing techniques can be differentiated: *spectrum-based*, *parameter-based* and *beamforming*.

Thanks to an existing equivalence between the model of a signal sampled in time and that of a signal sampled in space, spectrum-based techniques are analogous

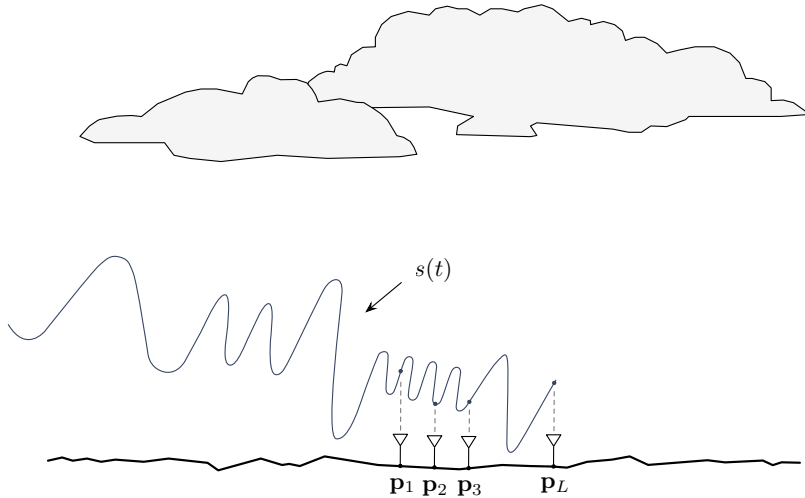


Figure 1.1: Illustration of a set of L spatially separated sensors at arbitrary positions $\mathbf{p}_1, \dots, \mathbf{p}_L$ collecting values of a common analog signal $s(t)$.

versions of the spectral estimation approaches for discrete-time signals [3]. They all form a spectrum-like function of the parameters to be estimated, and the locations of the highest peaks of the function are recorded as the true estimates of the parameters. These parameters are mostly the directions of arrival (DOAs) of the received signals at the array, just as their analogous approaches estimate the frequencies of received complex exponentials. Some noteworthy examples are quadratic algorithms, such as Bartlett [4] and Capon [5], and subspace algorithms, such as Pisarenko [6] and multiple signal classification (MUSIC) [7]. Interestingly enough, [5, 7] were initially designed for arrays and later adapted to the conventional spectral estimation problem.

Parameter-based techniques are an extension of the classical and Bayesian parameter estimation approaches for discrete-time signals [8]. They estimate the unknown parameters by explicitly writing them as a function of the received data and using mathematical expressions that take the probability density function of the data into account. They allow estimating any type of parameter included in the model of the received signal, and when applied to DOA estimation, they often result in more accurate estimates than the spectrum-based ones, although at the expense of increased computational complexity. A vast number of estimation techniques have been proposed so far, and some good examples can be found in [9–15]. They are mainly based on the maximum likelihood (ML) and maximum a posteriori (MAP) criteria, but other relevant approaches also exist [16–18].

Finally, beamforming techniques are versatile approaches to spatial filtering. They linearly combine the spatially shifted time series of each sensor through certain complex weights, just as finite impulse response (FIR) filters linearly combine temporally shifted time series. The result is an algorithm that separates signals originating from different directions, forming beams towards specific locations and attenuating signals from other locations. They are mainly intended for waveform estimation, and can be divided into two groups: *deterministic* and *optimum*.

On the one hand, deterministic or data-independent approaches calculate beam-

forming weights based on certain known, determined, and constant characteristics of the scenario. Thus, they are suitable for static and relatively controlled environments, and robust against calibration errors and other uncertainties in the signal parameters. The most common performance metrics are the mainlobe width and sidelobe level of the equivalent beam pattern of the array since many algorithms are drawn from the classical antenna and digital filter design literature [19, 20]. However, other widely used examples exist, such as [21–23] and the natural extension of Bartlett, the latter known as Bartlett beamformer or delay-and-sum (DAS).

On the other hand, optimum or data-dependent approaches calculate beamforming weights based on the statistics of the incoming data, and they are optimum in a statistical sense. Thus, they are very appropriate when little a priori information about the scenario is available, or when the scenario is likely to change with time. Furthermore, they serve as candidates for adaptive implementations. The most common performance metrics are mean squared error (MSE), signal-to-noise ratio (SNR) and signal-to-interference ratio (SIR). And essential examples are the multiple sidelobe canceller (MSC) [24], also known as power inversion (PI), the minimum mean squared error (MMSE) [25], the linearly constrained minimum variance (LCMV) [26], the maximum signal-to-noise ratio (MSNR) [27], and the natural extension of Capon, known as Capon beamformer or minimum variance distortionless response (MVDR).

1.2 Global Navigation Satellite Systems

The term global navigation satellite system (GNSS) is a generic expression referring to any system that allows its users to calculate their own position based on signals transmitted by a constellation of satellites [28]. Examples of these systems are the GPS from North America, GLONASS from Russia, Galileo from Europe, and BeiDou from China. As depicted in Figure 1.2, they are all structured in three major segments: space segment, ground segment and user segment.

The space segment consists of a constellation of satellites transmitting radio signals to the earth’s surface, which are responsible for providing direct signal reception and some ephemeris information to the user radio-receivers. The ground segment consists of a set of infrastructures deployed over the earth’s surface in charge of monitoring and controlling the system satellites, thus being responsible for their proper operation. Finally, the user segment consists of the user radio-receivers capturing the signals transmitted by all visible satellites, which are responsible for calculating their own position autonomously.

At the user segment, all user receivers have to estimate the time-delay of the received direct signal or line-of-sight signal (LOSS) from each available satellite. It is used for the calculation of the *pseudorange*, or apparent distance between the user and each available satellite, and leads to a system of equations from which the user position can be calculated. As an alternative, the carrier-phase of each received LOSS may also be used to calculate the user position, providing a much more precise measurement than the time-delay yet presenting some limitations, such as being ambiguous by an unknown integer number of wavelengths.

Standard GNSS receivers perform estimation of the time-delay and carrier-phase through a delay-locked loop (DLL) and a phase-locked loop (PLL). These mechanisms

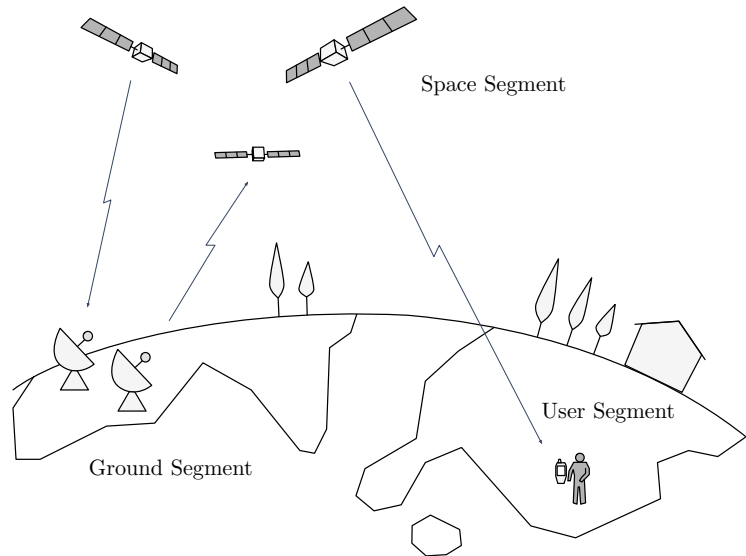


Figure 1.2: Illustration of the GNSS segments: Space, Ground and User.

keep track of the LOSS by comparing the received signals with a local reference signal with variable delay and phase and minimizing its matching error. This can be done thanks to the known structure of the GNSS signals. Specifically, these systems use direct-sequence spread-spectrum (DS-SS) modulations, which transform each navigation data bit into a known pseudorandom sequence before transmission, and reconstruct the navigation data bits at the receiver using the same sequence.

Due to the operating principle of GNSS, the receiving multipath reflections of a direct signal usually bias the pseudoranges by several tens of meters, and they also hamper the ambiguity resolution process needed for carrier-phase ranging [29]. For this reason, significant research and development efforts have been devoted to mitigating multipath effects, and many techniques have been proposed so far. Early approaches use the single antenna of standard GNSS receivers, and aim to discriminate the LOSS from the reflections by using temporal diversity. Important examples are the narrow correlator [30], the multipath estimating delay lock loop [31], the strobe correlator [32], the multipath elimination technique [33], the high resolution correlator [34], the a-posteriori multipath estimation [35], the multipath mitigation technique [36], and many others the reader can find in [37].

Although the performance of single-antenna techniques can be outstanding in many scenarios, it is still insufficient for some applications with high demand for accuracy. In such applications, the use of multiple-antenna techniques seems a promising alternative since they can discriminate the LOSS from the reflections by exploiting spatial diversity. The state of the art of GNSS multiple-antenna techniques is large [38], and many good solutions exist, such as applications of the MSC [39], ML estimation methods [40], extensions of the MVDR [41], hybrid beamforming [42], blind approaches [43], moving antenna arrays [44], and eigendecomposition-based methods [45]. Unfortunately, some limitations are still present, especially in the presence of multipath reflections with minimal delays relative to the LOSS, that is,

correlated multipath, and unknown directions of arrival.

In order to improve the multipath mitigation capabilities of an antenna array, it is also possible to exploit certain additional degrees of freedom available in GNSS. For example, the frequency diversity of GNSS signals, which allows precise mitigation of the frequency bands affected by multipath [46, 47]. Also, the polarization diversity through dual-polarization antenna arrays, which helps distinguishing the LOSS from multipaths [48, 49]. And even independent inertial sensors can be used, which provide useful assistance in the presence of severe multipath fading [50, 51]. All these examples can be remarkably helpful in highly spatially and temporally correlated scenarios, and may significantly increase the final performance.

1.3 Wireless Sensor Networks

Wireless sensor networks (WSNs) are groups of spatially dispersed sensors that wirelessly and cooperatively monitor large physical environments [52]. These environments are usually remote and inaccessible, and the developed applications include structural health, pipeline control, traffic control, underground mining and active volcanoes, among others. The features of the involved sensors can vary widely, from simple ones that monitor a single physical phenomenon to more complex devices that combine many different sensing techniques. And they can also differ in their communication technologies, with varying data rates and latencies.

WSNs are similar to wireless ad-hoc networks in the sense that they are decentralized. Specifically, sensor nodes rely on wireless connectivity, but they do not depend on preexisting infrastructures such as access points. Instead, each sensor node can participate in routing and which one forwards data is dynamically determined based on the routing algorithm in use. Moreover, as shown in Figure 1.3, sensors not only sense and communicate with each other, but they also transmit the collected data wirelessly to a centralized station, or *base station* (BS). This allows dissemination to more powerful systems for proper processing, analysis and storage.

One of the salient features of WSNs is that corresponding applications have an increasing demand for small and low-cost devices, which causes significant constraints on the available resources, such as scarce bandwidth to be shared and relatively limited battery lifetime. If these constraints are topped by the uneven distribution of channels between users, the networks' development is seriously hindered. A reasonable solution to this problem is to encourage users to cooperate in order to achieve more energy efficiency and reliability, as in cooperative communications, which allow users with diverse channel qualities to relay their messages to the destination [53].

Some examples of cooperative communications are amplify-and-forward, decode-and-forward [54], compress-and-forward [55], and coded cooperation [56]. They are all based on the pioneering work of [57], and when extended to large networks, the relay nodes form a distributed antenna array that relays the message from a given source to the destination. As a result, a given diversity gain is achieved as in multiple-input multiple-output (MIMO) wireless systems [58]. Similarly, the relay nodes can also focus on the simultaneous transmission towards the intended destination so that all bandpass transmissions are received constructively. In this case, a distributed antenna array is formed that emulates a transmit beamformer.

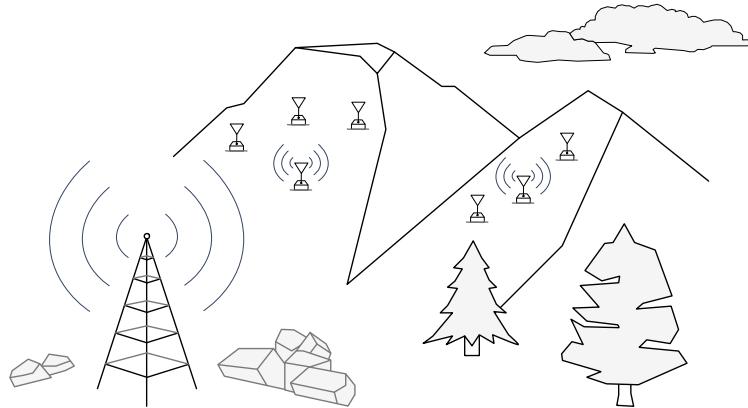


Figure 1.3: Illustration of a WSN collecting measures of certain seismic activities in a wild and remote area, and communicating with its corresponding base station.

The latter approach is known as *distributed beamforming* and requires less transmit power to achieve a desired SNR target at the destination, hence achieving a given beamforming gain as in traditional beamforming systems [59]. This gain is of much interest when energy efficiency is preferred over reliability and, for instance, when the destination is located so far away that communication cannot be established from any of the single sensors. However, sensors in a distributed beamformer require to precisely synchronize their carrier signals so that they arrive with proper phase alignment at the destination.

Many methods have been proposed to achieve synchronization. On the one hand, closed-loop approaches exist, which rely on external signaling sent from the destination, as in [60–62]. They are meant to steer beams to the involved destination only, but little coordination among sensors is required. On the other hand, there are open-loop approaches, which do not need external signaling to operate, as in [59, 63, 64]. They can steer beams to arbitrary directions, but higher coordination among sensors is required, and concretely, each node requires knowledge of its relative position from a predetermined reference point.

1.4 Avalanche Victim Detectors

Telecommunications engineering is increasingly bringing more than substantial benefits in the field of mountain sports. An example is the use of GNSS receivers by hikers, which allow them to be located on a topographic map with exceptional ease. This attribute can be used in various entertainment activities, and it can save hikers from severe problems in hostile and foggy environments. Another example that directly impacts the safety of hikers is the use of avalanche transceivers, or avalanche victim detectors (AVDs).

AVDs are portable electromagnetic devices that allow their wearers to radiolocate each other if they are placed reasonably close. Concretely, they are devices that can be located when buried by snow, and for this reason, they are used to rescue

avalanche victims. The most crucial particularity is that the search and subsequent digging up of a victim wearing an AVD may be conducted by the unburied members of the affected group also wearing the device. In this way, the rescue of the victims can be performed without having to wait for the arrival of external rescue teams.

This type of self-functioning is important, because the chance of survival of a completely buried person is higher than 90% when it is found and extricated within less than 15 minutes, but only about 30% when this time extends to 30 minutes [65]. Hence, although technologically and technically prepared, external rescue teams take excessive time to arrive, and the affected group itself must perform the rescue. As a consequence, the localization time must be reduced to a minimal, because the digging up process is remarkably slow when performed by few people.

Avalanche transceivers radiolocate each other through electrically small multi-turn loop antennas, and the radiated fields are thus equivalent to those of an infinitesimal magnetic dipole [20]. A ferrite core within the loop is usually included to raise the magnetic field intensity and hence the radiation resistance, which otherwise are very low due to the electrically small size of the antenna. This configuration, together with an on-off keying modulation at 457 kHz, offers a detection range equal to few tens of meters, hence lower than $1/(2\pi)$ times the wavelength and, as a result, within the so-called *near-field* region of the radiated fields.

In contrast with the *far-field*, where the radiated electric and magnetic components have similar amplitudes and are transverse to the direction of propagation, the near-field is mainly dominated by the magnetic component, which is well preserved through snow and nearby objects. This magnetic component is not transverse to the direction of propagation, behaves almost statically, and all its field lines, which are perpendicular to the equipotential lines, originate at the emitter. Figure 1.4 shows an avalanche victim and the corresponding magnetic field lines of its hypothetical attached device in an example scenario of two people.

Although localization with AVDs is simply accomplished by tracking magnetic field intensity and direction, doing so in a reasonable time is still quite challenging. The reasons are the short range of operation, the low resolution appearing close by the victim, and the intricacy of the techniques required to find multiple victims. Since AVDs are only intended for mountaineering applications, their state of the art is somewhat poor, progresses slowly, and is usually published in patent format. Some interesting articles are [66, 67], and examples of patent publications are [68–73]. In contrast, complementary studies exist on the use of GNSS receivers [74, 75], airborne ground-penetrating radar [76], and AVDs with unmanned aerial vehicles [77, 78].

Despite the current limitations, the first practical works related to the near-field magnetic localization problem appeared in the 1970s, and referred to applications such as the rescue of buried miners [79], the location of geological structures [80], and the tracking of earth penetrators [81]. Over time, algorithms improved substantially, from the use of three-axis multi-turn loop antennas [82] to more advanced and specific proposals [83–85]. These methods provide a solid mathematical basis to the problem and have the particularity of calculating the source position relative to the receiver. Thus, the localization is not accomplished by following field lines.

Noteworthy, magnetic localization is also found within the field of medical imaging and diagnosis due to an existing equivalence between certain neural activities and the

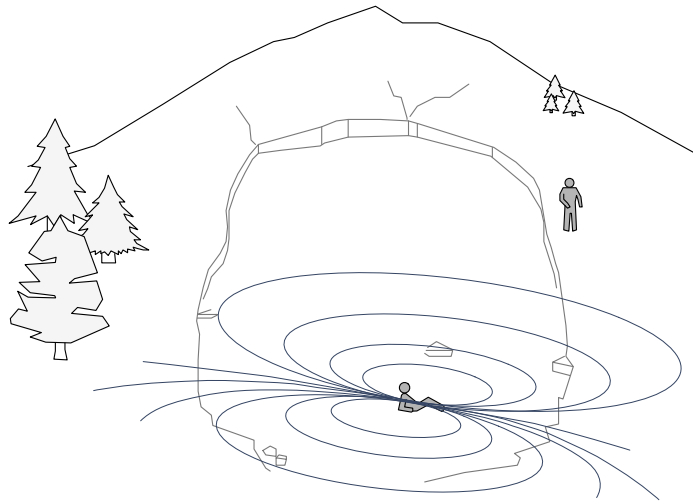


Figure 1.4: Illustration of an avalanche victim, one unburied partner, and the corresponding magnetic field lines emitted by the victim's attached device.

currents of a magnetic dipole [86]. In fact, many interesting publications appeared in the past [87–90] and still appear today [91, 92]. In this field, the achieved results demonstrate that array processing techniques can be extremely powerful. Specifically, they allow estimating the position of multiple sources simultaneously, thus forming the theoretical basis for the very useful magnetoencephalographies (MEG).

Chapter 2

Main Results

2.1 Deterministic Beamforming

Deterministic beamforming is a handy tool for many practical systems due to its robustness and simplicity of implementation, and it is an exceptional choice in relatively controlled scenarios. Examples of such scenarios can be found in the GNSS ground segment, where the desired and interfering signals received by reference stations are known to be confined in different spatial regions. This also happens in other applications, such as radio telescopes for interferometry and the over-the-horizon radar. Unfortunately, the inherent performance metrics of deterministic approaches are not functional enough to meet these systems' requirements.

In Paper A, new light is shed on the performance of the most relevant deterministic beamformers when they are chosen to operate in a scenario with predefined spatial regions. Specifically, the relationship between two crucial metrics for the design of practical systems is considered. These metrics are *array gain* and *attenuation*, or in other words, the ability to mitigate the overall noise and reject incoming interfering signals. The first significant result is that the Dolph-Chebyshev beamformer [23], which is usually adopted as the optimal solution to reject the signals coming from a given spatial sector, is not the best design from this system-level perspective.

The values of an optimal performance curve (OPC) are also worked out from the solution of an iterative algorithm that plots the best achievable array gain for a given attenuation, thus setting a reference to visualize how far the existing deterministic designs are from the optimal behavior. Interestingly enough, the corresponding beam patterns of the OPC present decreasing sidelobes in the desired signal region, and approximately constant sidelobes inside the interfering signal region. This is an intermediate behavior between those of the spectral weighting (SW) and Dolph-Chebyshev techniques [2].

As an example, Figure 2.1 shows numerical values corresponding to the most representative deterministic methods and the OPC, in a scenario with the desired signal at the direction of arrival 70° and interfering signals within the region bounded by 80° and 90° . A trade-off between the proposed performance metrics is shown, and also that the eligible designs are all placed below the OPC. For this reason, the OPC can be used to define the best possible trade-off of any deterministic beamformer, and also to delimit the area of eligible designs.

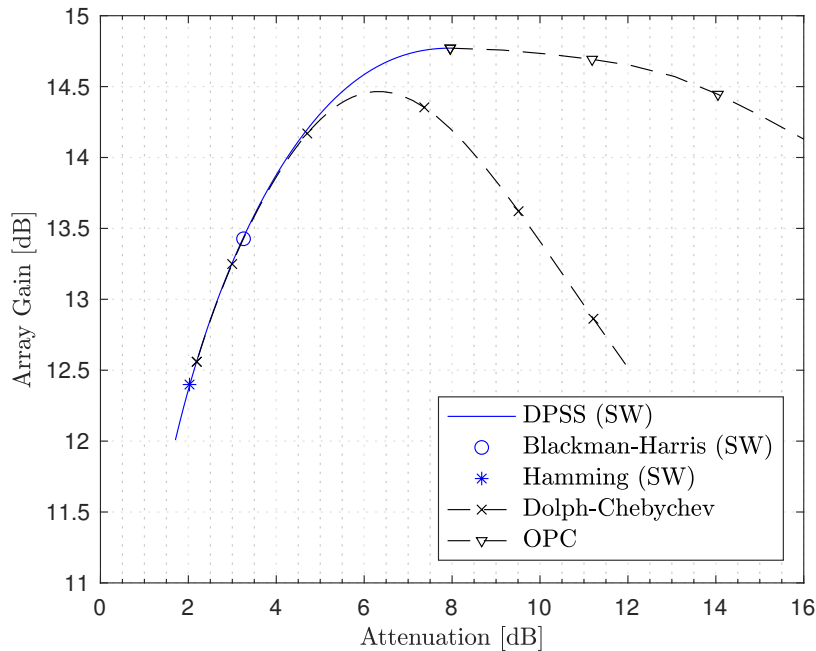


Figure 2.1: Array gain versus attenuation for several deterministic techniques and the OPC. The DOA of the desired signal is 70° , and the DOAs of the interfering signals lie in the region bounded by 80° and 90° . Linear array of 30 antennas.

2.2 Data-Dependent Beamforming

Data-dependent beamforming is an extremely powerful approach in very changing environments. With little information about the signals involved, these beamformers can spatially filter the incoming signals without the need to define specific spatial regions. Hence, they are very useful in the GNSS user segment, where user receivers are usually in motion and exposed to time-varying adversities. In this case, a typical choice is the Capon beamformer, which works extraordinarily well in the presence of uncorrelated interferences. However, it suffers from severe signal cancellation effects in the presence of correlated interferences, and therefore it is not applicable when multipath reflections are received with minimal delays relative to the LOSS.

In order to overcome this limitation, Paper B presents a novel analysis of the Capon beamformer in the presence of correlated multipath, and it explains that the mentioned cancellation effects are due to the existence of a non-zero cross-correlation vector $\mathbf{r}_{\mathbf{m}s}$ between direct signal and multipaths. Consequently, it proposes an innovative method to estimate and remove this vector from the spatial correlation matrix of the data received by the array. After that, the new correlation matrix is used instead of the original one for the calculation of the Capon weights.

The estimation of the vector $\mathbf{r}_{\mathbf{m}s}$ is performed through a given two-dimensional rank minimization problem, which has certain inherent numerical limitations and therefore needs to be relaxed by means of the so-called Schatten quasi-norm. Although this relaxation only provides an approximation to the problem, it allows the implementation of the method with outstanding performance. The method is finally referred to as power-based Capon (PBC) since it uses an estimate of the power of

the LOSS in one of its steps.

Figure 2.2 and Figure 2.3 show the multipath and noise powers present at the output of the array after PBC beamforming, normalized with respect to the power of the LOSS. These powers can be directly related to the attenuation and array gain considered in Section 2.1, but are plotted differently here to explicitly illustrate the existence of the cancellation effects. A parameter $\xi \in [0, 1]$ is defined as a delay scaling factor so that when $\xi = 0$, all the multipaths are received coherently, and when $\xi = 1$, they are received with certain non-zero maximum delays relative to the LOSS. Supplementary plotted techniques are the DAS, Capon (CAP), and Capon with additional spatial smoothing (SSC) or forward/backward (FBC).

From Figure 2.2, several things are appreciable. First, the multipath response of the CAP beamformer equals one when the delay factor is zero. This is due to the fact that full cancellation effects take place. Additionally, it can be seen that this response does not improve substantially when the delay factor increases. For their part, the smoothing approaches SSC and FBC offer enhanced performance compared to CAP, but just a bit because they only achieve a slight decrease in correlation. In contrast, the PBC beamformer immediately mitigates the multipaths when $\xi > 0$. For its part, the DAS approach offers an intermediate but insufficient performance.

From Figure 2.3, it can be observed that CAP, SSC and FBC offer a remarkably worse noise response than the rest. The reason is that Capon's formulation also implies merging the noise with the multipaths when they show some degree of correlation for short sample records. This effect is totally avoided by the PBC and DAS approaches, which show an exceptional noise response for all values of ξ .

Despite the good results obtained, having to solve a rank minimization problem can become a limitation for the successful implementation of the PBC technique. In this line, Paper C proposes a new mechanism to estimate the vector $\mathbf{r}_{\mathbf{m}s}$ that is equivalent to that of the rank but more accurate and reliable. Specifically, the rank minimization turns into a power minimization, whose new cost function is continuous and less sensitive to numerical deviations in the estimated correlation matrices.

Figures 2.4 and 2.5 show the accuracy of the new approach compared to that of the original one in a scenario with a direct signal and two multipaths. This accuracy is represented in terms of a given delay τ and phase φ of a local replica of the autocorrelation function of the considered GNSS despreading code. This replica is used in the PBC algorithm to convert an L -dimensional minimization problem to a two-dimensional one, and it leads to the correct estimate of $\mathbf{r}_{\mathbf{m}s}$ when the mentioned delay and phase are synchronized with the received post-despreading LOSS.

In the original PBC method, the delay and phase are calculated by minimizing the Schatten quasi-norm, denoted as $S(\tau, \varphi)$. In Paper C, two different functions are proposed: $F_1(\tau, \varphi)$ and $F_2(\tau, \varphi)$. While Figure 2.4 shows that the delays obtained from the distinct functions differ only by a few nanoseconds, Figure 2.5 shows that the differences obtained in the estimated phase can be as large as 0.2 rad. Thus, not only do the new functions offer more reliability due to specific inherent properties, but $F_2(\tau, \varphi)$ also provides more accurate results. Moreover, as detailed in Paper C, the new cost function simplifies the algorithm to generate the PBC weights, which is an additional advantage to what has been discussed so far.

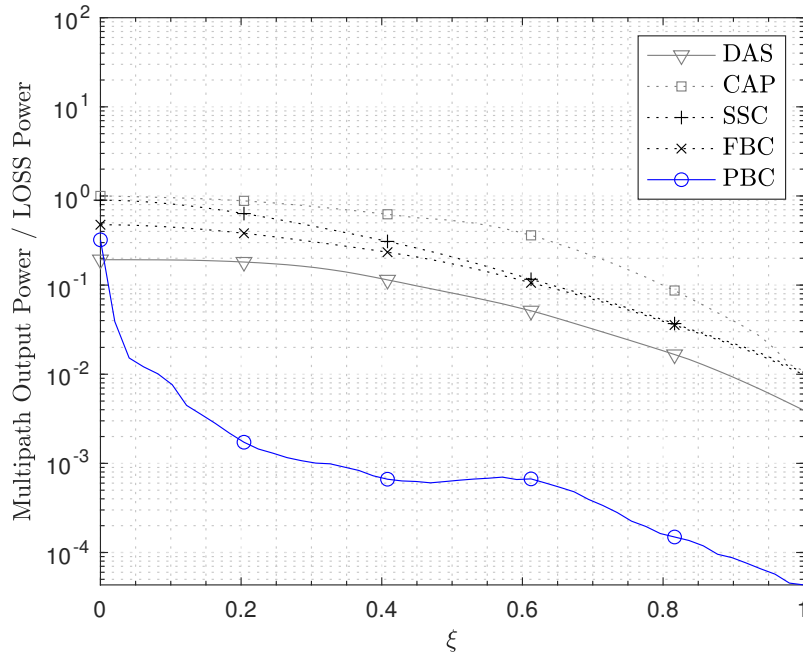


Figure 2.2: Multipath response of several beamformers versus delay factor ξ . The DOAs of the three multipaths and direct signal are -20° , 80° , 0° and 30° respectively. The maximum delays of the multipaths are $1.5\mu s$, $2\mu s$ and $2.5\mu s$. Linear array of 8 antennas.

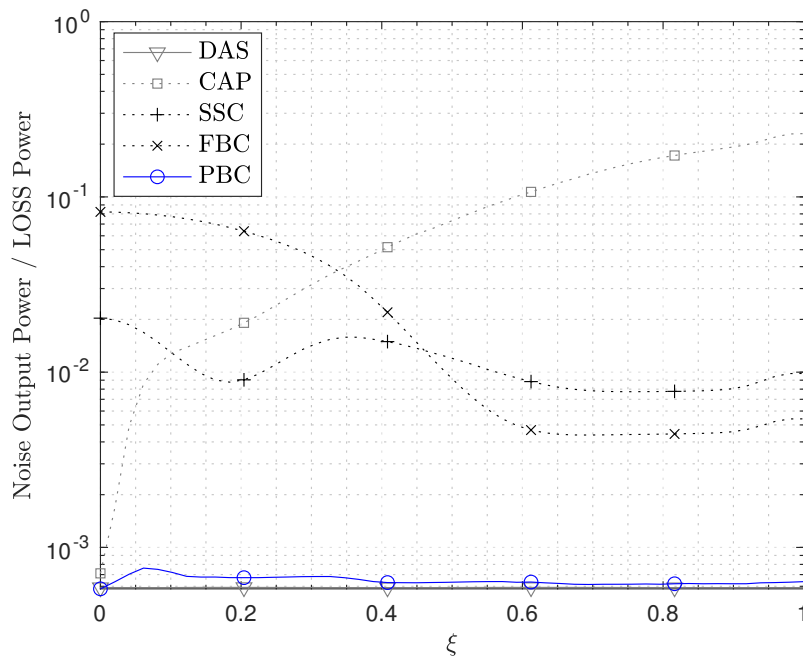


Figure 2.3: Noise response of several beamformers versus delay factor ξ . The DOAs of the three multipaths and direct signal are -20° , 80° , 0° and 30° respectively. The maximum delays of the multipaths are $1.5\mu s$, $2\mu s$ and $2.5\mu s$. Linear array of 8 antennas.

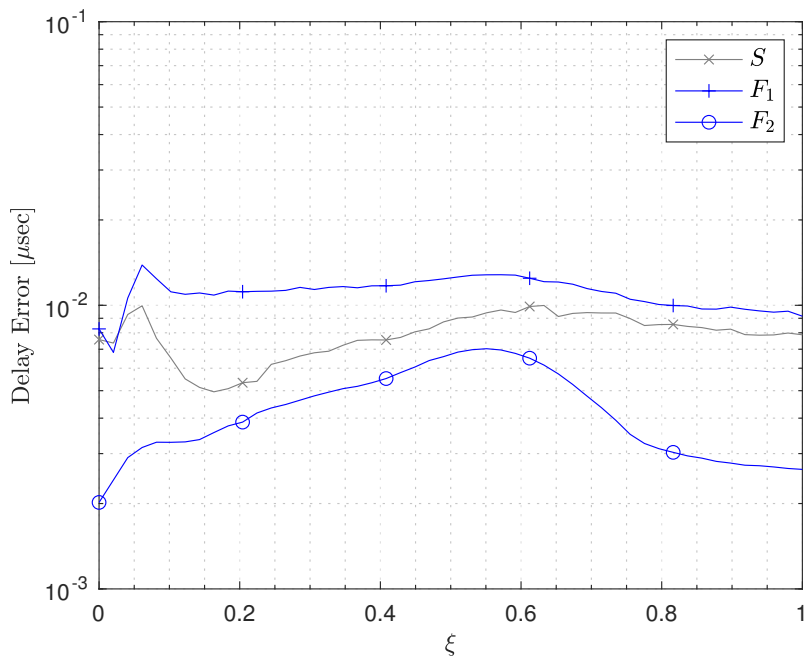


Figure 2.4: Synchronization error of the delay that minimize the functions $S(\tau, \varphi)$, $F_1(\tau, \varphi)$ and $F_2(\tau, \varphi)$, versus delay factor ξ . The DOAs of the two multipaths and direct signal are -20° , 80° and 30° respectively. The maximum delays of the multipaths are $1.5\mu\text{s}$ and $2.5\mu\text{s}$. Linear array of 5 antennas.

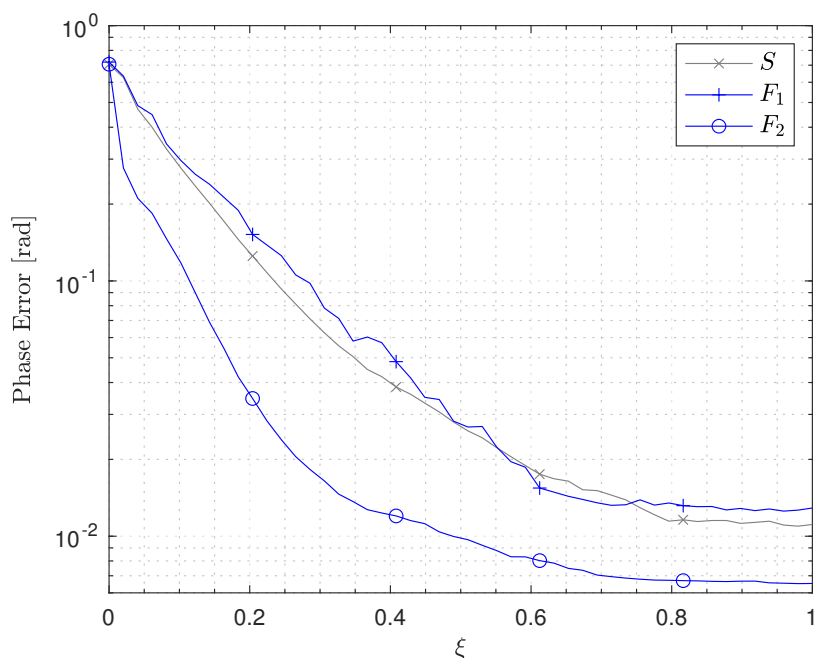


Figure 2.5: Synchronization error of the phase that minimize the functions $S(\tau, \varphi)$, $F_1(\tau, \varphi)$ and $F_2(\tau, \varphi)$, versus delay factor ξ . The DOAs of the two multipaths and direct signal are -20° , 80° and 30° respectively. The maximum delays of the multipaths are $1.5\mu\text{s}$ and $2.5\mu\text{s}$. Linear array of 5 antennas.

An alternative approach to PBC that also allows for multipath mitigation is the robust beamformer presented in Paper D. With very little knowledge of the power of the LOSS and the use of an additional FIR filter, this work proposes a mechanism to estimate the subspace spanned by the spatial signatures of the multipaths. Then, with this subspace at hand, designing a beamformer that mitigates the multipath contribution is straightforward, such as a distortionless beamformer that lies in the subspace orthogonal to the estimated multipath subspace.

A very interesting advantage of this approach with respect to the PBC is that it can decorrelate multipaths between them, thus allowing for subsequent multipath DOA estimation. Nevertheless, very small relative delays imply using a high sampling frequency, and the associated computational burden can increase significantly. Moreover, the time window taken for multipath subspace estimation may also be quite restrictive, since large windows become indispensable to reduce the impact of the low SNR characteristics of the proposed temporal filter.

Figure 2.6 shows the multipath response of the beamformer proposed in Paper D with respect to a design parameter of the filter $\rho \in [0, 1]$. Each curve corresponds to a different time window L in milliseconds. The results mainly demonstrate the effectiveness of the methodology, and the important role that the value of ρ plays in the achievable attenuations. More predictably, they also show that larger values of L perform better multipath attenuations, which happens because the estimation of the multipath subspace improves.

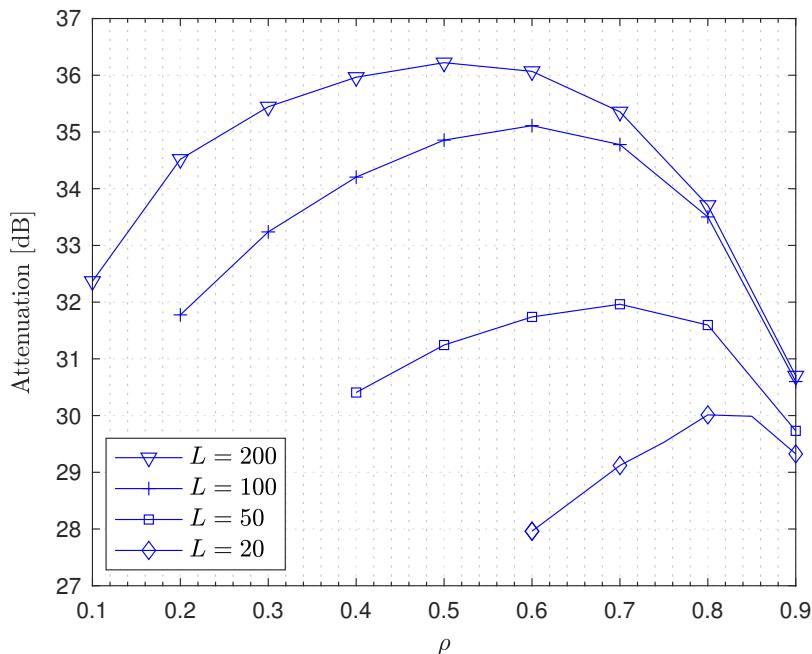


Figure 2.6: Multipath attenuation versus design parameter ρ . The DOAs of the two multipaths and direct signal are 90° , 140° and 40° respectively. The delays of the multipaths are $0.25\mu\text{s}$ and $1.25\mu\text{s}$. Sampling frequency of 4.092 MHz. Linear array of 5 antennas.

2.3 Distributed Synchronization

Distributed beamforming is a very attractive strategy for resource-constrained networks. Individual sources with common information can efficiently transmit to the intended destination by using phase and time aligned carriers so that all bandpass transmissions are received constructively. Nevertheless, each transmitter has an independent and imperfect oscillator, and for this reason synchronization among transmitters is fundamental.

Commonly, efforts are devoted to obtaining carrier phase alignment at the destination regardless of possible small time shifts between the corresponding baseband signals. Unfortunately, these time shifts may exist even with phase aligned carriers, for example when they are equal to an integer number of wavelengths. Then, a total constructive sum of the data at the destination may not be achieved. Another generally assumed situation is that all sensors are active during synchronization, which is not true when they leave the network without previous warning.

In Paper D, three types of synchronization procedures are distinguished that complement each other to achieve an effective total constructive sum of the data. They are frequency synchronization, phase synchronization and timing synchronization. A novel protocol is then proposed that explicitly considers these procedures and is valid when sensors leave the network without warning. The protocol is motivated by the previous work of [60], is based on the execution of simple rules at each sensor, and leaves freedom to choose those signals that provide better timing synchronization.

Figure 2.7 shows the probability that the proposed protocol achieves a given beamforming gain versus the time elapsed since the start of beamforming. While

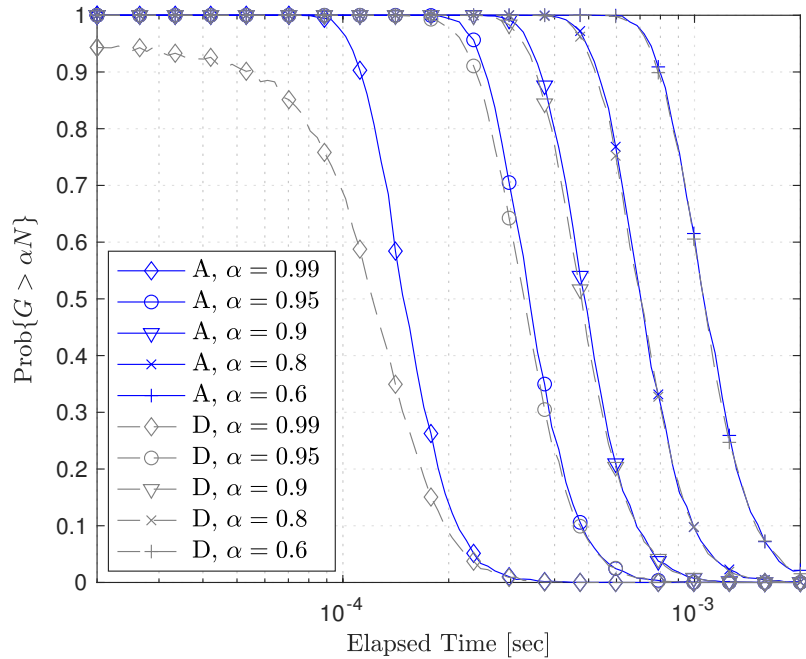


Figure 2.7: Probability of a beamforming gain G greater than α times the number of alive sensors N , versus elapsed time. Label A refers to all sensors alive. Label D refers to death ratios of 50%. Network of $N = 10$ sensors.

deterioration of beamforming is due to the fact that little frequency synchronization errors always exist, the plots show two essential aspects. First, that carrier phases are properly aligned at the destination up to $800\mu s$, where a 60% quality beamforming no longer can be achieved with probability greater than 0.9. Second, that sensors can disappear from the network with death ratios as high as 50% without severely affecting performance. Thus, the protocol shows reliability within a certain amount of time and successfully achieves beamforming in dynamic environments.

2.4 Magnetic Source Localization

The localization of magnetic sources is a problem addressed in many applications, and most algorithms enabling the localization of a magnetic dipole are highly refined. Nevertheless, some unconventional applications still need to be updated using the current state of the art, and further research can bring essential improvements. This is the case of avalanche victims rescue, where current techniques are anachronistic and the localization of victims often becomes slow and complicated.

Before improving existing localization algorithms, it is also important to inquire about available cutting-edge technologies and devise potential protocols. Along these lines, Paper E is a patent publication that suggests a novel localization device and an innovative protocol, both motivated by current solutions and the array processing literature. Its main novelty is the inclusion of an array of magnetic vector sensors at the receiver, which allows specific data processing depending on the level of spatial diversity of the signals present.

The localization protocol proposed with the new device is divided into three stages: detection, tracking and positioning. At detection, the outputs of the sensors are simply added together to increase the SNR and hence the sensibility of the device. At tracking, the magnetic field is calculated using one or more of the sensors available, and the corresponding field lines are followed by the rescuer. At positioning,

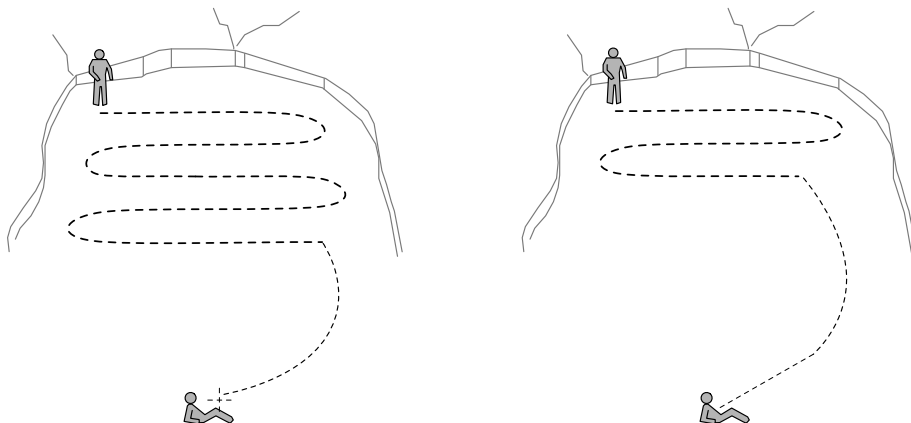


Figure 2.8: Hypothetical search paths of an avalanche victim corresponding to the traditional (left) and proposed (right) protocols. Different line widths indicate different stages of the protocol.

the victim's location is explicitly calculated using all sensors of the array, and a direct-path search towards the victim is performed.

This process contrasts with the traditional one, where four stages are defined with limiting particularities: the detection process is longer due to the lower sensibility of the device; the tracking stage is similar but starting and ending later; positioning is performed at ground level based on power measurements, hence becoming remarkably unhandy and inaccurate; and an additional cumbersome probe-based pinpointing is conducted to accurately find the victim. Figure 2.8 illustrates both protocols.

In general terms, the new protocol allows a more efficient and convenient search than the traditional one, since fewer meters need to be traced in total by the rescuer to reach the victim and pinpointing reduces to simply checking and marking the victim's location. Additionally, the detection range of the proposed device increases with the number of sensors used, and multiple victim localization can be drastically enhanced through parameter-based array processing techniques.

Chapter 3

General Conclusion

This thesis deals with several problems in the field of array signal processing that raise great interest within the telecommunication engineering community. The contributions can be summarized as follows:

First, a novel performance analysis of deterministic beamformers applied in a baseline GNSS scenario with interferences coming from low elevations is presented. The interference attenuation and array gain are considered parameters of interest, and the most outstanding deterministic techniques are analyzed showing that a trade-off exists between both metrics. Additionally, a method is presented to approximately calculate the performance that defines the best possible trade-off and thus delimit the region of eligible designs. As a result, it is found that the optimum beam patterns strike a balance between some aspects found in the Dolph-Chebyshev and others found in spectral weighting techniques.

Second, a new data-dependent beamforming technique is proposed for multipath mitigation in the context of GNSS. This technique is based on the well-known Capon beamformer, and it aims to avoid limiting cancellation effects between the direct signal and correlated multipaths. In order to do so, the known power and direction of arrival of the direct signal are exploited at the receiver, and as a result, the technique is referred to as PBC beamforming. The corresponding computational costs are estimating the spatial correlation matrix of the incoming signal, calculating the cross-correlation between this signal and a reference signal with variable delay and phase, and implementing a two-dimensional minimization problem.

The behavior of the PBC approach is justified mathematically, and also supported by several simulation results. Two important scenarios are distinguished depending on the degree of correlation between the direct signal and multipaths, with the most limiting situation occurring in the coherent multipath case. In either case, the obtained multipath attenuations are generally superior to those obtained by other representative techniques, and the noise response is highly satisfactory. The existing numerical limitations of the PBC approach are addressed later using a new cost function that is continuous and less sensitive to numerical deviations in the estimated correlation matrices. The equivalence between the new formulation and the original one is proven, and corresponding implementations are proposed. While the results obtained show that all implementations are valid, they also indicate that one of them provides significantly better results.

Third, a novel technique that estimates the subspace spanned by the spatial signatures of the multipaths received in an antenna array is presented. In order to estimate this subspace, a tunable FIR filter that offers a trade-off between multipath discrimination and output SNR is proposed. The estimated subspace can then be used for multipath mitigation via beamforming and for multipath DOA estimation. The obtained numerical results show that significant multipath attenuation can be achieved via beamforming for several configurations of the FIR filter, and that the tuning parameter can be adjusted to maximize the multipath attenuation.

Fourth, a robust time-slotted round-trip carrier and timing synchronization protocol is proposed for distributed beamforming in WSNs. The protocol is based on a simple exchange of few reference signals and a calibration signal, and leaves freedom to choose those signals that provide better simultaneity at destination. It also prevents the sensor nodes from being blocked when some disappear, thus allowing for beamforming in dynamic environments. The simulation results show that a significant delay estimation accuracy is required, and that a decent beamforming time can be achieved even when 50% of the nodes disappear at once.

Fifth and last, a novel localization device and an innovative protocol for the search of avalanche victims are presented. The main novelty is the inclusion of an array of magnetic vector sensors at the receiver, which allows specific data processing depending on the level of spatial diversity of the signals present. The method comprises performing three stages that contrast with the traditional ones for their simplicity and effectiveness. The detection stage is faster, the tracking stage is similar but starting and ending later, and the positioning stage is performed much more accurately and comfortably. As a consequence, the proposed method and localization device allow for a more convenient and quick search of the victims.

As a result of this thesis, there are several lines of research that suggest being exploited. It is natural, for example, to consider possible extensions of the proposed data-dependent beamforming techniques to scenarios other than GNSS, especially to those that do not use spread-spectrum modulations. However, it should be noted that in many cases the extensions can be resolved by simply incorporating pilot sequences in the data sent. Given the promising results, another issue to consider is how knowing the power of the desired signal can improve other existing beamforming techniques or even array processing techniques other than beamforming, such as the spectrum-based and parameter-based ones.

Regarding distributed synchronization, a rigorous study on the optimal design of the signals used for timing synchronization would be of great interest. With optimization, the advantages of the proposed protocol could be well exploited and thus lead to an outstanding synchronization. Concerning the localization of avalanche victims, the new device and protocol open the door to investigating array processing algorithms specifically designed for avalanche rescue. Although the use of existing multiple-antenna algorithms from other fields already brings with it an improvement over single-antenna avalanche rescue techniques, it is remarkably likely that new algorithms can slightly improve the rescue time.

Bibliography

- [1] R. C. Hansen. “Special issue on active and adaptive antennas”. In: *IEEE Transactions on Antennas and Propagation* 12.2 (Mar. 1964).
- [2] H. L. Van Trees. *Optimum Array Processing (Part IV of Detection, Estimation, and Modulation Theory)*. Wiley, 2002.
- [3] S. M. Kay. *Modern Spectral Estimation: Theory and Application*. Prentice Hall, 1988.
- [4] M. S. Bartlett. “Smoothing periodograms from time-series with continuous spectra”. In: *Nature* 161 (May 1948), pp. 686–687.
- [5] J. Capon. “High-resolution frequency-wavenumber spectrum analysis”. In: *Proceedings of the IEEE* 57.8 (Aug. 1969), pp. 1408–1418.
- [6] V. F. Pisarenko. “The retrieval of harmonics from a covariance function”. In: *Geophysical Journal International* 33.3 (Sept. 1973), pp. 347–366.
- [7] R. Schmidt. “Multiple emitter location and signal parameter estimation”. PhD thesis. Stanford University, Stanford, CA, 1981.
- [8] S. M. Kay. *Fundamentals of Statistical Signal Processing: Estimation Theory*. Prentice Hall, 1993.
- [9] M. Wax. “Detection and estimation of superimposed signals”. PhD thesis. Stanford University, Stanford, CA, 1985.
- [10] A. J. Weiss and B. Friedlander. “Array shape calibration using sources in unknown locations - a maximum likelihood approach”. In: *IEEE Transactions on Acoustics, Speech and Signal Processing* 37.12 (Dec. 1989), pp. 1958–1966.
- [11] K. M. Wong et al. “Estimation of the directions of arrival of signals in unknown correlated noise. Part I: The MAP approach and its implementation”. In: *IEEE Transactions on Signal Processing* 40.8 (Aug. 1992), pp. 2007–2017.
- [12] J. Li and R. T. Compton. “Maximum likelihood angle estimation for signals with known waveforms”. In: *IEEE Transactions on Signal Processing* 41.9 (Sept. 1993), pp. 2850–2862.
- [13] M. Viberg and A. L. Swindlehurst. “A Bayesian approach to auto-calibration for parametric array signal processing”. In: *IEEE Transactions on Signal Processing* 42.12 (Dec. 1994), pp. 3495–3507.
- [14] A. Jakobsson, A. L. Swindlehurst, and P. Stoica. “Subspace-based estimation of time delays and doppler shifts”. In: *IEEE Transactions on Signal Processing* 46.9 (Sept. 1998), pp. 2472–2483.

-
- [15] A. L. Swindlehurst. “Time delay and spatial signature estimation using known asynchronous signals”. In: *IEEE Transactions on Signal Processing* 46.2 (Feb. 1998), pp. 449–462.
- [16] R. Roy. “ESPRIT: estimation of signal parameters via rotational invariance techniques”. PhD thesis. Stanford University, Stanford, CA, 1987.
- [17] J. O. Smith and J. S. Abel. “Closed-form least-squares source location estimation from range-difference measurements”. In: *IEEE Transactions on Acoustics, Speech and Signal Processing* 35.12 (Dec. 1987), pp. 1661–1669.
- [18] M. Viberg and B. Ottersten. “Sensor array processing based on subspace fitting”. In: *IEEE Transactions on Signal Processing* 39.5 (May 1991), pp. 1110–1121.
- [19] A. V. Oppenheim and R. W. Schaffer. *Discrete-Time Signal Processing*. Pearson, 2010.
- [20] C. A. Balanis. *Antenna Theory: Analysis and Design*. Wiley, 2016.
- [21] S. A. Schelkunoff. “A mathematical theory of linear arrays”. In: *The Bell System Technical Journal* 22.1 (Jan. 1943), pp. 80–107.
- [22] P. M. Woodward. “A method for calculating the field over a plane aperture required to produce given polar diagram”. In: *Journal of the Institution of Electrical Engineers - Part IIIA: Radiolocation* 93.10 (Jan. 1946), pp. 1554–1558.
- [23] C. L. Dolph. “A current distribution for broadside arrays which optimizes the relationship between beam width and side-lobe level”. In: *Proceedings of the IRE* 34.6 (June 1946), pp. 335–348.
- [24] S. P. Applebaum. “Adaptive arrays”. In: *IEEE Transactions on Antennas and Propagation* 24.5 (Sept. 1976), pp. 585–598.
- [25] B. Widrow et al. “Adaptive antenna systems”. In: *Proceedings of the IEEE* 55.12 (Dec. 1967), pp. 2143–2159.
- [26] O. L. Frost. “An algorithm for linearly constrained adaptive array processing”. In: *Proceedings of the IEEE* 60.8 (Aug. 1972), pp. 926–935.
- [27] R. A. Monzingo and T. W. Miller. *Introduction to Adaptive Arrays*. Wiley, 1980.
- [28] E. D. Kaplan and C. J. Hegarty. *Understanding GPS/GNSS: Principles and Applications*. Artech House, 2017.
- [29] B. Hofmann-Wellenhof, H. Lichtenegger, and J. Collins. *Global Positioning System: Theory and Practice*. Springer, 2001.
- [30] A. J. Van Dierendonck, P. Fenton, and T. Ford. “Theory and performance of narrow correlator spacing in a GPS receiver”. In: *Navigation, Journal of the ION* 39.3 (Fall 1992), pp. 265–283.
- [31] R. D. J. Van Nee. “The multipath estimating delay lock loop”. In: *Proc. IEEE ISSSTA*. Yokohama, Japan, Nov. 1992, pp. 39–42.

- [32] L. Garin, F. Van Diggelen, and J.-M. Rousseau. “Strobe and edge correlator multipath mitigation for code”. In: *Proc. ION GPS*. Kansas City, MO, Sept. 1996, pp. 657–664.
- [33] B. Townsend and P. Fenton. “A practical approach to the reduction of pseudo-range multipath errors in a L1 GPS receiver”. In: *Proc. ION GPS*. Salt Lake City, UT, Sept. 1994, pp. 143–148.
- [34] G. A. McGraw and M. S. Braasch. “GNSS multipath mitigation using gated and high resolution correlator concepts”. In: *Proc. ION NTM*. San Diego, CA, Jan. 1999, pp. 333–342.
- [35] J. M. Sleewaegen and F. Boon. “Mitigating short-delay multipath: a promising new technique”. In: *Proc. ION GPS*. Salt Lake City, UT, Sept. 2001, pp. 204–213.
- [36] L. R. Weill. “Multipath mitigation using modernized GPS signals: how good can it get?” In: *Proc. ION GPS*. Portland, OR, Sept. 2002, pp. 493–505.
- [37] M. Z. H. Bhuiyan and E. S. Lohan. “Advanced multipath mitigation techniques for satellite-based positioning applications”. In: *International Journal of Navigation and Observation* (Dec. 2010), Article ID 412393.
- [38] C. Fernandez-Prades, J. Arribas, and P. Closas. “Robust GNSS receivers by array signal processing: theory and implementation”. In: *Proceedings of the IEEE* 104.6 (June 2016), pp. 1207–1220.
- [39] M. D. Zoltowski and A. S. Gecan. “Advanced adaptive null steering concepts for GPS”. In: *Proc. IEEE MILCOM*. San Diego, CA, Nov. 1995, pp. 1214–1218.
- [40] G. Seco-Granados and J. A. Fernández Rubio. “Maximum likelihood propagation-delay estimation in unknown correlated noise using antenna arrays: application to Global Navigation Satellite Systems”. In: *Proc. IEEE ICASSP*. Seattle, WA, May 1998, pp. 2065–2068.
- [41] R. G. Lorenz and S. P. Boyd. “Robust beamforming in GPS arrays”. In: *Proc. ION NTM*. San Diego, CA, Jan. 2002, pp. 409–427.
- [42] G. Seco-Granados, J. A. Fernandez-Rubio, and C. Fernandez-Prades. “ML estimator and hybrid beamformer for multipath and interference mitigation in GNSS receivers”. In: *IEEE Transactions on Signal Processing* 53.3 (Mar. 2005), pp. 1194–1208.
- [43] M. G. Amin and W. Sun. “A novel interference suppression scheme for Global Navigation Satellite Systems using antenna array”. In: *IEEE Journal on Selected Areas in Communications* 23.5 (May 2005), pp. 999–1012.
- [44] S. Daneshmand et al. “GNSS multipath mitigation with a moving antenna array”. In: *IEEE Transactions on Aerospace and Electronic Systems* 49.1 (Jan. 2013), pp. 693–698.
- [45] Y. Hu et al. “A novel array-based spoofing and jamming suppression method for GNSS receiver”. In: *IEEE Sensors Journal* 18.7 (Apr. 2018), pp. 2952–2958.

- [46] L. R. Weill. “High-performance multipath mitigation using the synergy of composite GPS signals”. In: *Proc. ION GPS/GNSS*. Portland, OR, Sept. 2003, pp. 829–840.
- [47] C. Fernandez-Prades and J. A. Fernández-Rubio. “Multi-frequency GPS/Galileo receiver design using direct RF sampling and antenna arrays”. In: *Proc. IEEE SAM*. Sitges, Spain, July 2004, pp. 475–479.
- [48] M. Brenneeman et al. “Mitigation of GPS multipath using polarization and spatial diversities”. In: *Proc. ION GNSS*. Fort Worth, TX, Sept. 2007, pp. 1221–1229.
- [49] F. Fohlmeister et al. “Dual polarization beamforming algorithm for multipath mitigation in GNSS”. In: *Signal Processing* 138 (Sept. 2017), pp. 86–97.
- [50] T. Bitner, S. Preston, and D. Bevly. “Multipath and spoofing detection using angle of arrival in a multi-antenna system”. In: *Proc. ION ITM*. Dana Point, CA, Jan. 2015, pp. 822–832.
- [51] S. Daneshmand and G. Lachapelle. “Integration of GNSS and INS with a phased array antenna”. In: *GPS Solutions* 22.3 (Nov. 2018), pp. 1–14.
- [52] W. Dargie and C. Poellabauer. *Fundamentals of Wireless Sensor Networks: Theory and Practice*. Wiley, 2010.
- [53] Y.-W. Hong et al. “Cooperative communications in resource-constrained wireless networks”. In: *IEEE Signal Processing Magazine* 24.3 (May 2007), pp. 47–57.
- [54] J. N. Laneman, D. N. C. Tse, and G. W. Wornell. “Cooperative diversity in wireless networks: efficient protocols and outage behavior”. In: *IEEE Transactions on Information Theory* 50.12 (Dec. 2004), pp. 3062–3080.
- [55] G. Kramer, M. Gastpar, and P. Gupta. “Cooperative strategies and capacity theorems for relay networks”. In: *IEEE Transactions on Information Theory* 51.9 (Sept. 2005), pp. 3037–3063.
- [56] M. Janani et al. “Coded cooperation in wireless communications: space-time transmission and iterative decoding”. In: *IEEE Transactions on Signal Processing* 52.2 (Feb. 2004), pp. 362–371.
- [57] T. M. Cover and A. A. Gamal. “Capacity theorems for the relay channel”. In: *IEEE Transactions on Information Theory* 25.5 (Sept. 1979), pp. 572–584.
- [58] L. Zheng and D. N. C. Tse. “Diversity and multiplexing: a fundamental tradeoff in multiple-antenna channels”. In: *IEEE Transactions on Information Theory* 49.5 (May 2003), pp. 1073–1095.
- [59] R. Mudumbai, G. Barriac, and U. Madhow. “On the feasibility of distributed beamforming in wireless networks”. In: *IEEE Transactions on Wireless Communications* 6.5 (May 2007), pp. 1754–1763.
- [60] D. R. Brown III and H. V. Poor. “Time-slotted round-trip carrier synchronization for distributed beamforming”. In: *IEEE Transactions on Signal Processing* 56.11 (Nov. 2008), pp. 5630–5643.

- [61] R. Mudumbai et al. “Distributed transmit beamforming using feedback control”. In: *IEEE Transactions on Information Theory* 56.1 (Jan. 2010), p. 426.
- [62] I. Thibault et al. “Design and analysis of deterministic distributed beamforming algorithms in the presence of noise”. In: *IEEE Transactions on Communications* 61.4 (Apr. 2013), pp. 1595–1607.
- [63] A. Bletsas, A. Lippman, and J. N. Sahalos. “Simple, zero-feedback, distributed beamforming with unsynchronized carriers”. In: *IEEE Journal on Selected Areas in Communications* 28.7 (Sept. 2010), pp. 1046–1054.
- [64] J. A. Nanzer et al. “Open-loop coherent distributed arrays”. In: *IEEE Transactions on Microwave Theory and Techniques* 65.5 (May 2017), pp. 1662–1672.
- [65] C. V. Tilburg et al. “Wilderness medical society practice guidelines for prevention and management of avalanche and nonavalanche snow burial accidents”. In: *Wilderness and Environmental Medicine* 28.1 (Mar. 2017), pp. 23–42.
- [66] N. Ayuso et al. “A deep insight into avalanche transceivers for optimizing rescue”. In: *Cold Regions Science and Technology* 111 (Mar. 2015), pp. 80–94.
- [67] J. R. Bourne and K. K. Leang. “Bayesian estimation of snow-avalanche victim pose: a method to assist human and/or robot first responders to quickly locate a buried victim”. In: *Proc. ASME DSCC*. Vol. 3. Park City, UT, Oct. 2019.
- [68] J. W. Hereford and M. X. Bond. *Avalanche Victim Locating Transceiving Apparatus*. Patent US/6167249/A. Backcountry Access, Dec. 2000.
- [69] D. Kashuba, E. G. Pachal, and C. G. Pachal. *Avalanche Transceiver*. Patent US/2005/0151662/A1. ORTOVOX, July 2005.
- [70] G. Kampel et al. *Search Device for Locating a Transmitter, in Particular an Avalanche-Victim Search Device*. Patent US/2005/0231359/A1. ORTOVOX, Oct. 2005.
- [71] E. A. Wolf and M. Clark. *Direction and Distance Finder for Locating Distress Signals*. Patent US/2005/0270234/A1. ACR Electronics, Dec. 2005.
- [72] P. Closas and N. Baldo. *Method and System for Locating Avalanche Victims Equipped with a Transceiver*. Patent WO/2016/062337/A1. CTTC, Apr. 2016.
- [73] M. Karaqui. *Safety Device, in Particular for Avalanche Victim Searching*. Patent WO/2017/109422/A1. June 2017.
- [74] J. Stepanek and D. W. Claypool. “GPS signal reception under snow cover: a pilot study establishing the potential usefulness of GPS in avalanche search and rescue operations”. In: *Wilderness and Environmental Medicine* 8.2 (May 1997), pp. 101–104.
- [75] J. B. Schleppe and G. Lachapelle. “Tracking performance of a HSGPS receiver under avalanche deposited snow”. In: *GPS Solutions* 12.1 (Mar. 2008), pp. 13–21.
- [76] L. Crocco and V. Ferrara. “A review on ground penetrating radar technology for the detection of buried or trapped victims”. In: *Proc. CTS*. Minneapolis, MN, July 2014, pp. 535–540.

- [77] M. Silvagni et al. “Multipurpose UAV for search and rescue operations in mountain avalanche events”. In: *Geomatics, Natural Hazards and Risk* 8.1 (2017), pp. 18–33.
- [78] N. Mimmo, P. Bernard, and L. Marconi. “Avalanche victim search via robust observers”. In: *IEEE Transactions on Control Systems Technology* 29.4 (July 2021), pp. 1450–1461.
- [79] J. R. Wait. “Criteria for locating an oscillating magnetic dipole buried in the earth”. In: *Proceedings of the IEEE* 59.6 (June 1971), pp. 1033–1035.
- [80] W. M. Wynn et al. “Advanced superconducting gradiometer/magnetometer arrays and a novel signal processing technique”. In: *IEEE Transactions on Magnetics* 11.2 (Mar. 1975), pp. 701–707.
- [81] T. W. H. Caffey. *Locating a buried earth penetrator*. Technical Report SAND77-0646. Sandia Laboratories, Albuquerque, CA, Nov. 1977.
- [82] F. H. Raab. “Quasi-static magnetic-field technique for determining position and orientation”. In: *IEEE Transactions on Geoscience and Remote Sensing* 19.4 (Oct. 1981), pp. 235–243.
- [83] D. D. Arumugam et al. “Three-dimensional position and orientation measurements using magneto-quasistatic fields and complex image theory”. In: *IEEE Antennas and Propagation Magazine* 56.1 (Feb. 2014), pp. 160–173.
- [84] O. Kypris, T. E. Abrudan, and A. Markham. “Magnetic induction-based positioning in distorted environments”. In: *IEEE Transactions on Geoscience and Remote Sensing* 54.8 (Aug. 2016), pp. 4605–4612.
- [85] V. Pasku et al. “Magnetic field-based positioning systems”. In: *IEEE Communications Surveys and Tutorials* 19.3 (Aug. 2017), pp. 2003–2017.
- [86] S. Baillet, J. C. Mosher, and R. M. Leahy. “Electromagnetic brain mapping”. In: *IEEE Signal Processing Magazine* 18.6 (Nov. 2001), pp. 14–30.
- [87] J. C. Mosher, P. S. Lewis, and R. M. Leahy. “Multiple dipole modeling and localization from spatio-temporal MEG data”. In: *IEEE Transactions on Biomedical Engineering* 39.6 (June 1992), pp. 541–557.
- [88] J. C. Mosher and R. M. Leahy. “Recursive MUSIC: a framework for EEG and MEG source localization”. In: *IEEE Transactions on Biomedical Engineering* 45.11 (Nov. 1998), pp. 1342–1354.
- [89] B. Lütkenhöner. “Dipole source localization by means of maximum likelihood estimation. I. Theory and simulations”. In: *Electroencephalography and Clinical Neurophysiology* 106.4 (Apr. 1998), pp. 314–321.
- [90] K. Sekihara et al. “Reconstructing spatio-temporal activities of neural sources using an MEG vector beamformer technique”. In: *IEEE Transactions on Biomedical Engineering* 48.7 (July 2001), pp. 760–771.
- [91] C. Hu et al. “A cubic 3-axis magnetic sensor array for wirelessly tracking magnet position and orientation”. In: *IEEE Sensors Journal* 10.5 (May 2010), pp. 903–913.

- [92] T. Piotrowski, J. Nikadon, and A. Moiseev. “Localization of brain activity from EEG/MEG using MV-PURE framework”. In: *Biomedical Signal Processing and Control* 64 (Feb. 2021), Article num. 102243.

Part II

Primary Publications

Paper A

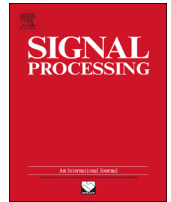
On the Performance of Deterministic Beamformers: A Trade-Off Between Array Gain and Attenuation

DOI: 10.1016/j.sigpro.2013.06.008

© 2013 Elsevier. Reprinted with permission from M. Mañosas-Caballú, J. L. Vicario and G. Seco-Granados, Signal Processing 94 (Jan. 2014), pp. 158-162.

Contents lists available at [ScienceDirect](#)

Signal Processing

journal homepage: www.elsevier.com/locate/sigpro

On the performance of deterministic beamformers: A trade-off between array gain and attenuation



Martí Mañosas-Caballú*, José López Vicario, Gonzalo Seco-Granados

Department of Telecommunications and Systems Engineering, Universitat Autònoma de Barcelona, Bellaterra 08193, Spain

ARTICLE INFO

Article history:

Received 22 February 2013

Received in revised form

10 May 2013

Accepted 10 June 2013

Available online 17 June 2013

Keywords:

Beamforming

Array gain

Attenuation

Deterministic

ABSTRACT

It is customary to look over deterministic beamforming techniques as designs that offer a trade-off between mainlobe width and sidelobe level. In this work, we take into consideration that noise reduction and interference rejection are actually more useful metrics for the design of practical systems, and we present a novel analysis as a first step to understand the behavior and limitations of the deterministic beamformers from this system level perspective. The obtained results show that a trade-off between both metrics exists, and they illustrate some misconceptions about the traditionally assumed optimal designs. Finally, a method to approximately calculate the best attainable performance of any deterministic beamformer is presented.

© 2013 Elsevier B.V. All rights reserved.

1. Introduction

Beamforming is an array signal processing technique that provides a versatile form of spatial filtering. The existing beamforming techniques can be mainly classified into two groups [1]: *deterministic beamforming* and *data-dependent beamforming*. In the former, the designs aim to generate a fixed response for all possible scenarios, where sidelobe level and mainlobe width are typical performance metrics. In the latter, the designs depend on the statistics of the incoming data, where output signal-to-interference plus noise ratio (SINR) is a common performance metric.

Currently, the application requirements at a system level are usually present in terms of interference power and noise power at the output of the beamformer [2–4], and normally they cannot be understood simply as a single requirement on the interference-plus-noise power. These requirements can be alternatively expressed in terms of the beamformer's ability to mitigate the noise (*array gain*) and reject the interferences (*attenuation*), and they can be represented in a curve that relates both metrics. On the

other hand, each beamforming technique is inherently characterized by a performance curve containing the array gain and attenuation values that it can offer, each point corresponding to a specific design. A natural concern is then to accurately quantify the performance curves, since they allow us to know which designs can be eligible for the application of interest. Fig. 1 depicts this idea. This clearly casts doubts on the optimality of some commonly used beamforming performance metrics, and it shows that array gain and attenuation may be better metrics.

Recently, the authors of [4] studied the trade-off between array gain and attenuation of some data-dependent beamformers, and they proposed a new beamformer that allows the control of this trade-off. However, a similar study about deterministic beamformers is also necessary since unfortunately most data-dependent beamformers do not allow this control and they fail in some scenarios [1,5–7]. In contrast, deterministic beamformers constitute a robust [1,8,9] and simpler option to be implemented. Moreover, they offer adequate solutions when the desired signal and the interferences are known to be confined in different spatial regions, as in GNSS reference stations [3], radio telescopes for interferometry and the over-the-horizon radar.

In this work we shed some light on the relation between attenuation and array gain of the most relevant deterministic techniques. We compare their behavior and

* Corresponding author. Tel.: +34 93 581 40 30; fax: +34 93 581 40 31.

E-mail addresses: marti.manosas@uab.cat (M. Mañosas-Caballú), jose.vicario@uab.cat (J. López Vicario), gonzalo.seco@uab.cat (G. Seco-Granados).

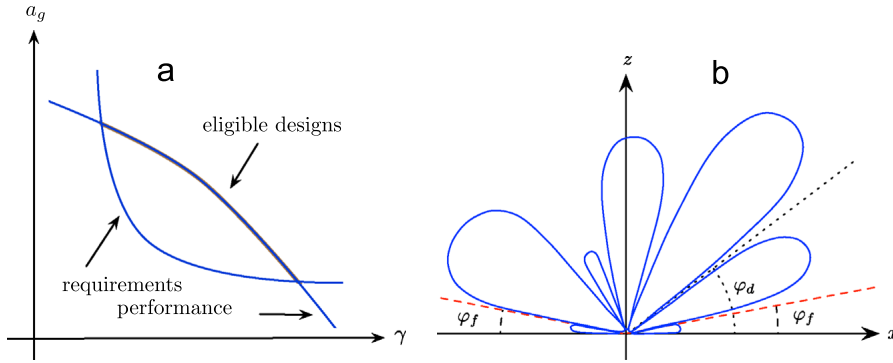


Fig. 1. (a) Example of the requirements and performance curves in terms of array gain (a_g) versus attenuation (γ). (b) Scenario of interest and example of a possible beam pattern.

limitations in a realistic scenario, and we show that the Dolph–Chebychev beamformer, which is usually adopted as the optimal solution to reject the signals coming from a given spatial sector, is not the best design from a system level perspective. In order to obtain a benchmark to evaluate the performance of any beamformer, we also present a method to approximately calculate the optimal performance curve.

2. Problem statement

Let us consider that an N -element uniform linear array receives $s(t)$, $m_1(t)$, \dots , $m_M(t)$ and $\mathbf{n}(t)$, which are the baseband representations of the desired signal, M interferences and additive white noise respectively. Assuming that the array narrow-band condition is fulfilled [1], the baseband equivalent of the beamformer output signal is

$$y(t) = \mathbf{w}^H \mathbf{v}(\theta_0) s(t) + \sum_{k=1}^M \mathbf{w}^H \mathbf{v}(\theta_k) m_k(t) + \mathbf{w}^H \mathbf{n}(t) \quad (1)$$

where $\mathbf{w} \in \mathbb{C}^N$ contains the beamforming weights, H denotes the conjugate transpose operation, $\mathbf{v}(\theta) \in \mathbb{C}^N$ is the steering vector at a given direction-of-arrival (DOA) θ , and $\theta_0, \theta_1, \dots, \theta_M$ are the DOAs of the desired signal and interferences respectively, defined as the arrival angles with respect to the array axis. Finally, $\mathbf{n}(t) \in \mathbb{C}^N$ contains the received noise at each element of the array.

In the applications of interest we cannot assume that the DOAs of the interferences are known. Instead, the interferences are assumed to arrive from elevations lower than a value φ_f , and we call this region *forbidden sector*. On the other hand, the desired signal arrives from an elevation higher than a value $\varphi_d > \varphi_f$, and we call this region *desired sector*. The remaining area is the *transition sector*. The elevations belonging to the forbidden sector correspond to $\theta \in [0, \varphi_f] \cup [\pi - \varphi_f, \pi]$, and for the desired one $\theta \in [\varphi_d, \pi - \varphi_d]$.

The aim of the beamformer is to find the weights \mathbf{w} that verify a particular requirements on the array response or *beam pattern* $\mathbf{w}^H \mathbf{v}(\theta)$. Fig. 1b shows a scheme of the described scenario and an example of a possible beam pattern. From all existing metrics related to \mathbf{w} , we are interested in the attenuation γ and the array gain a_g of the

corresponding beam pattern, defined as

$$\gamma^{-1} := \max\{|\mathbf{w}^H \mathbf{v}(\theta)|^2 / |\mathbf{w}^H \mathbf{v}(\theta_0)|^2 : \theta \in [0, \varphi_f] \cup [\pi - \varphi_f, \pi]\} \quad (2)$$

$$a_g := |\mathbf{w}^H \mathbf{v}(\theta_0)|^2 / |\mathbf{w}^H \mathbf{w}| \quad (3)$$

Note that the attenuation definition is consistent with the worst-case requirements of the considered applications, and the noise definition considers the special case of spatial white noise and identical noise spectra at each sensor [1].

The goal of the paper is then to study the relation between γ and a_g of the current deterministic beamformers for linear arrays and find an optimal performance curve to obtain a benchmark that let us evaluate their performance. The inter-element spacing of the array is chosen to be half wavelength through all the paper since the corresponding beam pattern presents the best resolution without ambiguity.

3. Array gain versus attenuation trade-off

3.1. Deterministic beamforming techniques

We discuss here how to adapt the existing deterministic techniques to our scenario. The first step is to select those methods in which either a_g or γ can be modified deliberately by the designer. This is only the case of the Main Response Axis (MRA) methods [1], which assure an accurate control of the sidelobe level.

The MRA methods mainly comprise the Spectral Weighting (SW) and the Minimum Beamwidth for Specified Sidelobe Level (MBSSL) approaches, which present a well known trade-off between sidelobe level and mainlobe width or *beamwidth*. Concretely, the MBSSL methods optimize the beamwidth for a given maximum level of sidelobes, and the Dolph–Chebychev is the best known representative because it has constant level of sidelobes. Furthermore, both approaches are characterized by having non-increasing sidelobes. This leads to a methodology of design based on building a spatial filter with pass-band given by the mainlobe and stop-band given by the sidelobes. In our scenario, the pass-band is located in the desired sector and the stop-band corresponds to the forbidden sector. The mainlobe is placed in the desired

direction θ_0 by means of *array steering* [1] since the mainlobe of all the MRA methods is located at $\theta_0 = \pi/2$ by default, and the first sidelobe level is meant to determine a lower-bound on the attainable attenuation.

Finally, note that this methodology of design may imply that a portion of the mainlobe is present in the forbidden sector because the closer to the endfire ($\theta = 0$ or π) the mainlobe is, the wider the beamwidth. Then, as γ is determined by the maximum value of sidelobes and mainlobe inside the forbidden sector, the mainlobe can reduce the attainable attenuation if it exceeds the sidelobe level. As a result, and being consistent with the considered worst case requirements, it is mandatory to focus on the designs where the DOA of $s(t)$ is close to the forbidden sector. Other cases are not so restrictive.

3.2. Trade-off analysis

We start by noting that the value of γ is generally improved by decreasing the sidelobes level. However, this generally widens the mainlobe. Thus, a situation may be attained where the mainlobe is present in the forbidden sector with a value that exceeds the sidelobes. As a result, each MRA technique has a maximum value of attenuation ϵ that is not possible to exceed, i.e. $\epsilon = \max \gamma$. We call it *maximum-attenuation design*, and it is achieved when the first sidelobe level equals the maximum mainlobe value inside the forbidden sector.

Without loss of generality, we can consider that our beam patterns are normalized with respect to the LOSS response, so ϵ corresponds to a minimum sidelobe level $1/\sqrt{\epsilon}$. In the case of the Dolph–Chebychev approach, it is possible to analytically deduce a formula for ϵ through simple algebraic manipulations on the beam pattern of the Dolph–Chebychev beamformer, whose basic formulation can be obtained from [1]

$$\epsilon = \cosh^2((N-1) \operatorname{sech}^{-1} \cos(\pi\rho/2)) \quad N \geq 2 \quad (4)$$

where $\rho = \cos(\varphi_f) - \cos(\varphi_d)$. In the case of the SW methods, the value of ϵ corresponds to the largest solution of

$$\sqrt{\epsilon}^{-1} = |\mathbf{w}(\epsilon)^H \mathbf{v}(\cos^{-1}\rho)| \quad \epsilon > 0 \quad (5)$$

where we use $\mathbf{w}(\epsilon)$ to emphasize that \mathbf{w} depends on the designed sidelobe level $1/\sqrt{\epsilon}$ through a MRA design parameter. Eq. (5) imposes that the value of the mainlobe at φ_f is equal to the first sidelobe level. Then, in practice one can obtain an approximate solution via beam pattern plots: increasing/decreasing the first sidelobe level until it equals the mainlobe value at φ_f . Analogously, an accurate solution of ϵ can be easily obtained from (5) via the bisection method.

As shown in (4) and (5), ϵ does not only depend on the particular design \mathbf{w} , but also on the value of N . Fig. 2 shows the minimum number of antennas N_{\min} needed to obtain a given value of ϵ . We can see that N_{\min} is a monotonically increasing function of ϵ . The reason is that an increase of ϵ requires a decrease of the beamwidth, which is achieved by increasing N . Note that the plot also shows that the SW methods can be classified into two groups [1]. On one hand, Hamming and Blackman-Harris, do not allow us to vary the sidelobe level deliberately, and they are

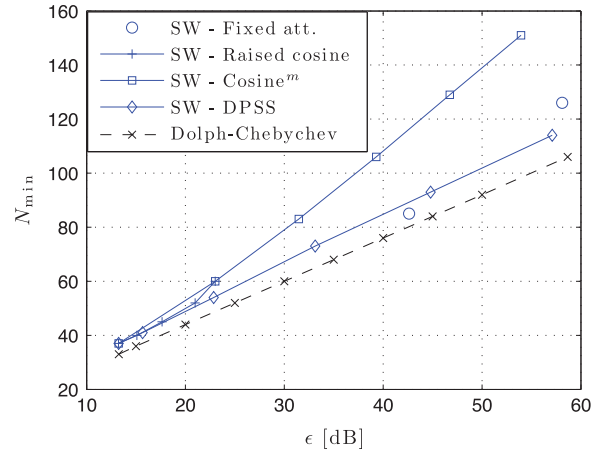


Fig. 2. Minimum number of antennas N_{\min} for achieving an attenuation ϵ . Scenario with $\varphi_f = 10^\circ$ and $\varphi_d = 20^\circ$.

represented as fixed attenuation points. On the other hand, Dolph–Chebychev, Raised Cosine, Cosine^m and Discrete Prolate Spheroidal Sequences (DPSS), allow us to increase or decrease the sidelobe level through a design parameter.

Finally, we analyze the points (a_g, γ) that an MRA method offers when varying the design parameter for a given value of N . This gives a curve for each value of N . Note first that if the designed sidelobes are higher or equal than $1/\sqrt{\epsilon}$, then γ is determined by the sidelobes level. However, when the designed sidelobes are lower than $1/\sqrt{\epsilon}$, then γ is determined by the mainlobe. Thus, two different designs may exist that produce the same γ . As each design corresponds to a different beamformer, a priori it has different values of a_g . The result is that some values of γ can be paired with two different values of a_g , except when $\gamma = \epsilon$. In fact, all simulated methods present an upper and lower curves ending at a common point with attenuation ϵ . In order to show only the most meaningful designs, we do not represent here the lower curve. Fig. 3 shows the upper curves obtained for the DPSS and Dolph–Chebychev methods.

3.3. Discussion

First note that, as the SW methods have decreasing sidelobes, there are sidelobes that are lower than the first sidelobe. But, as some of them are outside the forbidden region, they are not effectively used to attenuate interferences. In contrast, the Dolph–Chebychev approach offers a constant level of sidelobes, which is a less restrictive way of using the degrees of freedom of \mathbf{w} to increase γ , as corroborated by the results in Fig. 2. This advantage partially clarifies why the Dolph–Chebychev is usually adopted as the optimal solution to attenuate the signals coming from a given spatial sector. However, the Dolph–Chebychev method does not enjoy the same advantage in terms of a_g . For instance, Fig. 3 shows that for $N=40$ the SW techniques present the best values of a_g .

Second note that Fig. 3 shows that there exists a clear trade-off between a_g and γ . The SW methods present the best a_g when high sidelobes are used. This is due to both the narrow mainlobe of the beam patterns and the high filtration

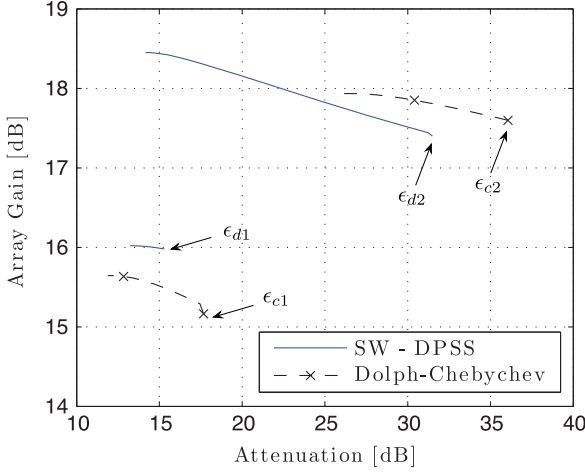


Fig. 3. Array gain versus attenuation for the DPSS and the Dolph-Chebyshev techniques. $N=40$ (lower curves) and $N=70$ (upper curves). The maximum-attenuation design values are $\epsilon_{d1} \approx 15.3$ dB, $\epsilon_{d2} \approx 31.5$ dB, $\epsilon_{c1} \approx 17.7$ dB and $\epsilon_{c2} \approx 36$ dB. Scenario with $\varphi_f = 10^\circ$ and $\varphi_d = 20^\circ$.

of the noise for low elevations. Then, when the designed sidelobes are lower, γ increases up to ϵ . But the mainlobe width increases and the higher noise reduction for low elevations does not compensate the incoming noise from the mainlobe, so a_g decreases. In contrast, in the case of the Dolph-Chebyshev, the noise is poorly mitigated in all the visible region for high sidelobes since the same low attenuation is applied for all the sidelobes, so a_g is low. Then, a_g is improved when the sidelobes are decreased, although the represented values are obtained once the sidelobes go under $1/\sqrt{\epsilon}$, so the attenuation decreases.

4. Optimal performance curve

We work out the values of the Optimal Performance Curve (OPC) from the solution of an iterative algorithm. Our goal is to solve

$$\begin{aligned} \max_{\mathbf{w}} \quad & |\mathbf{w}^H \mathbf{a}|^2 / |\mathbf{w}^H \mathbf{w}| \\ \text{s.t.} \quad & |\mathbf{w}^H \mathbf{v}(\theta)| / |\mathbf{w}^H \mathbf{a}| \leq \beta \quad \theta \in [0, \varphi_f] \cup [\pi - \varphi_f, \pi] \end{aligned} \quad (6)$$

where $\mathbf{a} = \mathbf{v}(\theta_0)$ to abbreviate and, without loss of generality, we can consider that $\mathbf{w}^H \mathbf{a} = 1$. Note that (6) maximizes a_g for a given attenuation $\gamma = \beta^2$, so its solution determines the optimal trade-off between a_g and γ . However, as this solution is very difficult to obtain (if possible at all), we present below an approximate solution by means of a modified version of the iterative algorithm presented in [10]. Although an analytical proof of the convergence of the proposed iterative algorithm to the approximate solution is not available, the results obtained in [10] and our extensive simulations have shown that in practice this is always the case as long as the constraint in (6) does not make the problem unfeasible. Note that in the considered scenarios a mathematical proof of the convergence is not really necessary since it can be just checked through simulations before using the weights for their final purpose.

The algorithm starts by creating a distortionless beamformer with maximum array gain, i.e. $\mathbf{w}_0 = \arg \min \mathbf{w}^H \mathbf{w}$

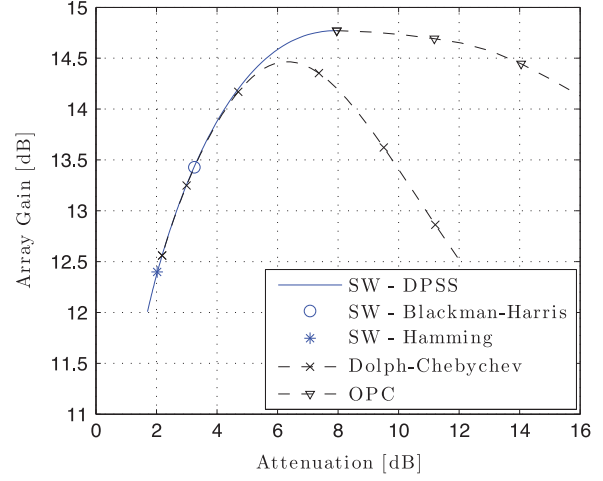


Fig. 4. Array gain versus attenuation for several MRA deterministic techniques and the OPC. $N=30$. Scenario with $\varphi_f = 10^\circ$ and $\varphi_d = 20^\circ$.

subject to $\mathbf{w}^H \mathbf{a} = 1$, whose solution is $\mathbf{w}_0 = (\mathbf{a}^H \mathbf{a})^{-1} \mathbf{a}$. Second, the algorithm iteratively updates the weights as $\mathbf{w}_{n+1} = \mathbf{w}_n + \Delta \mathbf{w}_n$ until the sidelobes do not exceed the desired level β in the forbidden sector. For a given value of $n \in \mathbb{N}$, $\Delta \mathbf{w}_n$ comes from

$$\begin{aligned} \min_{\Delta \mathbf{w}_n} \quad & (\mathbf{w}_n + \Delta \mathbf{w}_n)^H (\mathbf{w}_n + \Delta \mathbf{w}_n) \\ \text{s.t.} \quad & \Delta \mathbf{w}_n^H \mathbf{a} = 0 \\ & \Delta \mathbf{w}_n^H \mathbf{v}(\phi_{n,k}) = f_{n,k} \quad k = 1, \dots, K_n \end{aligned} \quad (7)$$

where $\phi_{n,k}$ is the direction of the k -th sidelobe of \mathbf{w}_n that exceeds β in the forbidden sector, K_n is the number of sidelobes that exceed β and $f_{n,k}$ is the value that we assign to the beam pattern of $\Delta \mathbf{w}_n$ in the direction $\phi_{n,k}$.

The goal of (7) is twofold. On one hand, using the new objective function and the constraint $\Delta \mathbf{w}_n^H \mathbf{a} = 0$, the maximization of the array gain of \mathbf{w}_{n+1} and the constraint $\mathbf{w}_{n+1}^H \mathbf{a} = 1$ are maintained. On the other hand, using the second constraint with $f_{n,k} := (\beta - |c_{n,k}|)c_{n,k}/|c_{n,k}|$ and defining $c_{n,k}$ as the value of the beam pattern of \mathbf{w}_n at $\phi_{n,k}$, the level of the selected sidelobes that exceed β is forced to be equal to β . In the case that $K_n > N-1$, only the highest $N-1$ sidelobes are considered, hence prioritizing the directions that exceed the sidelobe threshold in a greatest extent. Note that, assuming that convergence holds, $K_n \leq N-1$ must be verified from some iteration on. The solution of (7) is $\Delta \mathbf{w}_n = \mathbf{C}_n (\mathbf{C}_n^H \mathbf{C}_n)^{-1} \mathbf{g}_n - \mathbf{P}_{\mathbf{C}_n}^\perp \mathbf{w}_n$, where $\mathbf{C}_n = [\mathbf{a}, \mathbf{v}(\phi_{n,1}), \dots, \mathbf{v}(\phi_{n,K_n})]$, $\mathbf{g}_n = [0, f_{n,1}, \dots, f_{n,K_n}]^H$ and $\mathbf{P}_{\mathbf{C}_n}^\perp$ is the projection matrix onto the space orthogonal to the column space of \mathbf{C}_n .

Fig. 4 plots the OPC and the performance curves of the most representative MRA methods for $N=30$. As it is clearly shown, the OPC outperforms these deterministic designs, so it sets a reference to visualize how far they are from the optimal one. In addition, an interesting feature is observed when the OPC beam patterns are plotted: they present decreasing sidelobes outside the forbidden sector and approximately constant sidelobes in the forbidden sector. This is an intermediate behavior between those of the SW and the Dolph-Chebyshev and coincides with the fact that it may optimize the studied trade-off.

5. Conclusion

In this work we have presented a novel performance analysis of deterministic beamformers applied in a scenario with interferences coming from low elevations. We have argued that the well known trade-off between sidelobe level and mainlobe width is not useful to carry out performance assessment and design at system level. Therefore, we have considered the attenuation and the array gain as a parameters of interest, and we have analyzed the most outstanding deterministic techniques showing that a trade-off between both metrics exists. Finally, we have presented a method to approximately calculate the performance that defines the best possible trade-off and delimit the region of eligible designs. The corresponding beam patterns strike a balance between some aspects found in the Spectral Weighting techniques and others found in the Dolph–Chebychev.

References

- [1] H.L. Van Trees, *Optimum Array Processing. Detection, Estimation, and Modulation Theory. Part IV*, 1st edition, Wiley-Interscience, 2002.
- [2] J. Riba, J. Goldberg, G. Vazquez, Robust beamforming for interference rejection in mobile communications, *IEEE Transactions on Signal Processing* 45 (1997) 271–275.
- [3] J.L. Vicario, F. Antreich, M. Barcelo, N. Basta, J. Cebrian, M. Cuntz, O. Gago, L. Gonzales, V. Heckler, C. Lavin, M. Manosas-Caballu, J. Picanyol, G. Seco-Granados, M. Sgammini, F. Amarillo, ADIBEAM: Adaptive digital beamforming for Galileo reference ground stations, in: *Proceedings of ION GNSS, 2010*, Portland, OR, pp. 172–184.
- [4] M. Souden, J. Benesty, S. Affes, A study of the LCMV and MVDR noise reduction filters, *IEEE Transactions on Signal Processing* 58 (2010) 4925–4935.
- [5] Y. Bresler, V. Reddy, T. Kailath, Optimum beamforming for coherent signal and interferences, *IEEE Transactions on Acoustics Speech and Signal Processing* 36 (1988) 833–843.
- [6] S. Pillai, B. Kwon, Forward/backward spatial smoothing techniques for coherent signal identification, *IEEE Transactions on Acoustics Speech and Signal Processing* 37 (1989) 8–15.
- [7] G. Seco-Granados, J.A. Fernandez-Rubio, C. Fernandez-Prades, ML estimator and hybrid beamformer for multipath and interference mitigation in GNSS receivers, *IEEE Transactions on Signal Processing* 53 (2005) 1194–1208.
- [8] K.M. Buckley, L. Griffiths, Design of deterministic beamformers for arbitrarily configured arrays, in: *Proceedings of the IEEE ICASSP, 1987*, Minneapolis, MN, pp. 1995–1998.
- [9] C.-Y. Tseng, L.J. Griffiths, An iterative approach for deterministic beamformer design, in: *Proceedings of the Conference on Communication Computing and Signal Processing, 1989*, Victoria, BC, Canada, pp. 439–442.
- [10] C.-Y. Tseng, L. Griffiths, A simple algorithm to achieve desired patterns for arbitrary arrays, *IEEE Transactions on Signal Processing* 40 (1992) 2737–2746.

Paper B

Power-Based Capon Beamforming: Avoiding the Cancellation Effects of GNSS Multipath

DOI: 10.1016/j.sigpro.2020.107891

© 2020 Elsevier. Reprinted with permission from M. Mañosas-Caballú, A. L. Swindlehurst and G. Seco-Granados, Signal Processing 180 (Mar. 2021), num. 107891.



Contents lists available at ScienceDirect

Signal Processing

journal homepage: www.elsevier.com/locate/sigpro

Power-based Capon beamforming: Avoiding the cancellation effects of GNSS multipath



Martí Mañosas-Caballú^{a,*}, A. Lee Swindlehurst^b, Gonzalo Seco-Granados^a

^aDpt. Telecomm. and Syst. Engineering, Universitat Autònoma de Barcelona, Spain

^bDpt. Electrical Engineering and Comp. Science, University of California at Irvine, United States

ARTICLE INFO

Article history:

Received 25 March 2020

Revised 7 August 2020

Accepted 5 November 2020

Available online 10 November 2020

Keywords:

Beamforming

Capon

Arrays

Multipath

Correlated

Coherent

GNSS

Time-delay

Carrier-phase

ABSTRACT

This paper addresses the problem of GNSS multipath mitigation using antenna arrays. A new data-dependent beamforming technique is proposed that is based on the well-known Capon beamformer. This technique aims to avoid the typical cancellation phenomenon between signal and correlated multipaths, by exploiting the known power of the direct signal at the receiver. To this effect, a measure of the correlation between the signal and multipaths is obtained in matrix form, and it is then subtracted from the spatial correlation matrix of the received signal. This results in a new spatial correlation matrix that is used for the final Power-Based Capon beamformer. The behaviour of this technique is justified mathematically, and it is supported by several numerical results. These results show that the obtained multipath attenuations are generally superior to those obtained by other existing techniques, and also that the noise response is very satisfactory. The impact of the proposed technique on the time-delay and carrier-phase calculation at the GNSS receiver is also considered. While the obtained carrier-phase observables are reasonably accurate, the final distortion on the time-delay is exceptionally low for any multipath delay.

© 2020 Elsevier B.V. All rights reserved.

1. Introduction

Global Navigation Satellite Systems (GNSS) enable the calculation of a user position by using the signals transmitted by a constellation of specific satellites. In order to obtain this position, some essential parameters have to be estimated at the user receiver. For instance, the time-delay of the received signals is very important, and it has a great impact on the receiver accuracy. It is used for the calculation of the *pseudorange*, or apparent distance between the user and each available satellite. This distance does not typically match with the exact geometric distance due to, among other factors, synchronism errors between the receiver and satellite clocks, but it leads to a system of equations from which the position can be calculated [1]. The carrier-phase of the received signals may also be used to obtain a measure of the distance between the satellite and receiver, and it is particularly appealing because it provides a much more precise measurement than the time-delay. However, it also presents some limitations, such as being ambiguous by an unknown integer number of wavelengths.

For GNSS, only the received Line-Of-Sight Signal (LOSS) is exploited to obtain useful information about the receiver position. Multipath reflections usually bias the time-delay and carrier-phase estimates, so that pseudoranges may change by several tens of meters, and they also hamper the ambiguity resolution process needed for carrier-phase ranging [2]. For this reason, significant research and development efforts have been devoted to the mitigation of multipath effects, and many techniques have been proposed so far. On one hand, there are single-antenna techniques, which attempt to discriminate the LOSS from the reflections by exploiting their temporal diversity. Examples of such techniques are the narrow-correlator [3], the strobe-correlator [4] and the MEDLL [5], but there are other proposals as well [6–8]. Although these approaches improve on the standard positioning accuracy, their performance is still insufficient for many precise applications. On the other hand, there are multiple-antenna techniques, which exploit the spatial diversity, and are able to discriminate the reflections when they come from different directions [9]. So far, several multiple-antenna studies have been proposed that take into account the underlying particularities of a GNSS scenario. These include the application of the basic Howells-Applebaum and Power-Inversion methods [10], the use of Deterministic Beamforming techniques [11], specific methods based on Maximum Likelihood (ML) estimation [12], two-step approaches based on Eigen-decomposition [13], and many other examples [14–16]. A thor-

* Corresponding author.

E-mail addresses: marti.manosas@e-campus.uab.cat (M. Mañosas-Caballú), swindle@uci.edu (A.L. Swindlehurst), gonzalo.seco@uab.cat (G. Seco-Granados).

ough overview can be found in [17], and other recent studies are [18] and [19].

Overall, the best and most well-known multiple-antenna solutions are based on data-dependent beamforming, where the optimal beamforming weights depend on the statistics of the incoming data [9]. They are very appropriate for situations where little a priori information about the scenario is available, or when the scenario is likely to change with time. When the spatial and/or temporal signatures of the LOSS are assumed known, it is common to exploit them to improve performance at the output of the array [20]. Otherwise, there are also blind beamforming techniques that only exploit some specific properties of the involved signals, such as constant modulus and self-coherence, and hence they are robust to errors in the previous assumptions. In any case, the data that is used to compute the beamforming weights can be obtained either before or after the despreading process, since all present and planned navigation systems use Direct-Sequence Spread-Spectrum (DS-SS) signals. When mitigating the multipath is the main issue, it is recommended to employ the post-despreading signals because the despreading makes the multipath contribution more noticeable. The weights can then be applied to either the pre-despreading or the post-despreading signals.

Although data-dependent beamforming is very useful in many situations, it often fails when very correlated signals are present. Hence, it is not useful to mitigate multipath reflections with very small delay relative to the LOSS. For this reason, some robust beamforming techniques that combat highly correlated signals have been proposed, but they still present certain limitations. The first remarkable contribution was in 1982, with the work of Widrow et al. [21]. Then, Shan et al. [22] introduced the powerful spatial smoothing technique for Direction-Of-Arrival (DOA) estimation, which satisfactorily decorrelates a set of coherent signals impinging on an antenna array. However, the application of this technique to the beamforming problem involves a regular array geometry, such as a uniform linear array or a uniform rectangular array, and it also requires using a large amount of sensors. Other interesting alternatives were presented by Bresler et al. [23] afterwards. Also, a forward/backward extension of the spatial smoothing technique was presented in [24], which reduces the number of extra sensors needed for decorrelation. A ML estimation procedure for the location of coherent sources was presented in [25], and a quadratically constrained approach was implemented in [26]. Other important works have also been presented since [27–30]. Nonetheless, there is still no method that satisfactorily mitigates the effects of the multipath on the pseudoranges for all possible relative delays, unless it is at the expense of a loss of the array resolution or the computational need to estimate the DOA of each multipath.

Noteworthy characteristic of GNSS is that receivers are continuously provided with accurate information of the satellites' positions and with their own position estimates. Often, this particularity is exploited to calculate some useful parameters at the receiver for data-dependent beamforming. For instance, the DOA of the direct signal. Note that in very adverse multipath scenarios, the inaccuracies of the receiver and satellite positions are at most on the order of a few hundred meters, and hence they are not important in determining the DOA. In fact, many beamforming techniques use this parameter together with the known geometry of the array to determine the spatial signature of the LOSS [20]. The assumption of a known spatial signature relies on the availability of array calibration, since some modelling errors always exist that must be taken into account. This problem can be found in many applications of antenna arrays, and robust calibration methods developed for generic applications are also applicable here.

In a similar manner to the DOA, the theoretical value of the received power of the LOSS can also be calculated at the receiver. In this case, the knowledge of the satellite transmit power and a proper model for the direct-path loss are fundamental, in addition to the distance between the receiver and the satellite that is obtained from the receiver and satellite positions. The errors in the receiver position, even if they are on the order of hundreds of meters, have no significant impact on the calculation of the distance because the satellites are 20000 km or further away. Only the deviations due to model mismatches need to be considered, which can be further reduced by contrasting them with previous estimation records and some specific template functions [31]. Note that the knowledge of the LOSS power occurs on top of the more usual assumption that the noise power at each element of the array can be estimated, and we aim to show that it has a great potential to reduce the multipath effects.

In this paper, we propose a new data-dependent beamformer that exploits the previous GNSS particularities. The proposed technique is based on the well-known Capon beamformer [32], and it uses the post-despreading signals to calculate the weights. In particular, it attempts to attenuate interference, multipath and noise, exploiting the fact that the spatial signature and power of the LOSS are known at the receiver. In the next section, the model of the problem is presented formally. Then, a novel review of the Capon beamformer in the presence of multipaths follows. This new look motivates the proposed Power-Based Capon (PBC) beamformer, which is detailed in Section 4. Afterwards, some simulation results are presented, which demonstrate the behaviour of our methodology. Finally, conclusions about the work are drawn in Section 6.

2. Problem model

Let us consider that an arbitrary N -element antenna array receives the DS-SS signal transmitted by a given GNSS satellite together with $D < N$ multipath reflections. After the despreading process, the n th sample of the data received by the array is modeled as:

$$\mathbf{x}[n] = \mathbf{a}s[n] + \mathbf{B}\mathbf{m}[n] + \mathbf{v}[n] \quad (1)$$

where $s[n] \in \mathbb{C}$ is the LOSS, $\mathbf{a} \in \mathbb{C}^N$ is its corresponding spatial signature, $\mathbf{m}[n] := [m_1[n] \dots m_D[n]]^T$ is a vector containing all multipath contributions $m_k[n] \in \mathbb{C}$ for $k = 1, \dots, D$, the matrix $\mathbf{B} := [\mathbf{b}_1 \dots \mathbf{b}_D]$ contains at each column the spatial signature of each multipath, and $\mathbf{v}[n] \in \mathbb{C}^N$ is the received noise at each element of the array, which is assumed to be spatially white and with identical noise power at each sensor. In the scenario of interest, the multipath reflections can be either correlated or uncorrelated with the direct signal. When one or more reflections have zero relative delay, we refer to it as the coherent multipath case. As all the involved signals are assumed to impinge on the array from different directions, in this work we assume that \mathbf{a} , $\mathbf{b}_1, \dots, \mathbf{b}_D$ are linearly independent vectors. In addition, \mathbf{a} is considered known, whereas $\mathbf{b}_1, \dots, \mathbf{b}_D$ are unknown.

We process $\mathbf{x}[n]$ through a given *beamforming* technique, which uses some complex weights $\mathbf{w} \in \mathbb{C}^N$ to generate the signal $y[n] = \mathbf{w}^H \mathbf{x}[n]$ at the output of the processor. The purpose of this operation is to mitigate the multipath contribution, interference and noise, while keeping $s[n]$ undistorted. Then, the time-delay and carrier-phase of the LOSS can be estimated from $y[n]$, which are usually fed back to the despreading stage as illustrated in Fig. 1. A very interesting approach for the beamforming stage is the Capon beamformer, which calculates \mathbf{w} from the solution to:

$$\min_{\mathbf{w}} \mathbf{w}^H \mathbf{R}_{\mathbf{x}\mathbf{x}} \mathbf{w} \text{ subject to } \mathbf{w}^H \mathbf{a} = 1 \quad (2)$$

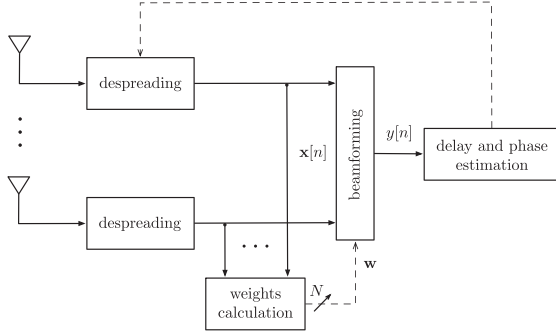


Fig. 1. Proposed GNSS multiple-antenna receiver.

where $\mathbf{R}_{\mathbf{x}\mathbf{x}} = \mathbb{E}\{\mathbf{x}[n]\mathbf{x}[n]^H\}$ is the spatial correlation matrix of $\mathbf{x}[n]$. This problem minimizes the output power $\sigma_y^2 = \mathbb{E}\{|y[n]|^2\}$ using the distortionless constraint $\mathbf{w}^H \mathbf{a} = 1$, aiming to place nulls at the directions of the interference and to keep the signal $s[n]$ undistorted. Unfortunately, it is well-known that (2) does not work properly in the presence of correlated multipaths, since it cancels them together with $s[n]$, and hence it eliminates the contribution of $s[n]$ at the output.

In this work, we seek a solution to this cancellation phenomenon of the Capon beamformer. Concretely, we aim to identify in $\mathbf{R}_{\mathbf{x}\mathbf{x}}$ the portion of the multipaths that contributes to the cancellation, and then counteract it before calculating the Capon weights. As a key aspect of the proposed procedure is to exploit the fact that the power of the LOSS is known at the receiver, we refer to the approach as Power-Based Capon beamforming.

3. Capon beamforming review

We begin with the general expression of the spatial correlation matrix of $\mathbf{x}[n]$:

$$\mathbf{R}_{\mathbf{x}\mathbf{x}} = \sigma_s^2 \mathbf{a}\mathbf{a}^H + \mathbf{a}\mathbf{r}_{\mathbf{m}\mathbf{s}}^H \mathbf{B}^H + \mathbf{B}\mathbf{r}_{\mathbf{m}\mathbf{s}} \mathbf{a}^H + \mathbf{B}\mathbf{R}_{\mathbf{m}}\mathbf{B}^H + \sigma_v^2 \mathbf{I} \quad (3)$$

where σ_s^2 is the power of the signal $s[n]$, σ_v^2 is the power of the noise $\mathbf{v}[n]$, $\mathbf{r}_{\mathbf{m}\mathbf{s}} = \mathbb{E}\{\mathbf{m}[n]s[n]^*\}$ contains the correlation between the LOSS and its multipaths, $\mathbf{R}_{\mathbf{m}} = \mathbb{E}\{\mathbf{m}[n]\mathbf{m}[n]^H\}$ is the correlation matrix of the multipaths, and \mathbf{I} is the identity matrix. From this expression, we can illustrate two different scenarios that explain the cancellation phenomenon of the Capon beamformer. They are based on the value of $\mathbf{r}_{\mathbf{m}\mathbf{s}}$, taking into account that the power at the output of the beamformer $\sigma_y^2 = \mathbf{w}^H \mathbf{R}_{\mathbf{x}\mathbf{x}} \mathbf{w}$ is minimized and the distortionless constraint $\mathbf{w}^H \mathbf{a} = 1$ is verified.

When the direct signal is uncorrelated with its multipaths, $\mathbf{r}_{\mathbf{m}\mathbf{s}} = \mathbf{0}$, and the spatial correlation matrix becomes $\mathbf{R}_{\mathbf{x}\mathbf{x}} = \sigma_s^2 \mathbf{a}\mathbf{a}^H + \mathbf{B}\mathbf{R}_{\mathbf{m}}\mathbf{B}^H + \sigma_v^2 \mathbf{I}$. As a result, the power at the output of the beamformer can be written as:

$$\sigma_y^2 = \sigma_s^2 + \mathbf{w}^H \mathbf{B}\mathbf{R}_{\mathbf{m}}\mathbf{B}^H \mathbf{w} + \sigma_v^2 \|\mathbf{w}\|^2 \quad (4)$$

Eq. (4) shows that the power at the output of the beamformer is the contribution of the power of the LOSS, the multipaths and the noise separately. Note that $\sigma_s^2 > 0$, $\mathbf{w}^H \mathbf{B}\mathbf{R}_{\mathbf{m}}\mathbf{B}^H \mathbf{w} \geq 0$ and $\sigma_v^2 \|\mathbf{w}\|^2 > 0$, so the weights \mathbf{w} cannot mix the direct signal with the multipaths and noise at the output to reduce the power σ_y^2 , but instead they can only reduce the multipaths and noise individually.

In contrast, when the direct signal and its multipaths are correlated, $\mathbf{r}_{\mathbf{m}\mathbf{s}} \neq \mathbf{0}$. Then, the power at the output is given by:

$$\sigma_y^2 = \sigma_s^2 + \mathbf{w}^H \mathbf{a}\mathbf{r}_{\mathbf{m}\mathbf{s}}^H \mathbf{B}^H \mathbf{w} + \mathbf{w}^H \mathbf{B}\mathbf{r}_{\mathbf{m}\mathbf{s}} \mathbf{a}^H \mathbf{w} + \mathbf{w}^H \mathbf{B}\mathbf{R}_{\mathbf{m}}\mathbf{B}^H \mathbf{w} + \sigma_v^2 \|\mathbf{w}\|^2 \quad (5)$$

Eq. (5) shows that the power at the output it is not just formed by the contribution of the LOSS, multipaths and noise separately, but

it also contains the term $\mathbf{w}^H \mathbf{a}\mathbf{r}_{\mathbf{m}\mathbf{s}}^H \mathbf{B}^H \mathbf{w} + \mathbf{w}^H \mathbf{B}\mathbf{r}_{\mathbf{m}\mathbf{s}} \mathbf{a}^H \mathbf{w}$, which is due to the correlation between the direct signal and multipaths. This term is real and can be negative, so the weights \mathbf{w} can mix it with the contribution of the direct signal and multipaths at the output in order to reduce the power σ_y^2 . This is the well-known cancellation phenomenon of the Capon beamformer, and as we have seen it is due to the existence of a non-zero $\mathbf{r}_{\mathbf{m}\mathbf{s}}$.

4. Power-based Capon beamforming

As we have seen in the previous section, the value of $\mathbf{r}_{\mathbf{m}\mathbf{s}}$ in (3) determines the behaviour of the Capon beamformer in the presence of multipaths, and the cancellation phenomenon only appears when $\mathbf{r}_{\mathbf{m}\mathbf{s}} \neq \mathbf{0}$. Therefore, a reasonable approach to avoid the cancellation is to eliminate the contribution of $\mathbf{r}_{\mathbf{m}\mathbf{s}}$ from the correlation matrix $\mathbf{R}_{\mathbf{x}\mathbf{x}}$. In order to eliminate this contribution, the Power-Based Capon beamformer calculates the terms $\mathbf{a}\mathbf{r}_{\mathbf{m}\mathbf{s}}^H \mathbf{B}^H$ and $\mathbf{B}\mathbf{r}_{\mathbf{m}\mathbf{s}} \mathbf{a}^H$, and subtracts them from $\mathbf{R}_{\mathbf{x}\mathbf{x}}$. Since \mathbf{a} is known and \mathbf{B} is unknown, we estimate the cross-correlation parameter $\alpha_0 := \mathbf{B}\mathbf{r}_{\mathbf{m}\mathbf{s}}$, and then calculate the terms $\alpha\alpha_0^H$ and $\alpha_0\alpha^H$.

4.1. Cross-correlation estimation

In order to estimate α_0 , we first generate a modified correlation matrix $\mathbf{C}_{\mathbf{x}\mathbf{x}}$ defined as:

$$\mathbf{C}_{\mathbf{x}\mathbf{x}} := \mathbf{R}_{\mathbf{x}\mathbf{x}} - \sigma_s^2 \mathbf{a}\mathbf{a}^H - \sigma_v^2 \mathbf{I} \quad (6)$$

where both the power of the direct signal σ_s^2 and the power of the noise σ_v^2 need to be used. This allows us to work with a matrix with the following structure:

$$\mathbf{C}_{\mathbf{x}\mathbf{x}} = \begin{bmatrix} \mathbf{a} & \mathbf{B} \end{bmatrix} \begin{bmatrix} 0 & \mathbf{r}_{\mathbf{m}\mathbf{s}}^H \\ \mathbf{r}_{\mathbf{m}\mathbf{s}} & \mathbf{R}_{\mathbf{m}} \end{bmatrix} \begin{bmatrix} \mathbf{a}^H \\ \mathbf{B}^H \end{bmatrix}$$

where the term $\mathbf{r}_{\mathbf{m}\mathbf{s}}$ appears somewhat isolated. Then, if we subtract the term $\alpha\alpha_0^H + \alpha_0\alpha^H$ from $\mathbf{C}_{\mathbf{x}\mathbf{x}}$, we obtain:

$$\mathbf{C}_{\mathbf{x}\mathbf{x}} - \alpha\alpha_0^H - \alpha_0\alpha^H = \begin{bmatrix} \mathbf{a} & \mathbf{B} \end{bmatrix} \begin{bmatrix} 0 & \mathbf{0}^H \\ \mathbf{0} & \mathbf{R}_{\mathbf{m}} \end{bmatrix} \begin{bmatrix} \mathbf{a}^H \\ \mathbf{B}^H \end{bmatrix}$$

which indicates that the rank of $\mathbf{C}_{\mathbf{x}\mathbf{x}}$ has been decreased. Based on this observation, it is then natural to think that $\alpha = \alpha_0$ may minimize the rank of $\mathbf{C}_{\mathbf{x}\mathbf{x}} - \alpha\alpha^H - \alpha\alpha^H$. In order to understand when this minimization occurs, the following lemma has been developed. Note that $\mathcal{R}\{q\}$ indicates the real part of q .

Lemma 1. *The rank of the matrix $\mathbf{C}_{\mathbf{x}\mathbf{x}} - \alpha\alpha^H - \alpha\alpha^H$ attains its minimum if and only if $\alpha = \alpha_0 - q\mathbf{a} - \mathbf{B}\mathbf{R}_{\mathbf{m}}\mathbf{p}$ with $q \in \mathbb{C}$, $\mathbf{p} \in \mathbb{C}^D$ such that $\mathbf{p}^H \mathbf{R}_{\mathbf{m}} \mathbf{p} = 2\mathcal{R}\{q\}$.*

Proof. First assume that $\alpha_0 - \alpha \in \text{span}\{\mathbf{a}, \mathbf{B}\}$. Then $\exists q \in \mathbb{C}, \mathbf{z} \in \mathbb{C}^D$ such that $\alpha_0 - \alpha = q\mathbf{a} + \mathbf{B}\mathbf{z}$. Then $\mathbf{C}_{\mathbf{x}\mathbf{x}} - \alpha\alpha^H - \alpha\alpha^H$ can be written as:

$$\mathbf{C}_{\mathbf{x}\mathbf{x}} - \alpha\alpha^H - \alpha\alpha^H = \begin{bmatrix} \mathbf{a} & \mathbf{B} \end{bmatrix} \begin{bmatrix} 2\mathcal{R}\{q\} & \mathbf{z}^H \\ \mathbf{z} & \mathbf{R}_{\mathbf{m}} \end{bmatrix} \begin{bmatrix} \mathbf{a}^H \\ \mathbf{B}^H \end{bmatrix}$$

As \mathbf{a} and $\mathbf{b}_1, \dots, \mathbf{b}_D$ are linearly independent, the rank of $\mathbf{C}_{\mathbf{x}\mathbf{x}} - \alpha\alpha^H - \alpha\alpha^H$ is the same as the rank of $\begin{bmatrix} 2\mathcal{R}\{q\} & \mathbf{z}^H \\ \mathbf{z} & \mathbf{R}_{\mathbf{m}} \end{bmatrix}$, see [33], which is equal to $\text{rank}(\mathbf{R}_{\mathbf{m}})$ if and only if $\exists \mathbf{p} \in \mathbb{C}^D$ such that $\mathbf{z} = \mathbf{R}_{\mathbf{m}}\mathbf{p}$ and $2\mathcal{R}\{q\} = \mathbf{z}^H \mathbf{p}$. In the case that there does not exist such \mathbf{p} , the rank is equal to $\text{rank}(\mathbf{R}_{\mathbf{m}}) + 1$.

Now assume that $\alpha_0 - \alpha \notin \text{span}\{\mathbf{a}, \mathbf{B}\}$. In this case we cannot write $\alpha_0 - \alpha$ as a linear combination of \mathbf{a}, \mathbf{B} . Instead, we must say that $\alpha_0 - \alpha$ is linearly independent of \mathbf{a}, \mathbf{B} . Then $\mathbf{C}_{\mathbf{x}\mathbf{x}} - \alpha\alpha^H - \alpha\alpha^H$

can be written as:

$$\mathbf{C}_{\mathbf{x}\mathbf{x}} - \boldsymbol{\alpha}\boldsymbol{\alpha}^H - \boldsymbol{\alpha}\mathbf{a}^H = \begin{bmatrix} \boldsymbol{\alpha}_0 - \boldsymbol{\alpha} & \mathbf{a} & \mathbf{B} \\ \mathbf{0} & \mathbf{0} & \mathbf{0} \\ \vdots & \vdots & \mathbf{R}_m \\ \mathbf{0} & \mathbf{0} & \mathbf{0} \end{bmatrix} \begin{bmatrix} \mathbf{0} & 1 & 0 & \cdots & 0 \\ 1 & 0 & 0 & \cdots & 0 \\ 0 & 0 & & & \\ \vdots & \vdots & & & \\ 0 & 0 & & & \mathbf{R}_m \end{bmatrix}$$

$$\begin{bmatrix} \boldsymbol{\alpha}_0^H - \boldsymbol{\alpha}^H \\ \mathbf{a}^H \\ \mathbf{B}^H \end{bmatrix}$$

As $\boldsymbol{\alpha}_0 - \boldsymbol{\alpha}$, \mathbf{a} and $\mathbf{b}_1, \dots, \mathbf{b}_D$ are linearly independent, the rank of the previous matrix is the same as the rank of

$$\begin{bmatrix} 0 & 1 & 0 & \cdots & 0 \\ 1 & 0 & 0 & \cdots & 0 \\ 0 & 0 & & & \\ \vdots & \vdots & & & \\ 0 & 0 & & & \mathbf{R}_m \end{bmatrix}, \text{ which is equal to } \text{rank}(\mathbf{R}_m) + 2.$$

As a result, we see that the minimum achievable rank is $\text{rank}(\mathbf{R}_m)$, and that this is attained if and only if $\boldsymbol{\alpha}_0 - \boldsymbol{\alpha} = \mathbf{q}\mathbf{a} + \mathbf{B}\mathbf{z}$ with $\mathbf{z} = \mathbf{R}_m\mathbf{p}$ and $2\mathcal{R}\{q\} = \mathbf{z}^H\mathbf{p}$, or equivalently, when $\boldsymbol{\alpha}_0 - \boldsymbol{\alpha} = \mathbf{q}\mathbf{a} + \mathbf{B}\mathbf{R}_m\mathbf{p}$ with $\mathbf{p}^H\mathbf{R}_m\mathbf{p} = 2\mathcal{R}\{q\}$. \square

Lemma 1 shows us that, effectively, $\boldsymbol{\alpha} = \boldsymbol{\alpha}_0$ minimizes the rank of $\mathbf{C}_{\mathbf{x}\mathbf{x}} - \boldsymbol{\alpha}\boldsymbol{\alpha}^H - \boldsymbol{\alpha}\mathbf{a}^H$. In addition, it also tells us that an infinite set of possible $\boldsymbol{\alpha}$ exist that minimize the rank, and it gives us a characterisation of them. As a result, we can try to find the solution $\boldsymbol{\alpha}_0$ by minimizing the rank of $\mathbf{C}_{\mathbf{x}\mathbf{x}} - \boldsymbol{\alpha}\boldsymbol{\alpha}^H - \boldsymbol{\alpha}\mathbf{a}^H$, but some additional information should be used. Along these lines, next we construct a parametrisation for $\boldsymbol{\alpha}$ that is based on the fact that the received signals are DS-SS, and the corresponding waveforms are known by the receiver. In particular, we exploit the fact that a replica of the post-despreading signal $s[n]$ can be created by the receiver, with only some unknown delay τ_e and phase φ_e synchronization errors.

We can assume then that a reference signal $c[n] = 1/\sqrt{\sigma_s^2}s[n + \tau_e]e^{-j\varphi_e}$ is available at the receiver. If we correlate it with the received data $\mathbf{x}[n]$ of (1), then we can obtain the following correlation vector:

$$\mathbf{r}_{\mathbf{x}\mathbf{c}} := \mathbb{E}\{\mathbf{x}[n]c^*[n]\} = \frac{e^{j\varphi_e}}{\sqrt{\sigma_s^2}}r_s(\tau_e)\mathbf{a} + \frac{e^{j\varphi_e}}{\sqrt{\sigma_s^2}}\mathbf{B}\mathbf{r}_{\mathbf{m}\mathbf{s}}(\tau_e)$$

where $r_s(\tau_e) = \mathbb{E}\{s[n]s^*[n + \tau_e]\}$ and $\mathbf{r}_{\mathbf{m}\mathbf{s}}(\tau_e) = \mathbb{E}\{\mathbf{m}[n]s^*[n + \tau_e]\}$. Then, by tuning the delay and phase of the reference by an amount τ and φ , we can generate the following correlation vectors:

$$\mathbf{r}_{\mathbf{x}\mathbf{c}}(\tau, \varphi) = \frac{e^{j(\varphi_e - \varphi)}}{\sqrt{\sigma_s^2}}r_s(\tau_e - \tau)\mathbf{a} + \frac{e^{j(\varphi_e - \varphi)}}{\sqrt{\sigma_s^2}}\mathbf{B}\mathbf{r}_{\mathbf{m}\mathbf{s}}(\tau_e - \tau) \quad (7)$$

which, when synchronized with $\tau = \tau_e$ and $\varphi = \varphi_e$ yield:

$$\mathbf{r}_{\mathbf{x}\mathbf{c}}(\tau_e, \varphi_e) = \sqrt{\sigma_s^2}\mathbf{a} + \frac{1}{\sqrt{\sigma_s^2}}\boldsymbol{\alpha}_0$$

Thus, when the received and reference signal are synchronized in this way, we can solve for $\boldsymbol{\alpha}_0$:

$$\boldsymbol{\alpha}_0 = (\mathbf{r}_{\mathbf{x}\mathbf{c}}(\tau_e, \varphi_e) - \sqrt{\sigma_s^2}\mathbf{a})\sqrt{\sigma_s^2}$$

Although we obviously do not know the values of delay and phase that achieve synchronization, we can change the delay τ and phase φ deliberately and compute:

$$\boldsymbol{\alpha}(\tau, \varphi) := (\mathbf{r}_{\mathbf{x}\mathbf{c}}(\tau, \varphi) - \sqrt{\sigma_s^2}\mathbf{a})\sqrt{\sigma_s^2} \quad (8)$$

which gives us a parametrisation for $\boldsymbol{\alpha}$ that verifies $\boldsymbol{\alpha}(\tau_e, \varphi_e) = \boldsymbol{\alpha}_0$.

Now, we solve the following 2-dimensional minimization problem in order to estimate $\boldsymbol{\alpha}_0$:

$$\min_{\tau, \varphi} \text{rank}(\mathbf{C}_{\mathbf{x}\mathbf{x}} - \boldsymbol{\alpha}(\tau, \varphi)\boldsymbol{\alpha}(\tau, \varphi)^H - \boldsymbol{\alpha}(\tau, \varphi)\mathbf{a}^H) \quad (9)$$

The following theorem tells us which are the solutions to (9).

Theorem 1. *In the non-coherent multipath case, the minimum of (9) is attained at the unique point $(\tau, \varphi) = (\tau_e, \varphi_e)$. In the coherent multipath case, the minimum is attained at multiple points, and the ones with the smallest τ correspond to the pairs (τ, φ) with $\tau = \tau_e$ regardless of the value of φ .*

Proof. First assume that $\text{rank}(\mathbf{C}_{\mathbf{x}\mathbf{x}} - \boldsymbol{\alpha}(\tau, \varphi)\boldsymbol{\alpha}(\tau, \varphi)^H - \boldsymbol{\alpha}(\tau, \varphi)\mathbf{a}^H)$ is minimum. Using **Lemma 1**, we have that $\boldsymbol{\alpha}(\tau, \varphi)$ satisfies:

$$\begin{aligned} \boldsymbol{\alpha}(\tau, \varphi) &= \boldsymbol{\alpha}_0 - \mathbf{q}\mathbf{a} - \mathbf{B}\mathbf{R}_m\mathbf{p} \\ &= \mathbf{B}\mathbf{r}_{\mathbf{m}\mathbf{s}} - \mathbf{q}\mathbf{a} - \mathbf{B}\mathbf{R}_m\mathbf{p} \\ &= -\mathbf{q}\mathbf{a} - \mathbf{B}(\mathbf{R}_m\mathbf{p} - \mathbf{r}_{\mathbf{m}\mathbf{s}}) \end{aligned} \quad (10)$$

Substituting (7) in (8), we also have:

$$\begin{aligned} \boldsymbol{\alpha}(\tau, \varphi) &= \left[r_s(\tau_e - \tau)\mathbf{a} + \frac{e^{j(\varphi_e - \varphi)}}{\sqrt{\sigma_s^2}}\mathbf{B}\mathbf{r}_{\mathbf{m}\mathbf{s}}(\tau_e - \tau) - \sqrt{\sigma_s^2}\mathbf{a} \right] \sqrt{\sigma_s^2} \\ &= (r_s(\tau_e - \tau)e^{j(\varphi_e - \varphi)} - \sigma_s^2)\mathbf{a} + \mathbf{B}\mathbf{r}_{\mathbf{m}\mathbf{s}}(\tau_e - \tau)e^{j(\varphi_e - \varphi)} \end{aligned} \quad (11)$$

Then, comparing (10) and (11), and using that \mathbf{a} and $\mathbf{b}_1, \dots, \mathbf{b}_D$ are linearly independent, results in:

$$\begin{aligned} -\mathbf{q}\mathbf{a} &= (r_s(\tau_e - \tau)e^{j(\varphi_e - \varphi)} - \sigma_s^2)\mathbf{a} \\ -\mathbf{B}(\mathbf{R}_m\mathbf{p} - \mathbf{r}_{\mathbf{m}\mathbf{s}}) &= \mathbf{B}\mathbf{r}_{\mathbf{m}\mathbf{s}}(\tau_e - \tau)e^{j(\varphi_e - \varphi)} \end{aligned}$$

which, solving for q , leads to:

$$q = \sigma_s^2 - r_s(\tau_e - \tau)e^{j(\varphi_e - \varphi)} \quad (12)$$

and solving for \mathbf{p} leads to:

$$\mathbf{R}_m\mathbf{p} = \mathbf{r}_{\mathbf{m}\mathbf{s}} - \mathbf{r}_{\mathbf{m}\mathbf{s}}(\tau_e - \tau)e^{j(\varphi_e - \varphi)} \quad (13)$$

With this information at hand, now we can exploit the fact that $\mathbf{p}^H\mathbf{R}_m\mathbf{p} = 2\mathcal{R}\{q\}$, as stated by **Lemma 1**, and we obtain:

$$\begin{aligned} 2\sigma_s^2 - 2r_s(\tau_e - \tau)\cos(\varphi_e - \varphi) \\ = (\mathbf{r}_{\mathbf{m}\mathbf{s}}^H - \mathbf{r}_{\mathbf{m}\mathbf{s}}^H(\tau_e - \tau)e^{-j(\varphi_e - \varphi)})\mathbf{R}_m^+(\mathbf{r}_{\mathbf{m}\mathbf{s}} - \mathbf{r}_{\mathbf{m}\mathbf{s}}(\tau_e - \tau)e^{j(\varphi_e - \varphi)}) \end{aligned} \quad (14)$$

While we expect \mathbf{R}_m to be generically invertible for the GNSS application, in other applications it may not be full rank, and so to be more general we use the pseudoinverse \mathbf{R}_m^+ here.

Eq. (14) shows us a necessary and sufficient condition for the minimization of $\text{rank}(\mathbf{C}_{\mathbf{x}\mathbf{x}} - \boldsymbol{\alpha}(\tau, \varphi)\boldsymbol{\alpha}(\tau, \varphi)^H - \boldsymbol{\alpha}(\tau, \varphi)\mathbf{a}^H)$. In practice, this condition must be rewritten using the sample averages $\mathbf{R}_m = (1/N)\mathbf{M}^H\mathbf{M}$, $\mathbf{r}_{\mathbf{m}\mathbf{s}}(\tau) = (1/N)\mathbf{M}^H\mathbf{s}(\tau)$ and $r_s(\tau) = (1/N)\mathbf{s}^H(\tau)\mathbf{s}(\tau)$ from a set of N consecutive samples, where $\mathbf{M} = [\mathbf{m}[1] \dots \mathbf{m}[N]]^H$ and $\mathbf{s}(\tau) = [s[1 + \tau] \dots s[N + \tau]]^H$. With this notation, the condition (14) can be transformed to:

$$\|\mathbf{s} - \mathbf{s}(\tau_e - \tau)e^{j(\varphi_e - \varphi)}\|^2 = \|\mathbf{P}_M(\mathbf{s} - \mathbf{s}(\tau_e - \tau)e^{j(\varphi_e - \varphi)})\|^2 \quad (15)$$

where $\mathbf{P}_M = \mathbf{M}(\mathbf{M}^H\mathbf{M})^+\mathbf{M}^H$ is the projection matrix onto the subspace defined by the columns of \mathbf{M} . The two possible solutions of (15) are $\mathbf{s} - \mathbf{s}(\tau_e - \tau)e^{j(\varphi_e - \varphi)} = \mathbf{0}$ and $\mathbf{s} - \mathbf{s}(\tau_e - \tau)e^{j(\varphi_e - \varphi)} \in \text{span}\{\mathbf{M}\}$. Note that the first solution is valid for any possible type of multipath, since it does not depend on the matrix \mathbf{M} , and it is equivalent to $\mathbf{s} = \mathbf{s}(\tau_e - \tau)e^{j(\varphi_e - \varphi)}$, which gives $\tau = \tau_e$ and $\varphi = \varphi_e$. In contrast, the second solution is only valid if $\mathbf{s} \in \text{span}\{\mathbf{M}\}$, or equivalently, if one or more multipaths have zero relative delay. In this case, we have that $\mathbf{s}(\tau_e - \tau)e^{j(\varphi_e - \varphi)} \in \text{span}\{\mathbf{M}\}$, which gives $\tau = \tau_e + \tau_k$ for $k = 1, \dots, D$ regardless of the value of φ , if we denote the relative delay of the k th multipath by τ_k . Among all these solutions, the ones with the smallest τ correspond to the pairs (τ, φ) with $\tau = \tau_e$. \square

From **Theorem 1**, we know that $\boldsymbol{\alpha}_0$ can be obtained from the unique point (τ_e, φ_e) that minimizes (9) in a scenario with non-coherent multipath. On the other hand, when one or more multipaths are coherent with the direct signal, vectors of the type

$\alpha(\tau_e, \varphi) : \varphi \in [-\pi, \pi]$ are obtained from the points that minimize (9) with the smallest τ . Taking into account these two possible situations, in the following section we discuss the final implementation of the Power-Based Capon beamformer.

4.2. Implementation

As we have introduced at the beginning of Section 4, the idea behind the Power-Based Capon beamformer is to estimate the cross-correlation vector α_0 and calculate $\mathbf{R}_{\mathbf{x}\mathbf{x}} - \alpha_0 \alpha_0^H - \alpha_0 \mathbf{a}^H$. Then, the resulting matrix is treated as the correlation matrix used to calculate the Capon weights. Given that the solution to (2) is:

$$\mathbf{w}_{\text{cap}} = \frac{\mathbf{R}_{\mathbf{x}\mathbf{x}}^{-1} \mathbf{a}}{\mathbf{a}^H \mathbf{R}_{\mathbf{x}\mathbf{x}}^{-1} \mathbf{a}} \quad (16)$$

the resulting PBC beamformer is:

$$\mathbf{w}_{\text{pbc}} = \frac{(\mathbf{R}_{\mathbf{x}\mathbf{x}} - \alpha_0 \alpha_0^H - \alpha_0 \mathbf{a}^H)^{-1} \mathbf{a}}{\mathbf{a}^H (\mathbf{R}_{\mathbf{x}\mathbf{x}} - \alpha_0 \alpha_0^H - \alpha_0 \mathbf{a}^H)^{-1} \mathbf{a}} \quad (17)$$

In the non-coherent multipath case, we have already seen that α_0 is estimated from the unique solution of (9). However, in the coherent multipath case, any vector $\alpha(\tau_e, \varphi)$ is obtained regardless of the value of φ . In order to understand the effect of using an arbitrary value of φ , observe that the resulting correlation matrix $\mathbf{R}_{\mathbf{x}\mathbf{x}} - \alpha(\tau_e, \varphi) \alpha(\tau_e, \varphi)^H - \alpha(\tau_e, \varphi) \mathbf{a}^H$ can be written as the sum of $\sigma_s^2 \mathbf{a} \mathbf{a}^H$ plus another term corresponding to the correlation matrix of $\mathbf{a} s[n](1 - e^{j(\varphi_e - \varphi)}) + \mathbf{B} \mathbf{m}[n] + \mathbf{v}[n]$. As a result, the PBC beamformer must cancel $s[n](1 - e^{j(\varphi_e - \varphi)})$ with $\mathbf{m}[n]$ in order to minimize the output power, that is:

$$\mathbf{w}_{\text{pbc}}^H \mathbf{a} s[n](1 - e^{j(\varphi_e - \varphi)}) + \mathbf{w}_{\text{pbc}}^H \mathbf{B} \mathbf{m}[n] = 0$$

Then, when we apply \mathbf{w}_{pbc} to the actual scenario of Eq. (1), the resulting signal at the output is:

$$y[n] = \mathbf{w}_{\text{pbc}}^H \mathbf{x}[n] = s[n] e^{j(\varphi_e - \varphi)} + \mathbf{w}_{\text{pbc}}^H \mathbf{v}[n]. \quad (18)$$

That is, $s[n]$ is distorted by a factor $e^{j(\varphi_e - \varphi)}$, but the multipaths are eliminated. This behaviour is clearly better than the behaviour of the traditional Capon. Furthermore, if we set $\varphi = 0$, then we guarantee that the resulting distortion is always equal to $e^{j\varphi_e}$, which corresponds to the standard carrier-phase synchronisation error of the GNSS receiver. In this way, we do not perform any additional correction in the estimated carrier-phase, but we assure that the proposed methodology does not worsen the performance of the system. Algorithm 1 summarizes the whole process.

Finally note that, in order to implement the proposed methodology, a cost function that properly approximates the rank needs to be chosen to avoid errors caused by the use of numerical rank. A typical choice found in the literature is the nuclear norm [34], because it is a convex approximation to the rank and it leads to

Algorithm 1 PBC Beamforming.

Given the received signal $\mathbf{x}[n]$ and local reference $c[n]$

- 1) Calculate $\mathbf{R}_{\mathbf{x}\mathbf{x}}$ and $\mathbf{r}_{\mathbf{x}c}(\tau, \varphi)$
- 2) Obtain $\mathbf{C}_{\mathbf{x}\mathbf{x}}$ and $\alpha(\tau, \varphi)$
- 3) Solve $\arg \min_{\tau, \varphi} \text{rank}(\mathbf{C}_{\mathbf{x}\mathbf{x}} - \alpha \alpha^H - \alpha \mathbf{a}^H)$

if solution is not unique **then**

take the one with smallest τ and $\varphi = 0$

end if

- 4) Obtain corresponding $\alpha(\tau, \varphi)$
 - 5) Compute \mathbf{w}_{pbc} using $\alpha_0 = \alpha(\tau, \varphi)$
-

the optimal solution under some optimality conditions. However, simulations show that in this work it is necessary to use a more precise heuristic to approximate the rank. Since there are only two independent variables τ and φ in (9), which take values in very small intervals of \mathbb{R} , in practice it makes sense to perform a two-dimensional grid search. This opens the doors to use non-convex approximations such as the so-called Schatten p -norm. This norm can be understood as a generalisation of the nuclear norm, and it is defined as:

$$\|\mathbf{Q}\|_p = \left(\sum_k \sigma_k^p(\mathbf{Q}) \right)^{\frac{1}{p}} \quad \text{with } 1 \leq p < \infty \quad (19)$$

where $\mathbf{Q} \in \mathbb{C}^{N \times N}$, and $\sigma_k(\mathbf{Q})$ is the k th eigenvalue of \mathbf{Q} . Note that the Schatten p -norm corresponds to the nuclear norm for $p = 1$.

The definition (19) also includes the Frobenius norm $\|\mathbf{Q}\|_2$ and the spectral norm $\|\mathbf{Q}\|_\infty$, and with special interest here, it can be extended to $p \in (0, 1)$. If it is extended, then the Schatten p -norm becomes a quasinorm, but we can exploit the fact that $\|\mathbf{Q}\|_p$ to the power of p tends to $\text{rank}(\mathbf{Q})$ when $p \rightarrow 0$. Indeed, raising $\|\mathbf{Q}\|_p$ to the power of p does not change the points where the minimum is attained. Then, the lower the value of p , the closer to the minimum rank solution. In practice, however, very low values of p are not recommended, since they can increase significantly the contribution of those singular values that are not exactly zero but correspond to the null space of \mathbf{Q} . As a result, an intermediate value must be chosen instead. In the results presented in the following section, we have used $p = 0.2$.

5. Simulation results

In this section, we present some numerical examples related to the implementation of the proposed PBC beamformer. In order to show the effectiveness of the methodology, we have first calculated the response of the beamformer to multipath and noise, and we plot the results together with those of other representative methodologies. In addition, we have also calculated the time-delay and carrier-phase of the direct signal that are obtained after applying these beamforming techniques, and the output error is represented. For this purpose, we have used a Delay-Locked Loop (DLL) and a Phase-Locked Loop (PLL), but note that any other specific technique can be used after beamforming, including one that exploits the temporal diversity of the multipath as in [6–8].

Throughout all the simulations, we assume that a linear antenna array receives a Global Positioning System (GPS) signal and several multipath reflections, and that $C/N_0 = 45$ dBHz. The corresponding post-despreading versions of the signals have been calculated from a triangle function of duration $t_c = 1/1023$ ms, with a given delay, amplitude and phase specified in each figure. This triangle function has also been used to generate the filtered additive white Gaussian noise. Then, we assume that $N_p = 31$ samples are taken at each correlation peak, within an interval approximately $\pm t_c$, and centered at the time-delay obtained from the DLL. The integration time of the GPS receiver was set to $T_{\text{int}} = 20$ ms, and the observation time to $T = 200$ ms. The result of this configuration is $\mathbf{x}[n]$ in (1), from which the beamformer is calculated.

To begin, we evaluate the response of the proposed PBC beamformer to three received multipaths when an 8-element antenna array is used. Fig. 2 plots the expected value of the total multipath power at the output of the beamformer. This power is normalized with respect to the power of the LOSS with the aim of

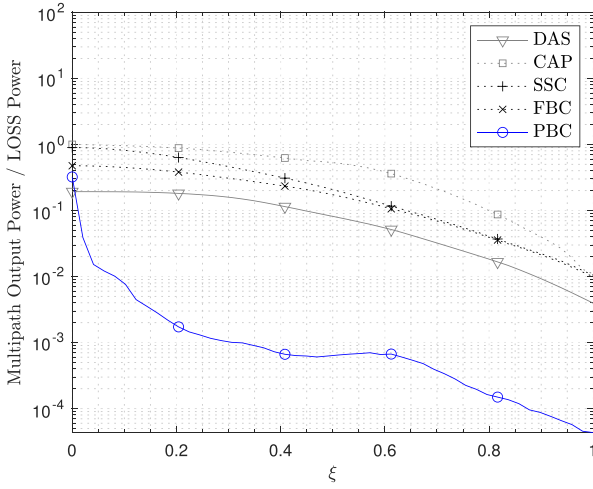


Fig. 2. Multipath response of different beamformers, versus delay factor ξ . The relative powers, delays and phases of the multipaths are given by $\kappa_{\mathbf{m}} = [0.9 \ 0.5 \ 0.25]$, $\tau_{\mathbf{m}} = [1.5 \ 2 \ 2.5]t_c$ and $\phi_{\mathbf{m}} = [-\pi/4 \ \pi/2 \ 0]$ rad respectively. The DOA's of the multipaths and direct signal are -20° , 80° , 0° and 30° respectively.

emphasizing the LOSS cancellation with the multipaths. In order to get the performance for a broad range of correlations, the delays of the multipaths are defined by the product of a delay factor $\xi \in [0, 1]$ and a vector $\tau_{\mathbf{m}} = [1.5 \ 2 \ 2.5]t_c$ containing each maximum multipath delay, and the results are represented as a function of ξ . When ξ is zero, all the multipaths are received coherently, and when $\xi = 1$, they are received with delays given by $\tau_{\mathbf{m}}$. The results corresponding to the Capon (CAP) beamformer are also represented, together with those obtained by additional pre-processing: spatial smoothing (SSC) and forward/backward (FBC). Finally, the Delay-And-Sum (DAS) beamformer is also evaluated, which uses the deterministic weights $\mathbf{w}_{\text{das}} = (1/N)\mathbf{a}$ in all possible scenarios.

As we can see in Fig. 2, the PBC beamformer clearly outperforms the presented methods for all values of ξ . When $\xi = 0$, the exact value of φ_e cannot be estimated from the two-dimensional search given by (9), and $\varphi = 0$ is chosen. Thus, the response to the multipaths is given by the squared absolute value of $1 - e^{j(\varphi_e - 0)}$. In contrast, the response of the CAP beamformer equals one when the delay factor is zero, since the cancellation phenomenon takes place. The DAS beamformer performs then better than CAP at this point. On the other hand, when the delay factor increases, the PBC beamformer immediately mitigates the multipaths, achieving multipath-to-LOSS ratios as low as 10^{-2} for $\xi > 0.1$. The response of the CAP beamformer is also improved, but not as much as PBC unless the multipaths are completely uncorrelated. For its part, SSC and FBC approaches offer enhanced performance compared to CAP, but they are still far from PBC because they only achieve a small decrease in correlation. Finally, note that the response of the DAS beamformer does not change significantly as a function of ξ , since it is a deterministic beamformer.

In order to provide some insights into the robustness of the proposed technique against possible mismatches between the received power of the LOSS and the corresponding estimated value, the response of the PBC has also been calculated with respect to errors in this estimation. Concretely, Fig. 3 considers the previous scenario and shows the output multipath power as a function of $e_s = (\hat{\sigma}_s^2 - \sigma_s^2)/\sigma_s^2$, where $\hat{\sigma}_s^2$ is used to denote the es-

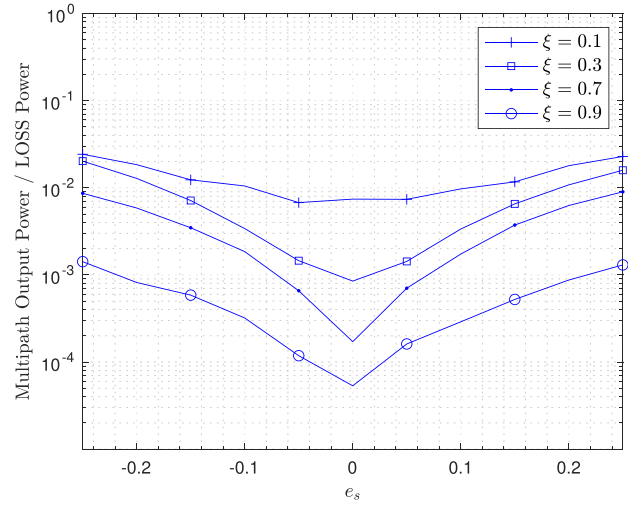


Fig. 3. Multipath response of PBC versus LOSS power estimation error e_s . Each line corresponds to a different value of ξ . The relative powers, delays and phases of the multipaths are given by $\kappa_{\mathbf{m}} = [0.9 \ 0.5 \ 0.25]$, $\tau_{\mathbf{m}} = [1.5 \ 2 \ 2.5]t_c$ and $\phi_{\mathbf{m}} = [-\pi/4 \ \pi/2 \ 0]$ rad respectively. The DOA's of the multipaths and direct signal are -20° , 80° , 0° and 30° respectively.

timated value of σ_s^2 . Different lines correspond to different values of ξ , so that several correlations can be considered. As it could be expected, the greater the mismatch, the more multipath power is present at the output. However, as Fig. 3 shows, the obtained multipath-to-LOSS ratios are about $2 \cdot 10^{-2}$ when the estimation errors are as high as 25% of σ_s^2 , and they do not exceed 10^{-2} unless the errors on the estimation are greater than 10%. Then, while precision in power estimation may play an important role in mitigating the multipath effects, the results provided here show that errors as high as 10% may be tolerated with little consequences.

Fig. 4 shows the expected value of the noise power at the output of the beamformer, also normalized with respect to the power of the LOSS. In this case, we notice that the PBC beamformer has a good response for all values of ξ . For its part, the CAP beamformer offers a remarkably higher response than the rest. The reason is that minimization of the output power implies merging the noise with the multipaths, due to the fact that they show some degree of correlation for short sample records. Additional simulations show that this effect can be limited by increasing the time window T , since the noise becomes less correlated. For instance, responses that do not exceed 10^{-2} can be obtained for $T > 1$ s. This effect is somewhat modified by the SSC and FBC approaches. Finally, the DAS curve shows a lower bound among all beamformers, which is consistent with the fact that it is the beamformer with maximum array gain.

In Fig. 5, we show the expected value of the time-delay estimation error at the DLL when a 5-element antenna array is used. We consider that an early-late tracking loop is configured with an early-minus-late power discriminator [35] and a correlator spacing equal to $t_c/4$. Two multipath reflections with $\tau_{\mathbf{m}} = [1.5 \ 2.5]t_c$ are received together with the LOSS, and a dashed line is additionally plotted that corresponds to PBC when the reference and received signals are synchronized with $\tau = \tau_e$ and $\varphi = \varphi_e$. As we can see, the most remarkable aspect of the plots is that the PBC curve does not show any significant variation with ξ . In particular, it shows time-delay errors below 3m for any delay factor. Thus, the case $\xi = 0$ is not critical for the DLL if it is used together with the PBC beamformer. In contrast,

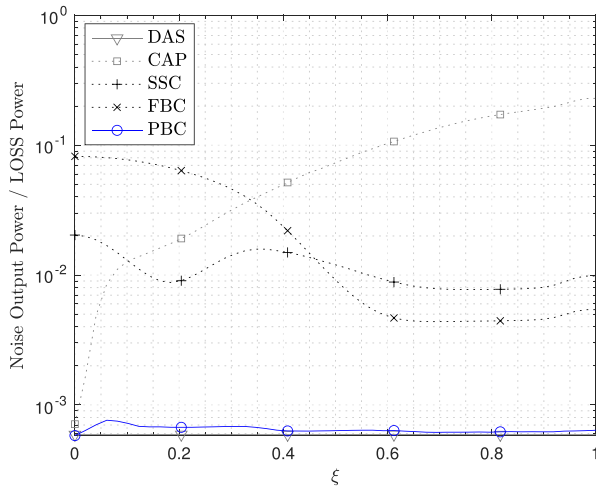


Fig. 4. Noise response of different beamformers, versus delay factor ξ . The relative powers, delays and phases of the multipaths are given by $\kappa_m = [0.9 \ 0.5 \ 0.25]$, $\tau_m = [1.5 \ 2 \ 2.5]t_c$ and $\phi_m = [-\pi/4 \ \pi/2 \ 0]$ rad respectively. The DOA's of the multipaths and direct signal are -20° , 80° , 0° and 30° respectively.

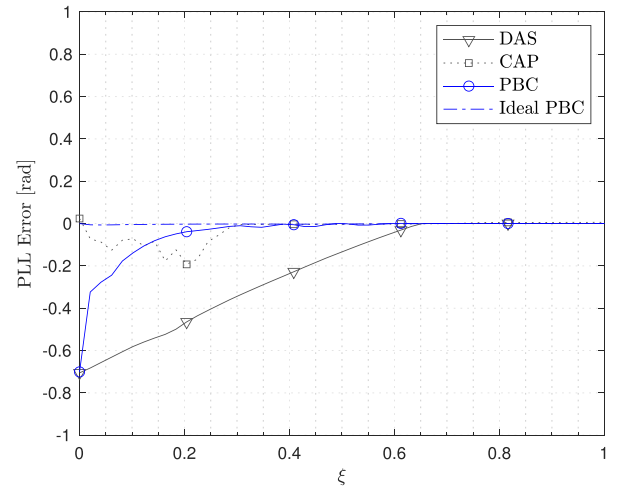


Fig. 6. Output error of a PLL when it is used together with different beamformers, versus delay factor ξ . The relative powers, delays and phases of the multipaths are given by $\kappa_m = [0.9 \ 0.5]$, $\tau_m = [1.5 \ 2.5]t_c$ and $\phi_m = [-\pi/4 \ \pi/2]$ rad respectively. The DOA's of the multipaths and direct signal are -20° , 80° and 30° respectively.

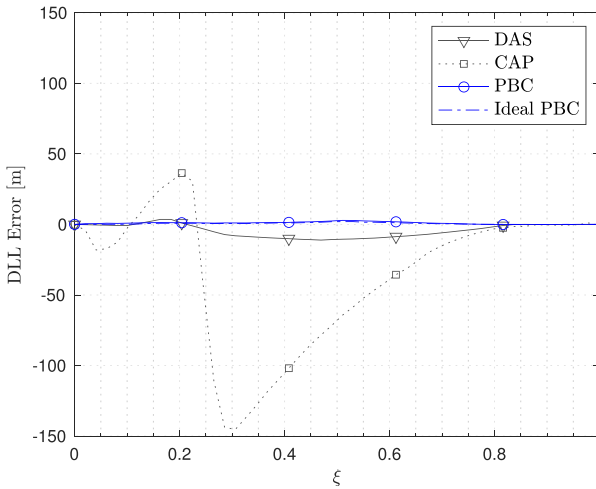


Fig. 5. Output error of a DLL when it is used together with different beamformers, versus delay factor ξ . The relative powers, delays and phases of the multipaths are given by $\kappa_m = [0.9 \ 0.5]$, $\tau_m = [1.5 \ 2.5]t_c$ and $\phi_m = [-\pi/4 \ \pi/2]$ rad respectively. The DOA's of the multipaths and direct signal are -20° , 80° and 30° respectively.

the DAS and CAP techniques show large variations with ξ , and they generate errors as high as 145 m. For its part, the shape of the DAS curve is a subtle variation of the curve that would be obtained without beamforming, which happens because this beamformer has a spatial attenuation that does not depend on ξ .

Fig. 6 shows the expected value of the carrier-phase estimation error at the PLL considering that it is calculated from the prompt correlation output and using the previous configuration. In this case, note that the results can be misleading in that the CAP beamformer performs reasonably well, because this technique generates

very random phase values for small and medium ξ , and hence they cannot be treated as reliable. This occurs because the multipaths cancel the LOSS, and the noise becomes dominant. For its part, the PBC approach does not perform any additional correction in the carrier-phase when $\xi = 0$, and hence it generates exactly the same phase as the DAS approach. The former, however, performs better when the delay factor increases, allowing for very precise phase estimates when $\xi > 0.1$. In contrast, the DAS beamformer leads to significant errors until the multipaths are received with large relative delays, similarly to what would be obtained without beamforming.

Finally, in order to consider the effect of the multipath phase relative to the LOSS, Figs. 7 and 8 show the delay and phase envelopes of the multipath when a 5-element antenna array is used. They have been calculated as the noiseless time-delay and carrier-phase estimation errors at the DLL and PLL respectively, when just one multipath reflection is received together with the LOSS. The beamformers have been evaluated in two different situations that depict the worst possible cases depending on the value of the relative multipath phase. For a fair comparison, the results corresponding to a single-antenna receiver are also represented, and they are labeled as *traditional*. In Fig. 7, the time-delay error is calculated in the two situations where the multipath is received either constructively or destructively with the LOSS. The plots show that the CAP beamformer may reach time-delay errors that are even worse than the traditional ones, while the time-delay errors of PBC are approximately zero for any multipath delay. For its part, the results of the DAS beamformer are better than the traditional ones, but they show a similar behaviour. In Fig. 8, the carrier-phase error is calculated in the two situations where the multipath is received orthogonally to the total received signal. In this case, both the CAP and PBC beamformers generate very low carrier-phase errors except when $\xi = 0$. At this point, the CAP beamformer generates an error equal to φ_e , since the residual of the cancellation phenomenon becomes significant in the absence of noise. For its part, the DAS beamformer is again better than the traditional case, but it has a similar behaviour.

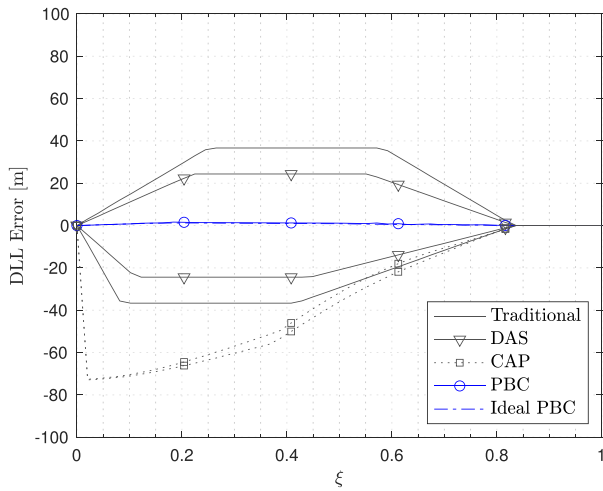


Fig. 7. Multipath delay envelope: worst output error of a DLL when it is used together with different beamformers, versus delay factor ξ . The relative power, delay and phase of the multipath is given by $\kappa_m = 0.25$, $\tau_m = 1.5t_c$ and $\phi_m \in \{0, \pi\}$ rad respectively. The DOA's of the multipath and direct signal are -20° and 30° respectively.

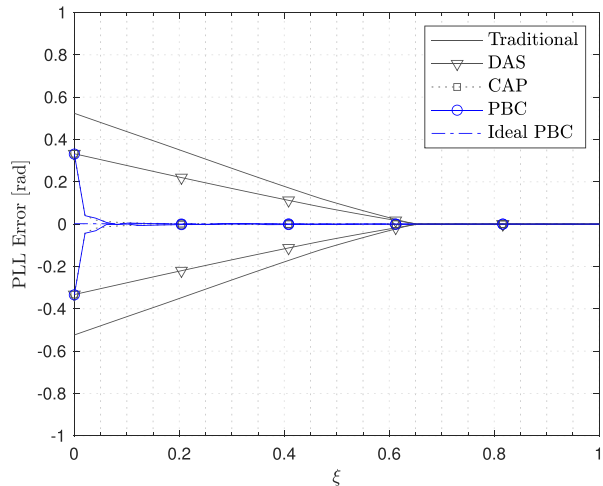


Fig. 8. Multipath phase envelope: worst output error of a PLL when it is used together with different beamformers, versus delay factor ξ . The relative power, delay and phase of the multipath is given by $\kappa_m = 0.25$, $\tau_m = 1.5t_c$ and $\phi_m \in \{-2\pi/3, 2\pi/3\}$ rad respectively. The DOA's of the multipath and direct signal are -20° and 30° respectively.

6. Conclusion

In this work, we have proposed a novel data-dependent beamforming technique that is based on the well-known Capon beamformer. This technique aims to avoid the typical cancellation phenomenon between signal and correlated multipaths, and it exploits the fact that the direction-of-arrival and power of the direct signal can be known at the receiver. The proposed procedure first identifies the portion of multipaths that contributes to the cancellation, and then counteracts it before calculating the traditional Capon weights. It involves calculating the spatial correlation matrix of the incoming signal, the cross-correlation between the incoming signal and a reference signal with variable delay and phase, and implementing a two-dimensional minimization problem. The behaviour of this technique was justified mathematically, and was supported by several numerical results. The analysis and simula-

tions indicate two important scenarios depending on the degree of correlation between the signal and multipaths, with the most limiting situation occurring in the coherent multipath case. In either case, the multipath attenuations obtained by PBC are generally superior to those obtained by other existing techniques, and also, the noise response is very satisfactory. Finally, the time-delay and carrier-phase observables obtained after the beamforming stage by a DLL and a PLL are calculated. We show that, while the obtained time-delay error is approximately zero for any multipath delay, the carrier-phase observables strongly depend on the type of scenario. In the coherent multipath case, the proposed technique does not introduce any additional correction in the carrier-phase, and in the non-coherent multipath case, the obtained carrier-phase is significantly better than that obtained by other existing techniques.

Declaration of Competing Interest

The authors declare that they have no known competing financial interests or personal relationships that could have appeared to influence the work reported in this paper.

CRediT authorship contribution statement

Martí Mañosas-Caballú: Conceptualization, Methodology, Software, Formal analysis, Writing - original draft. **A. Lee Swindlehurst:** Conceptualization, Writing - review & editing, Funding acquisition. **Gonzalo Seco-Granados:** Conceptualization, Writing - review & editing, Supervision, Funding acquisition.

References

- [1] E.D. Kaplan, C.J. Hegarty, *Understanding GPS/GNSS: Principles and Applications*, third ed., Artech House, 2017.
- [2] B. Hofmann-Wellenhof, H. Lichtenegger, J. Collins, *Global Positioning System: Theory and Practice*, Springer, 2001.
- [3] A.J.V. Dierendonck, P. Fenton, T. Ford, Theory and performance of narrow correlator spacing in a GPS receiver, *ION Navig.* 39 (3) (1992) 265–283.
- [4] L. Garin, F.V. Diggelen, J.-M. Rousseau, Strobe and edge correlator multipath mitigation for code, in: *Proc. ION Int. Tech. Meeting of the Sat. Division*, Kansas City, MO, 1996, pp. 657–664.
- [5] R.D.J.V. Nee, The multipath estimating delay lock loop, in: *Proc. IEEE Int. Symp. on Spread Spectrum Tech. and App.*, Yokohama, Japan, 1992, pp. 39–42.
- [6] M.Z.H. Bhuiyan, E.S. Lohan, Advanced multipath mitigation techniques for satellite-based positioning applications, *Hindawi Int. Journal of Navig. and Obs.* (2010). Article ID 412393.
- [7] X. Chen, F. Doyis, S. Peng, Y. Morton, Comparative studies of GPS multipath mitigation methods performance, *IEEE Trans. Aerosp. Electron. Syst.* 49 (3) (2013) 1555–1568.
- [8] C. Cheng, J.-Y. Tournet, An EM-based multipath interference mitigation in GNSS receivers, *Signal Process.* 162 (2019) 141–152.
- [9] H.L.V. Trees, *Optimum Array Processing (Part IV of Detection, Estimation, and Modulation Theory)*, first edition, Wiley-Interscience, 2002.
- [10] D.-J. Moelker, E.V.d. Pol, Y. Bar-Ness, Adaptive antenna arrays for interference cancellation in GPS and GLONASS receivers, in: *Proc. IEEE PLANS*, Atlanta, GA, 1996, pp. 191–198.
- [11] M. Manosas-Caballú, J.L. Vicario, G. Seco-Granados, On the performance of deterministic beamformers: a trade-off between array gain and attenuation, *Signal Process.* 94 (1) (2014) 158–162.
- [12] G. Seco-Granados, J.A.F. Rubio, Maximum likelihood propagation-delay estimation in unknown correlated noise using antenna arrays: application to global navigation satellite systems, in: *Proc. IEEE ICASSP*, Seattle, WA, 1998, pp. 2065–2068.
- [13] M. Sgammini, F. Antreich, L. Kurz, M. Meurer, T.G. Noll, Blind adaptive beamformer based on orthogonal projections for GNSS, in: *Proc. ION GNSS*, Nashville, TN, 2012, pp. 926–935.
- [14] R.G. Lorenz, S.P. Boyd, Robust beamforming in GPS arrays, in: *Proc. ION Nation. Technic. Meeting*, San Diego, CA, 2002, pp. 409–427.
- [15] D. Lu, Q. Feng, R. Wu, Survey on interference mitigation via adaptive array processing in GPS, in: *Proc. EA PERS*, Cambridge, MA, vol. 2, 2006, pp. 357–362.
- [16] H. Zhao, B. Lian, J. Feng, Adaptive beamforming and phase bias compensation for GNSS receiver, *J. Syst. Eng. Electron.* 26 (1) (2015) 10–18.
- [17] C. Fernandez-Prades, J. Arribas, P. Closas, Robust GNSS receivers by array signal processing: theory and implementation, *Proc. IEEE* 104 (6) (2016) 1207–1220.
- [18] S. Daneshmand, G. Lachapelle, Integration of GNSS and INS with a phased array antenna, *GPS Solutions* 22 (2018). Article num. 3.
- [19] Y. Hu, S. Bian, B. Li, L. Zhou, A novel array-based spoofing and jamming suppression method for GNSS receiver, *IEEE Sens. J.* 18 (7) (2018) 2952–2958.

- [20] A.L. Swindlehurst, B.D. Jeffs, G. Seco-Granados, J. Li, Applications of array signal processing, in: Academic Press Library in Signal Processing, vol. 3, chapter 20, Elsevier, 2014, pp. 859–953.
- [21] B. Widrow, K. Duvall, R. Gooch, W. Newman, Signal cancellation phenomena in adaptive antennas: causes and cures, *IEEE Trans. Ant. Prop.* 30 (3) (1982) 469–478.
- [22] T.-J. Shan, M. Wax, T. Kailath, On spatial smoothing for direction-of-arrival estimation of coherent signals, *IEEE Trans. ASSP* 33 (4) (1985) 806–811.
- [23] Y. Bresler, V.U. Reddy, T. Kailath, Optimum beamforming for coherent signal and interferences, *IEEE Trans. ASSP* 36 (6) (1988) 833–843.
- [24] S.U. Pillai, B.H. Kwon, Forward/backward spatial smoothing techniques for coherent signal identification, *IEEE Trans. ASSP* 37 (1) (1989) 8–15.
- [25] I. Ziskind, M. Wax, Maximum likelihood localization of multiple sources by alternating projection, *IEEE Trans. ASSP* 36 (10) (1988) 1553–1560.
- [26] F. Qian, B.D.V. Veen, Quadratically constrained adaptive beamforming for coherent signals and interference, *IEEE Trans. Signal Process.* 43 (8) (1995) 1890–1900.
- [27] G. Seco-Granados, J.A. Fernandez-Rubio, C. Fernandez-Prades, ML estimator and hybrid beamformer for multipath and interference mitigation in GNSS receivers, *IEEE Trans. Signal Process.* 53 (3) (2005) 1194–1208.
- [28] M.G. Amin, W. Sun, A novel interference suppression scheme for global navigation satellite systems using antenna array, *IEEE J. Sel. Areas Commun.* 23 (5) (2005) 999–1012.
- [29] M. Manosas-Caballú, G. Seco-Granados, A.L. Swindlehurst, Robust beamforming via FIR filtering for GNSS multipath mitigation, in: Proc. IEEE ICASSP, Vancouver, BC, 2013, pp. 4173–4177.
- [30] J. Wu, X. Tang, Z. Li, C. Li, F. Wang, Cascaded interference and multipath suppression method using array antenna for GNSS receiver, *IEEE Access* 7 (2019) 69274–69282.
- [31] F.K. Brunner, H. Hartinger, L. Troyer, GPS signal diffraction modelling: the stochastic SIGMA-d model, *J. Geodesy* 73 (1999) 259–267.
- [32] J. Capon, High-resolution frequency-wavenumber spectrum analysis, *Proc. IEEE* 57 (8) (1969) 1408–1418.
- [33] C.D. Meyer, *Matrix Analysis and Applied Linear Algebra*, first edition, SIAM, 2000.
- [34] B. Recht, M. Fazel, P.A. Parrilo, Guaranteed minimum-rank solutions of linear matrix equations via nuclear norm minimization, *SIAM Rev.* 52 (3) (2010) 471–501.
- [35] K. Borre, D.M. Akos, N. Bertelsen, P. Rinder, S.H. Jensen, *A Software-Defined GPS and GALILEO Receiver*, Birkhäuser, 2007.

Paper C

Alternative Implementations of the GNSS Power-Based Capon Beamformer

DOI: 10.1109/lsp.2021.3092229

© 2021 IEEE. Reprinted with permission from M. Mañosas-Caballú and G. Seco-Granados, IEEE Signal Processing Letters 28 (June 2021), pp. 1435-1439.

Alternative Implementations of the GNSS Power-Based Capon Beamformer

Martí Mañosas-Caballú  and Gonzalo Seco-Granados , Senior Member, IEEE

Abstract—Power-Based Capon beamforming has recently been proposed to avoid the well-known cancellation effects between direct signal and correlated multipaths of the Capon beamformer. This novel technique exploits the fact that in some applications the power of the direct signal can be known at the receiver, in addition to the more usual assumptions of known spatial and temporal signatures. At the implementation stage, however, it involves solving a given two-dimensional rank minimization problem, which must be approximated to avoid inherent numerical limitations. In this work, we present an equivalent minimization problem that overcomes such limitations, and therefore leads to alternative implementations that can provide more precise and reliable results. The new approach is justified mathematically, and also supported by several simulations results.

Index Terms—Arrays, beamforming, Capon, coherent, correlated, GNSS, multipath.

I. INTRODUCTION

GLOBAL Navigation Satellite Systems (GNSS) enable the calculation of a user position by using the signals transmitted by a constellation of specific satellites. For GNSS, only the received Line-Of-Sight Signal (LOSS) is useful to obtain information about the user position. Multipath reflections usually bias the apparent distance between the user and each available satellite, and they also hamper the ambiguity resolution process needed for carrier-phase ranging [1]. For this reason, significant research has been devoted to the mitigation of multipath effects, and many techniques have been proposed so far. On one hand, there are single-antenna techniques, that attempt to discriminate the received signals by exploiting temporal diversity [2]–[8]. On the other hand, there are multiple-antenna techniques, that attempt to discriminate the received signals by exploiting spatial diversity [9]–[22].

The most practical multiple-antenna solutions are based on data-dependent beamforming, where specifically designed weights are calculated that depend on the statistics of the incoming data [23]. These weights are used to spatially filter the incoming signals by the antenna array, and thus attenuate the interference and noise present. Since all GNSS use

Direct-Sequence Spread-Spectrum modulations, the data used to compute the beamforming weights can be obtained either before or after the despreading process [24]. The current techniques can be mainly grouped into those that exploit knowledge of the LOSS spatial signature, as in [25]–[29], into those that exploit knowledge of the LOSS temporal signature, as in [30]–[33], or into the blind ones, that only exploit some specific properties of the signals involved [34]–[40]. Although all these techniques are very useful in GNSS scenarios, they have serious limitations when correlated multipaths are present. A great example is that of Capon [41], which works extraordinarily well in the presence of uncorrelated interferences, but suffers from direct signal cancellation in the presence of correlated multipaths.

Recently, a modification of the Capon beamformer has been proposed exploiting the known power of the direct signal at the receiver, and it is referred to as Power-Based Capon (PBC) beamforming [42]. By estimating some particular cross-correlation terms and subtracting them from the spatial correlation matrix of the received signal, this novel technique prevents great part of the cancellation effects between direct signal and correlated multipaths. In this work, we review the most important features of the PBC and propose more practical and better performing implementations. In Section II, we formally state the problem to be addressed. In Section III, we derive an equivalent formulation of the PBC that leads to enhanced implementations. In Section IV, we show numerical examples that support the theoretical discussions. Finally, we draw conclusions about the work in Section V.

II. PROBLEM STATEMENT

Let us assume that the n -th sample of the post-despreading baseband equivalent signal received by an arbitrary L -element array can be written as follows:

$$\mathbf{x}[n] = \mathbf{a}s[n] + \sum_{k=1}^D \mathbf{b}_k m_k[n] + \mathbf{v}[n] \quad (1)$$

where $s[n] \in \mathbb{C}$ is the LOSS, $\mathbf{a} \in \mathbb{C}^L$ is its corresponding spatial signature, $m_k[n] \in \mathbb{C}$ is the k -th multipath reflection, $\mathbf{b}_k \in \mathbb{C}^L$ is its corresponding spatial signature, and $\mathbf{v}[n] \in \mathbb{C}^L$ is the received spatially white noise with identical power at each sensor. The signals involved in (1) impinge on the array from different directions, so that \mathbf{a} , $\mathbf{b}_1, \dots, \mathbf{b}_D$ are linearly independent. The vector \mathbf{a} is considered to be known, whereas $\mathbf{b}_1, \dots, \mathbf{b}_D$ are unknown. In the scenario of interest, the multipath reflections can be either correlated or uncorrelated with the direct signal, and verify $D < L$. Specifically, they can be written as $m_k[n] = \beta_k s[n - \tau_k] e^{-j\varphi_k} \forall k \in \{1, \dots, D\}$, where

Manuscript received April 14, 2021; revised June 16, 2021; accepted June 21, 2021. Date of publication June 24, 2021; date of current version July 29, 2021. This work was supported in part by the Ministry of Science and Innovation Grant TEC2017-89925-R and in part by the ICREA Academia Program. The associate editor coordinating the review of this manuscript and approving it for publication was Prof. Jun Liu. (Corresponding author: Martí Mañosas-Caballú.)

The authors are with the Department of Telecommunications and Systems Engineering, Universitat Autònoma de Barcelona, 08193 Bellaterra, Spain (e-mail: marti.manosas@e-campus.uab.cat; gonzalo.seco@uab.cat).

Digital Object Identifier 10.1109/LSP.2021.3092229

$\beta_k \in \mathbb{R}$, $\tau_k \in \mathbb{R}$ and $\varphi_k \in \mathbb{R}$ are the corresponding amplitude, delay and phase relative to the LOSS.

At the receiver, a reference signal $c[n, \tau, \varphi]$ is also available. It is a non-synchronized replica of the direct signal $s[n]$, and can be tuned through a delay τ and phase φ :

$$c[n, \tau, \varphi] = s[n + \tau - \tau_e]e^{j(\varphi - \varphi_e)}$$

where τ_e and φ_e are the unknown delay and phase synchronization errors. The spatial cross-correlation vector between $\mathbf{x}[n]$ and $c[n, \tau, \varphi]$ can be easily calculated, which is defined as $\mathbf{r}_{xc}(\tau, \varphi) = \mathbb{E}\{\mathbf{x}[n]c[n, \tau, \varphi]^*\}$ and can be written as:

$$\mathbf{r}_{xc}(\tau, \varphi) = (\mathbf{a} r_s(\tau - \tau_e) + \mathbf{B} \mathbf{r}_{ms}(\tau - \tau_e)) e^{-j(\varphi - \varphi_e)} \quad (2)$$

where $r_s(\tau) = \mathbb{E}\{s[n]s[n + \tau]^*\}$, $\mathbf{r}_{ms}(\tau) = \mathbb{E}\{\mathbf{m}[n]s[n + \tau]^*\}$, $\mathbf{m}[n] = [m_1[n] \dots m_D[n]]^T$ and $\mathbf{B} = [\mathbf{b}_1 \dots \mathbf{b}_D]$. In addition, the spatial correlation matrix of $\mathbf{x}[n]$ can also be calculated. It is defined as $\mathbf{R}_{xx} = \mathbb{E}\{\mathbf{x}[n]\mathbf{x}[n]^H\}$ and can be written as:

$$\mathbf{R}_{xx} = \sigma_s^2 \mathbf{a} \mathbf{a}^H + \mathbf{a} \mathbf{r}_{ms}^H \mathbf{B}^H + \mathbf{B} \mathbf{r}_{ms} \mathbf{a}^H + \mathbf{B} \mathbf{R}_m \mathbf{B}^H + \sigma_v^2 \mathbf{I}$$

where σ_s^2 is the known power of $s[n]$, σ_v^2 is the power of $\mathbf{v}[n]$, $\mathbf{r}_{ms} = \mathbb{E}\{\mathbf{m}[n]s[n]^*\}$, $\mathbf{R}_m = \mathbb{E}\{\mathbf{m}[n]\mathbf{m}[n]^H\}$ and \mathbf{I} denotes the identity matrix.

If we evaluate (2) at $\tau = \tau_e$ and $\varphi = \varphi_e$, then $\mathbf{r}_{xc}(\tau, \varphi)$ is equal to the vector $\mathbf{a} \sigma_s^2 + \mathbf{B} \mathbf{r}_{ms}$, which in turn can be transformed to $\mathbf{B} \mathbf{r}_{ms}$ because \mathbf{a} and σ_s^2 are known. This procedure further allows to calculate the cross-correlation terms $\mathbf{B} \mathbf{r}_{ms} \mathbf{a}^H$ and $\mathbf{a} \mathbf{r}_{ms}^H \mathbf{B}^H$, and to subtract them to \mathbf{R}_{xx} . The result is a new correlation matrix that would correspond to the scenario where the multipaths are totally uncorrelated with the LOSS. Then, if the Capon beamformer is calculated using the new correlation matrix, the typical cancellation effects between the direct signal and multipaths are avoided. This procedure is known as Power-Based Capon (PBC) beamforming [42], and the estimates of τ_e and φ_e are obtained from the solution to:

$$\min_{\tau, \varphi} \text{rank}(\mathbf{R}(\tau, \varphi)) \quad (3)$$

where $\mathbf{R}(\tau, \varphi)$ is defined as $\mathbf{R}_{xx} - \sigma_s^2 \mathbf{a} \mathbf{a}^H - \sigma_v^2 \mathbf{I} - \mathbf{a} \alpha(\tau, \varphi)^H - \alpha(\tau, \varphi) \mathbf{a}^H$, and $\alpha(\tau, \varphi) = \mathbf{r}_{xc}(\tau, \varphi) - \mathbf{a} \sigma_s^2$. Here, the value of σ_v^2 must be assumed known.

In practice, the discontinuities of the rank function and the need to use a threshold for the calculation of the numerical rank make the minimization problem (3) very difficult to implement. For this reason, the original PBC uses a generalization of the Schatten p -norm to approximate the rank:

$$S(\tau, \varphi) = \left(\sum_k \sigma_k^p(\tau, \varphi) \right)^{\frac{1}{p}} \quad \text{with } 0 < p < \infty$$

where $\sigma_k(\tau, \varphi)$ is the k -th singular value of $\mathbf{R}(\tau, \varphi)$. This cost function is relatively simple to calculate, and does not present neither the discontinuities of the rank nor its numerical limitations. However, it only provides the exact values of τ_e and φ_e when $p \rightarrow 0$, and very low values of p are not numerically recommended [42]. With the goal of providing more accurate and reliable results, in the following we develop an equivalent approach to (3) that leads to new implementations of the PBC.

III. EQUIVALENT APPROACH

A. Theoretical Bases

Let us start by noting that the matrix $\mathbf{R}(\tau, \varphi)$ can be written as follows:

$$\begin{bmatrix} \mathbf{a} & \mathbf{B} \end{bmatrix} \begin{bmatrix} 2\sigma_s^2 - 2\mathcal{R}\{r_s(\bar{\tau})e^{-j\bar{\varphi}}\} & \mathbf{r}_{ms}^H - \mathbf{r}_{ms}^H(\bar{\tau})e^{j\bar{\varphi}} \\ \mathbf{r}_{ms} - \mathbf{r}_{ms}(\bar{\tau})e^{-j\bar{\varphi}} & \mathbf{R}_m \end{bmatrix} \begin{bmatrix} \mathbf{a}^H \\ \mathbf{B}^H \end{bmatrix}$$

where $\bar{\tau}$ and $\bar{\varphi}$ are used to denote $\tau - \tau_e$ and $\varphi - \varphi_e$ respectively, and $\mathcal{R}\{\}$ denotes the real part operator. A direct consequence of this formulation is that $\mathbf{R}(\tau, \varphi)$ can be considered as the spatial correlation matrix of an hypothetically received signal $\mathbf{x}_0[n]$:

$$\mathbf{x}_0[n] = \mathbf{a} s[n] - \mathbf{a} s[n + \bar{\tau}]e^{j\bar{\varphi}} + \sum_{k=1}^D \mathbf{b}_k m_k[n] \quad (4)$$

If we evaluate (4) at $\tau = \tau_e$ and $\varphi = \varphi_e$, then there is no contribution of \mathbf{a} in $\mathbf{x}_0[n]$, and therefore it is natural that in this case the rank of $\mathbf{R}(\tau, \varphi)$ is minimal. Further, when we process $\mathbf{x}_0[n]$ with a beamformer $\mathbf{w} \in \mathbb{C}^L$ that satisfies the distortionless constraint $\mathbf{w}^H \mathbf{a} = 1$, it is expected that the minimum achievable power at the output of the beamformer is zero. In contrast, if $\tau \neq \tau_e$ or $\varphi \neq \varphi_e$, then there is contribution of \mathbf{a} in $\mathbf{x}_0[n]$, and some amount of power must be present at the output unless the direct signal is fully correlated with some multipaths. This observation suggests that minimizing the rank of $\mathbf{R}(\tau, \varphi)$ may provide the same minimizers as:

$$\min_{\tau, \varphi} P_{\min}(\tau, \varphi) \quad (5)$$

where $P_{\min}(\tau, \varphi)$ is the minimum achievable power at the output of a distortionless beamformer with input equal to $\mathbf{x}_0[n]$, and thus it is defined as the minimum value of $\mathbf{w}^H \mathbf{R}(\tau, \varphi) \mathbf{w}$ subject to $\mathbf{w}^H \mathbf{a} = 1$. The following lemma has been developed to prove the equivalence.

Lemma 1: The minima of problems (3) and (5) are attained at the same values of (τ, φ) .

Proof: Let us find first an analytical expression of $P_{\min}(\tau, \varphi)$. If we exploit the known structure of $\mathbf{R}(\tau, \varphi)$ together with $\mathbf{w}^H \mathbf{a} = 1$, then $\mathbf{w}^H \mathbf{R}(\tau, \varphi) \mathbf{w}$ can be replaced with the following function:

$$\begin{aligned} P(\mathbf{w}) &= 2\sigma_s^2 - 2\mathcal{R}\{r_s(\bar{\tau})e^{-j\bar{\varphi}}\} + (\mathbf{r}_{ms}^H - \mathbf{r}_{ms}^H(\bar{\tau})e^{j\bar{\varphi}}) \mathbf{B}^H \mathbf{w} \\ &\quad + \mathbf{w}^H \mathbf{B} (\mathbf{r}_{ms} - \mathbf{r}_{ms}(\bar{\tau})e^{-j\bar{\varphi}}) + \mathbf{w}^H \mathbf{B} \mathbf{R}_m \mathbf{B}^H \mathbf{w} \end{aligned}$$

Thus, using the Lagrange multiplier theorem to find the minimum of $P(\mathbf{w})$ subject to $\mathbf{w}^H \mathbf{a} = 1$, we shall define:

$$L(\mathbf{w}, \lambda) = P(\mathbf{w}) + \lambda(\mathbf{w}^H \mathbf{a} - 1) + \lambda^*(\mathbf{a}^H \mathbf{w} - 1)$$

and solve the system:

$$\nabla L(\mathbf{w}, \lambda) = 0 \quad (6)$$

$$\mathbf{a}^H \mathbf{w} = 1 \quad (7)$$

where $\lambda \in \mathbb{C}$ is the Lagrange multiplier and ∇ is the complex gradient operator with respect to \mathbf{w}^H .

The solution to (6) gives $\lambda = 0$ because the columns of \mathbf{B} and \mathbf{a} are linearly independent, and also as a result:

$$\mathbf{B} \mathbf{R}_m \mathbf{B}^H \mathbf{w} = -\mathbf{B} (\mathbf{r}_{ms} - \mathbf{r}_{ms}(\bar{\tau})e^{-j\bar{\varphi}})$$

which can be reduced to:

$$\mathbf{R}_m \mathbf{B}^H \mathbf{w} = -(\mathbf{r}_{ms} - \mathbf{r}_{ms}(\bar{\tau})e^{-j\bar{\varphi}})$$

These last two equations are compatible with (7), and if we substitute them into $\mathbf{P}(\mathbf{w})$, and we rewrite \mathbf{R}_m as $\mathbf{R}_m \mathbf{R}_m^+ \mathbf{R}_m$ by means of the pseudoinverse \mathbf{R}_m^+ , we finally obtain that the minimum achievable power is:

$$\begin{aligned} P_{\min}(\tau, \varphi) &= 2\sigma_s^2 - 2\mathcal{R}\{r_s(\bar{\tau})e^{-j\bar{\varphi}}\} \\ &\quad - (\mathbf{r}_{ms}^H - \mathbf{r}_{ms}^H(\bar{\tau})e^{j\bar{\varphi}}) \mathbf{R}_m^+ (\mathbf{r}_{ms} - \mathbf{r}_{ms}(\bar{\tau})e^{-j\bar{\varphi}}) \end{aligned} \quad (8)$$

Now note that $P_{\min}(\tau, \varphi)$ is positive by definition. Therefore its minimum over τ and φ is attained when $P_{\min}(\tau, \varphi) = 0$. This leads to the condition $2\sigma_s^2 - 2\mathcal{R}\{r_s(\bar{\tau})e^{-j\bar{\varphi}}\} = (\mathbf{r}_{ms}^H - \mathbf{r}_{ms}^H(\bar{\tau})e^{j\bar{\varphi}}) \mathbf{R}_m^+ (\mathbf{r}_{ms} - \mathbf{r}_{ms}(\bar{\tau})e^{-j\bar{\varphi}})$, which is the one obtained in [42] starting from the minimization of the rank of $\mathbf{R}(\tau, \varphi)$ and extended to complex $r_s(\bar{\tau})$. ■

Lemma 1 tells us that the PBC beamformer can be implemented from the points (τ, φ) that minimize $P_{\min}(\tau, \varphi)$. This is inherently better than minimizing $\text{rank}(\mathbf{R}(\tau, \varphi))$, because $P_{\min}(\tau, \varphi)$ is continuous, and also because small numerical deviations in $\mathbf{R}(\tau, \varphi)$ do not change $P_{\min}(\tau, \varphi)$ dramatically.

B. Implementation Aspects

At the receiver, the calculation of $P_{\min}(\tau, \varphi)$ needs to be performed from an estimate of $\mathbf{R}(\tau, \varphi)$. Then, the Lagrange multiplier theorem can be applied to the function $\mathbf{w}^H \mathbf{R}(\tau, \varphi) \mathbf{w}$ subject to the constraint $\mathbf{w}^H \mathbf{a} = 1$, leading to the system:

$$\mathbf{R}(\tau, \varphi) \mathbf{w} = -\mu \mathbf{a} \quad (9)$$

$$\mathbf{a}^H \mathbf{w} = 1 \quad (10)$$

where $\mu \in \mathbb{C}$ is the associated Lagrange multiplier.

The solution to (9)-(10) is straightforward and well-known when $\mathbf{R}(\tau, \varphi)$ is invertible. However, the matrix $\mathbf{R}(\tau, \varphi)$ may not be full rank in the scenario of interest, and in fact we know that it degenerates for some τ and φ [42]. When $\mathbf{R}(\tau, \varphi)$ is not full rank, two distinct scenarios must be contemplated that depend on the space spanned by $\mathbf{R}(\tau, \varphi)$. If $\mathbf{a} \notin \text{span}\{\mathbf{R}(\tau, \varphi)\}$, then (9) can only be fulfilled when $\mu = 0$, which gives $\mathbf{w} \in \text{null}\{\mathbf{R}(\tau, \varphi)\}$ and leads to $P_{\min}(\tau, \varphi) = 0$. In contrast, if $\mathbf{a} \in \text{span}\{\mathbf{R}(\tau, \varphi)\}$, then (9) has multiple solutions that together with (10) lead to $P_{\min}(\tau, \varphi) = (\mathbf{a}^H \mathbf{R}(\tau, \varphi)^+ \mathbf{a})^{-1}$. This results into a piecewise definition of $P_{\min}(\tau, \varphi)$ with sub-domains defined by $\text{span}\{\mathbf{R}(\tau, \varphi)\}$. Unfortunately, these sub-domains are very delicate to calculate numerically.

In order to avoid the need of piecewise definitions, one can attempt to directly find a point (τ_0, φ_0) where $P_{\min}(\tau, \varphi)$ is minimum by using the sole function:

$$F_1(\tau, \varphi) = (\mathbf{a}^H \mathbf{R}(\tau, \varphi)^+ \mathbf{a})^{-1} \quad (11)$$

This function is strictly positive, and must satisfy:

$$\lim_{(\tau, \varphi) \rightarrow (\tau_0, \varphi_0)} F_1(\tau, \varphi) = 0$$

because (8) implies that $P_{\min}(\tau, \varphi)$ must be continuous due to the continuity of all its terms, and because (τ_0, φ_0) verifies $\mathbf{a} \notin \text{span}\{\mathbf{R}(\tau_0, \varphi_0)\}$. As a result, (τ_0, φ_0) can be approached accurately by minimizing $F_1(\tau, \varphi)$. What is certain is that a jump

discontinuity exists, since $F_1(\tau_0, \varphi_0) \neq 0$. A discontinuity in $F_1(\tau, \varphi)$ implies a discontinuity in $\mathbf{R}(\tau, \varphi)^+$, and this carries some numerical consequences. In essence, it becomes crucial to select very carefully a threshold for the singular values of $\mathbf{R}(\tau, \varphi)$ that are taken as zero. A threshold that is too large can cause $F_1(\tau, \varphi)$ jump close to the discontinuity value $F_1(\tau_0, \varphi_0)$ when (τ, φ) is still far from (τ_0, φ_0) . In contrast, a threshold that is too small allows numerical deviations of the null singular values of $\mathbf{R}(\tau, \varphi)$ to be translated to $F_1(\tau, \varphi)$.

A reasonable approach to avoid the need of a threshold in the computation of (11) is to add a small amount of diagonal loading $\varepsilon > 0$ to the matrix $\mathbf{R}(\tau, \varphi)$. In this way, the function $F_1(\tau, \varphi)$ is approximated by the continuous function $F_2(\tau, \varphi) = (\mathbf{a}^H (\mathbf{R}(\tau, \varphi) + \varepsilon \mathbf{I})^{-1} \mathbf{a})^{-1}$. Not only the use of an standard inverse avoids the discontinuity problem, but also the strictly positive singular values of $\mathbf{R}(\tau, \varphi) + \varepsilon \mathbf{I}$ prevent the numerical instability associated with the null singular values. In order to see how similar $F_2(\tau, \varphi)$ is to the desired function $P_{\min}(\tau, \varphi)$, the following lemma has been developed.

Lemma 2: The function $F_2(\tau, \varphi) \rightarrow P_{\min}(\tau, \varphi)$ when $\varepsilon \rightarrow 0$.

Proof: Let us start by writing $F_2(\tau, \varphi)$ as:

$$\left(\sum_{k=1}^{\rho} \frac{1}{\lambda_k + \varepsilon} |\phi_k^H \mathbf{a}|^2 + \sum_{k=\rho+1}^L \frac{1}{\varepsilon} |\phi_k^H \mathbf{a}|^2 \right)^{-1} \quad (12)$$

where λ_k and ϕ_k are the k -th singular value and k -th singular vector of $\mathbf{R}(\tau, \varphi)$ respectively, and ρ is the rank of $\mathbf{R}(\tau, \varphi)$. The sets $\{\phi_1, \dots, \phi_\rho\}$ and $\{\phi_{\rho+1}, \dots, \phi_L\}$ form orthonormal bases of $\text{span}\{\mathbf{R}(\tau, \varphi)\}$ and $\text{null}\{\mathbf{R}(\tau, \varphi)\}$ respectively. If $\mathbf{a} \notin \text{span}\{\mathbf{R}(\tau, \varphi)\}$, then $|\phi_k^H \mathbf{a}| \neq 0$ for some $k \in \{\rho+1, \dots, L\}$, and the limit of (12) when $\varepsilon \rightarrow 0$ is zero. In contrast, if $\mathbf{a} \in \text{span}\{\mathbf{R}(\tau, \varphi)\}$, then $|\phi_k^H \mathbf{a}| = 0$ for all $k \in \{\rho+1, \dots, L\}$, and the limit of (12) when $\varepsilon \rightarrow 0$ is $(\sum_{k=1}^{\rho} \frac{1}{\lambda_k} |\phi_k^H \mathbf{a}|^2)^{-1} = (\mathbf{a}^H \mathbf{R}(\tau, \varphi)^+ \mathbf{a})^{-1}$. ■

The asymptotic equivalence shown in Lemma 2 means that for a sufficiently small ε , the function $F_2(\tau, \varphi)$ is a good enough estimate of $P_{\min}(\tau, \varphi)$, so that the minimizers of $F_2(\tau, \varphi)$ are also good enough estimates of the minimizers of $P_{\min}(\tau, \varphi)$. In addition, $F_2(\tau, \varphi)$ presents a great advantage in terms of simplicity if the value of ε is set to σ_v^2 . The noise term that had to be subtracted from \mathbf{R}_{xx} in the calculation of $\mathbf{R}(\tau, \varphi)$ is then reintroduced, eliminating the need to estimate σ_v^2 . And since $\sigma_s^2 \mathbf{a} \mathbf{a}^H$ can also be added to $\mathbf{R}(\tau, \varphi)$ without influencing the minimization problem (5), we can use:

$$F_2(\tau, \varphi) = (\mathbf{a}^H \bar{\mathbf{R}}(\tau, \varphi)^{-1} \mathbf{a})^{-1} \quad (13)$$

where $\bar{\mathbf{R}}(\tau, \varphi)$ is $\mathbf{R}_{xx} - \mathbf{a} \mathbf{a}^H + \sigma_v^2 \mathbf{I} - \mathbf{a} \mathbf{a}^H$. Similarly to [42], the process to calculate the PBC beamforming weights is then as shown in Algorithm 1.

IV. SIMULATION RESULTS

In this section, we present some numerical examples related to the implementation of (5). Specifically, we compare the accuracy of the proposed functions to estimate the delay and phase that minimize $P_{\min}(\tau, \varphi)$, and also analyze the response of the corresponding PBC beamformers to multipath and noise.

Throughout all the simulations, we assume that a 5-element array receives a Global Positioning System (GPS) signal and

Algorithm 1: PBC Beamforming.

Given the signals $\mathbf{x}[n]$ and $c[n, \tau, \varphi]$:

- 1) Calculate $\mathbf{R}_{\mathbf{xx}}$ and $\mathbf{r}_{\mathbf{x}c}(\tau, \varphi)$, and then $\bar{\mathbf{R}}(\tau, \varphi)$
- 2) Solve $(\tau_0, \varphi_0) = \arg \min_{\tau, \varphi} (\mathbf{a}^H \bar{\mathbf{R}}(\tau, \varphi)^{-1} \mathbf{a})^{-1}$

if solution is not unique **then**
 take the one with smallest τ and $\varphi = 0$
end if

- 3) Compute Capon using $\bar{\mathbf{R}}(\tau_0, \varphi_0)$ instead of $\mathbf{R}_{\mathbf{xx}}$

two multipath reflections with angles of arrival equal to 30° , -20° and 80° respectively. The post-despreading versions of the received signals are calculated from a triangle function of duration $T_c = 1/1023$ ms. This function is also used as the shape of the autocorrelation of the Gaussian noise. After each integration time $T_{\text{int}} = 20$ ms, 31 samples are taken within an interval approximately $\pm T_c$, centered at the time-delay obtained from a standard Delay-Locked Loop. The relative amplitudes and phases of the multipaths are set to $\beta_1 = 0.95$, $\beta_2 = 0.7$ and $\varphi_1 = -\pi/4$ rad, $\varphi_2 = \pi/2$ rad. The relative delays of the multipaths are defined as $\tau_1 = \xi \cdot 1.5 T_c$ and $\tau_2 = \xi \cdot 2.5 T_c$, where $\xi \in [0, 1]$ is a scaling factor. When ξ is zero, all the multipaths are received coherently. When $\xi = 1$, they are received with delays $1.5 T_c$ and $2.5 T_c$. Then, the simulation results are represented as a function of ξ , allowing a wide range of correlations to be taken into account. The Carrier-to-Noise-density (C/N₀) is set to 45 dBHz, and the observation time of the GPS receiver to $T = 200$ ms.

Fig. 1 and Fig. 2 plot the Root Mean Squared Error (RMSE) of the estimated delay and phase that minimize the functions $S(\tau, \varphi)$, $F_1(\tau, \varphi)$ and $F_2(\tau, \varphi)$, with respect to the desired values τ_e and φ_e . Unlike in [42], the value of p in $S(\tau, \varphi)$ is set here to 0.4. In this way, the resulting mean of the estimates worsens slightly, but the variance improves and so does the RMSE. The threshold needed for the calculation of the pseudoinverse in $F_1(\tau, \varphi)$ is set to 10^{-4} , and the value of ε in $F_2(\tau, \varphi)$ to σ_v^2 . Fig. 3 plots the expected value of the Signal-to-Noise-plus-Multipath Ratio (SNMR) at the output of different beamformers. The dotted line corresponds to the traditional Capon (CAP), and each solid line corresponds to a specific implementation of the PBC, with either $S(\tau, \varphi)$, $F_1(\tau, \varphi)$ or $F_2(\tau, \varphi)$. Looking at the plots, Fig. 1 shows that the delays estimated by the distinct functions differ only by a few nanoseconds. Fig. 2 shows that the differences obtained in the estimated phase can be as large as 0.2 rad. Fig. 3 shows that, while CAP suffers serious cancellation effects for $\xi = 0$ and only achieves SNMR < 8 dB for the remaining ξ , all PBC implementations start with SNMR = 1 dB and approach SNMR = 26 dB as ξ grows. Remarkable enough, $F_2(\tau, \varphi)$ leads to SNMR > 10 dB for $\xi > 0.02$.

V. CONCLUSION

This article reviews the most fundamental aspects of a recently proposed beamforming technique, referred to as Power-Based Capon. In order to overcome the numerical limitations of the original formulation, we have approached the problem to be solved from a different perspective, based on a new cost function

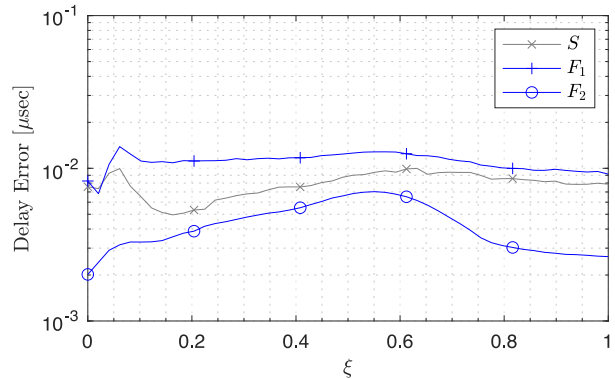


Fig. 1. Root Mean Squared Error of the estimated delay that minimize the functions $S(\tau, \varphi)$, $F_1(\tau, \varphi)$ and $F_2(\tau, \varphi)$, versus delay factor ξ .

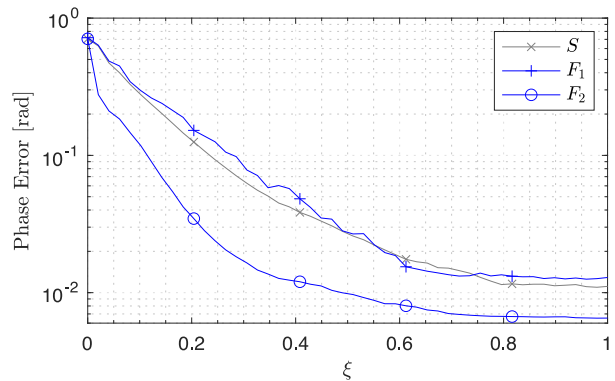


Fig. 2. Root Mean Squared Error of the estimated phase that minimize the functions $S(\tau, \varphi)$, $F_1(\tau, \varphi)$ and $F_2(\tau, \varphi)$, versus delay factor ξ .

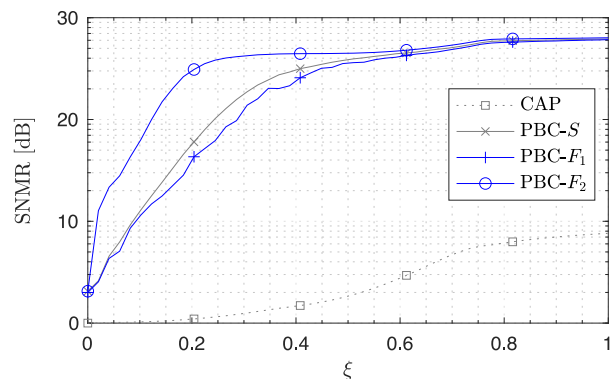


Fig. 3. Expected Signal-to-Noise-plus-Multipath Ratio at the output of different beamformers, versus delay factor ξ .

that is continuous and less sensitive to numerical deviations in the estimated correlation matrices. The equivalence between the new formulation and the original one is proven, and corresponding implementations are proposed. While the results obtained show that all implementations are valid, they also indicate that $F_2(\tau, \varphi)$ in (13) provides the best results.

REFERENCES

- [1] B. Hofmann-Wellenhof, H. Lichtenegger, and J. Collins, *Global Positioning System: Theory and Practice*. Vienna, Austria: Springer, 2001.
- [2] A. J. V. Dierendonck, P. Fenton, and T. Ford, "Theory and performance of narrow correlator spacing in a GPS receiver," *ION Navigation*, vol. 39, no. 3, pp. 265–283, 1992.
- [3] R. D. J. V. Nee, "The multipath estimating delay lock loop," in *Proc. IEEE Int. Symp. Spread Spectr. Tech. Appl.*, Yokohama, Japan, Nov. 1992, pp. 39–42.
- [4] L. Garin, F. V. Diggelen, and J.-M. Rousseau, "Strobe and edge correlator multipath mitigation for code," in *Proc. ION Int. Tech. Meeting Satell. Div.*, Kansas City, MO, USA, Sep. 1996, pp. 657–664.
- [5] M. Sahnoudi and M. G. Amin, "Robust tracking of weak GPS signals in multipath and jamming environments," *Signal Process.*, vol. 89, no. 7, pp. 1320–1333, Jul. 2009.
- [6] K. D. Wesson, B. L. Evans, and T. E. Humphreys, "A combined symmetric difference and power monitoring GNSS anti-spoofing technique," in *Proc. IEEE Global Conf. Signal Inf. Process.*, Austin, TX, USA, Feb. 2013, pp. 217–220.
- [7] X. Chen, F. DAVIS, S. Peng, and Y. Morton, "Comparative studies of GPS multipath mitigation methods performance," *IEEE Trans. Aerosp. Electron. Syst.*, vol. 49, no. 3, pp. 1555–1568, Jul. 2013.
- [8] C. Cheng and J.-Y. Tourneret, "An EM-based multipath interference mitigation in GNSS receivers," *Signal Process.*, vol. 162, pp. 141–152, Sep. 2019.
- [9] T.-J. Shan, M. Wax, and T. Kailath, "On spatial smoothing for direction-of-arrival estimation of coherent signals," *IEEE Trans. Acoust., Speech, Signal Process.*, vol. ASSP-33, no. 4, pp. 806–811, Aug. 1985.
- [10] M. D. Zoltowski and F. Haber, "A vector space approach to direction finding in a coherent multipath environment," *IEEE Trans. Antennas Propag.*, vol. ASSP-34, no. 9, pp. 1069–1079, Sep. 1986.
- [11] I. Ziskind and M. Wax, "Maximum likelihood localization of multiple sources by alternating projection," *IEEE Trans. Acoust., Speech, Signal Process.*, vol. 36, no. 10, pp. 1553–1560, Oct. 1988.
- [12] G. Seco-Granados and J. A. F. Rubio, "Maximum likelihood propagation-delay estimation in unknown correlated noise using antenna arrays: Application to global navigation satellite systems," in *Proc. IEEE Int. Conf. Acoust., Speech, Signal Process.*, Seattle, WA, USA, May 1998, pp. 2065–2068.
- [13] R. L. Fante and J. J. Vaccaro, "Cancellation of jammers and jammer multipath in a GPS receiver," *IEEE Aerosp. Electron. Syst. Mag.*, vol. 13, no. 11, pp. 25–28, Nov. 1998.
- [14] R. L. Fante and J. J. Vaccaro, "Wideband cancellation of interference in a GPS receive array," *IEEE Trans. Aerosp. Electron. Syst.*, vol. 36, no. 2, pp. 549–564, Apr. 2000.
- [15] G. Seco-Granados, J. A. Fernandez-Rubio, and C. Fernandez-Prades, "ML estimator and hybrid beamformer for multipath and interference mitigation in GNSS receivers," *IEEE Trans. Signal Process.*, vol. 53, no. 3, pp. 1194–1208, Mar. 2005.
- [16] S. Daneshmand, A. Broumandan, N. Sokhandan, and G. Lachapelle, "GNSS multipath mitigation with a moving antenna array," *IEEE Trans. Aerosp. Electron. Syst.*, vol. 49, no. 1, pp. 693–698, Jan. 2013.
- [17] M. Manosas-Caballú, G. Seco-Granados, and A. L. Swindlehurst, "Robust beamforming via FIR filtering for GNSS multipath mitigation," in *Proc. IEEE Int. Conf. Acoust., Speech, Signal Process.*, Vancouver, BC, Canada, May 2013, pp. 4173–4177.
- [18] M. Manosas-Caballú, J. L. Vicario, and G. Seco-Granados, "On the performance of deterministic beamformers: A trade-off between array gain and attenuation," *Signal Process.*, vol. 94, no. 1, pp. 158–162, 2014.
- [19] N. Vagle, A. Broumandan, A. Jafarnia-Jahromi, and G. Lachapelle, "Performance analysis of GNSS multipath mitigation using antenna arrays," *J. Global Positioning Syst.*, vol. 14, no. 4, pp. 1–15, Nov. 2016.
- [20] S. Daneshmand and G. Lachapelle, "Integration of GNSS and INS with a phased array antenna," *GPS Solutions*, vol. 22, no. 3, pp. 1–14, Nov. 2018.
- [21] Y. Hu, S. Bian, B. Li, and L. Zhou, "A novel array-based spoofing and jamming suppression method for GNSS receiver," *IEEE Sensors J.*, vol. 18, no. 7, pp. 2952–2958, Apr. 2018.
- [22] J. Wu, X. Tang, Z. Li, C. Li, and F. Wang, "Cascaded interference and multipath suppression method using array antenna for GNSS receiver," *IEEE Access*, vol. 7, pp. 69274–69282, May 2019.
- [23] H. L. Van Trees, *Optimum Array Processing (Part IV of Detection, Estimation, and Modulation Theory)*. New York, NY, USA: Wiley, 2002.
- [24] A. L. Swindlehurst, B. D. Jeffs, G. Seco-Granados, and J. Li, *Applications of Array Signal Processing, Academic Press Library in Signal Processing*. Amsterdam, The Netherlands: Elsevier, 2014, vol. 3, ch. 20, pp. 859–953.
- [25] O. L. Frost, "An algorithm for linearly constrained adaptive array processing," *Proc. IEEE*, vol. 60, no. 8, pp. 926–935, Aug. 1972.
- [26] M. D. Zoltowski and A. S. Gecan, "Advanced adaptive null steering concepts for GPS," in *Proc. IEEE MILCOM*, San Diego, CA, USA, Nov. 1995, pp. 1214–1218.
- [27] R. G. Lorenz and S. P. Boyd, "Robust beamforming in GPS arrays," in *Proc. ION Nat. Tech. Meeting*, San Diego, CA, USA, Jan. 2002, pp. 409–427.
- [28] M. Sahnoudi and M. Amin, "Optimal robust beamforming for interference and multipath mitigation in GNSS arrays," in *Proc. IEEE Int. Conf. Acoust., Speech, Signal Process.*, vol. 3, Honolulu, HI, USA, Apr. 2007, pp. 693–696.
- [29] Y. Jiang, P. Stoica, Z. Wang, and J. Li, "Capon beamforming in the presence of steering vector errors and coherent signals," in *Proc. MIT ASAP Workshop*, Lexington, MA, USA, Jun. 2007, pp. 1–6.
- [30] B. Widrow, P. E. Mantez, L. J. Griffiths, and B. B. Goode, "Adaptive antenna systems," *Proc. IEEE*, vol. 55, no. 12, pp. 2143–2159, Dec. 1967.
- [31] J. Miller and S. Miller, "An adaptive antenna array for multiple received signals in direct-sequence code-division multiple-access communication systems," in *Proc. IEEE MILCOM*, Fort Monmouth, NJ, USA, Oct. 1994, pp. 733–737.
- [32] G. Seco-Granados and J. A. Fernández-Rubio, "Multipath and interference errors reduction in GNSS by joint pseudorange measurement and array beamforming," in *Proc. Eur. Symp. GNSS*, Munich, Germany, Apr. 1997, pp. 605–614.
- [33] D. S. D. Lorenzo, F. Antreich, H. Denks, A. Hornbostel, C. Weber, and P. Enge, "Testing of adaptive beamsteering for interference rejection in GNSS receivers," in *Proc. ENC GNSS*, Geneva, Switzerland, Jun. 2007.
- [34] R. Gooch and J. Lundell, "The CM array: An adaptive beamformer for constant modulus signals," in *Proc. IEEE Int. Conf. Acoust., Speech, Signal Process.*, Tokyo, Japan, Apr. 1986, pp. 2523–2526.
- [35] S.-S. Hwang and J. J. Shynk, "Blind GPS receiver with a modified spreader for interference suppression," *IEEE Trans. Aerosp. Electron. Syst.*, vol. 42, no. 2, pp. 503–513, Jun. 2006.
- [36] M. G. Amin and W. Sun, "A novel interference suppression scheme for global navigation satellite systems using antenna array," *IEEE J. Sel. Areas Commun.*, vol. 23, no. 5, pp. 999–1012, May 2005.
- [37] B. Suard, A. F. Naguib, G. Xu, and A. Paulraj, "Performance of CDMA mobile communication systems using antenna arrays," in *Proc. IEEE Int. Conf. Acoust., Speech, Signal Process.*, vol. 4, Minneapolis, MN, USA, Apr. 1993, pp. 153–156.
- [38] D.-J. Moelker, E. V. der Pol, and Y. Bar-Ness, "Adaptive antenna arrays for interference cancellation in GPS and GLONASS receivers," in *Proc. IEEE Position, Location Navigation Symp.*, Atlanta, GA, USA, Apr. 1996, pp. 191–198.
- [39] W. L. Myrick, M. D. Zoltowski, and J. S. Goldstein, "Anti-jam space-time preprocessor for GPS based on multistage nested Wiener filter," in *Proc. IEEE MILCOM*, Atlantic City, NJ, USA, Nov. 1999, pp. 675–681.
- [40] M. Sgammini, F. Antreich, L. Kurz, M. Meurer, and T. G. Noll, "Blind adaptive beamformer based on orthogonal projections for GNSS," in *Proc. ION GNSS*, Nashville, TN, USA, Sep. 2012, pp. 926–935.
- [41] J. Capon, "High-resolution frequency-wavenumber spectrum analysis," *Proc. IEEE*, vol. 57, no. 8, pp. 1408–1418, Aug. 1969.
- [42] M. Manosas-Caballú, A. L. Swindlehurst, and G. Seco-Granados, "Power-based capon beamforming: Avoiding the cancellation effects of GNSS multipath," *Signal Process.*, vol. 180, Mar. 2021, Art no. 107891.

Part III

Supplementary Publications

Paper D

Robust Beamforming via FIR Filtering for GNSS Multipath Mitigation

DOI: 10.1109/icassp.2013.6638445

© 2013 IEEE. Reprinted with permission from M. Mañosas-Caballú, G. Seco-Granados and A. L. Swindlehurst, Proc. IEEE ICASSP (May 2013), pp. 4173-4177.

ROBUST BEAMFORMING VIA FIR FILTERING FOR GNSS MULTIPATH MITIGATION

Martí Mañosas-Caballú[†] Gonzalo Seco-Granados[†] A. Lee Swindlehurst^{*}

[†] Dpt. Telecomm. and Syst. Engineering, Universitat Autònoma de Barcelona

^{*}Dpt. Electrical Engineering and Comp. Science, University of California at Irvine

ABSTRACT

This paper addresses the problem of multipath mitigation with GNSS antenna arrays. A beamformer that is able to cancel the multipath components regardless of their relative delay and directions of arrival is proposed. The weights are obtained from a set of spatial correlation matrices that allows us to estimate the multipath subspace. These matrices are generated after a FIR filter that reduces the correlation between the multipath components and the line-of-sight signal, and it is only used for spatial processing. Some representative simulation results show the multipath attenuation provided by the proposed method under different conditions.

Index Terms— Beamforming, GNSS, multipath, correlation.

1. INTRODUCTION

The term Global Navigation Satellite Systems (GNSS) is a generic expression referring to any system that enables the calculation of the user position based on signals transmitted by a constellation of satellites. Due to the operating principle of the GNSS, only the time-delay (referred to as code-phase) and the carrier-phase of the received Line-Of-Sight Signal (LOSS) bears useful information about the receiver position. Multipath reflections may bias the pseudoranges by several tens of meters, and at the same time, they hamper the ambiguity resolution process needed for carrier-phase ranging [1]. For this reason, significant research and development efforts have been devoted to the mitigation of multipath effects, and many techniques have been proposed so far [2]. However, these single-antenna techniques discriminate the LOSS from the reflections by using only temporal diversity, and hence, their performance is still insufficient for many precise applications.

In contrast, the use of multiple-antenna techniques in GNSS is a promising alternative. They exploit spatial diversity and hence they are able to discriminate the received signals when they come from different directions. The best and most well-known approaches are based on data-dependent beamforming, where the optimal beamforming weights depend on the statistics of the incoming data [3]. However, these methods fail in the presence of signals that are very correlated with the LOSS, and hence they are not useful to mitigate the multipath reflections with very small relative delay, i.e. coherent multipath. Some robust methods for highly correlated signals have been proposed, e.g. [4–12], but they present certain limitations.

In the field of GNSS, many beamforming techniques have been proposed so far that take into account the underlying particularities of a GNSS scenario, e.g. [13–31]. Since all present and planned navigation systems use a Direct-Sequence Spread-Spectrum (DS-SS) signal, the information that is used to compute the weights can be extracted from the signal obtained either before or after the despreading process [30, 32]. When mitigating the multipath is the

main issue, the post-despreading signal is usually used since it contains the most noticeable contribution of the multipath. Although all robust GNSS methods improve on the performance of conventional beamforming techniques when coherent multipath is present, there are still important limitations.

In this work we address the problem of finding a beamformer that is robust against several GNSS multipath signals regardless of their relative delays and with arbitrary directions of arrival. In order to do so, we do not compute the weights from either the pre-despreading signal or the post-despreading signal. Instead, we propose to compute them from the output of an additional FIR filter that allows us to estimate the space spanned by the spatial signatures of the multipath reflections. This filter is only valid for the computation of the beamforming weights, which are then applied to either the pre-despreading signal or the post-despreading signal. The key idea behind the results presented in the paper comes from the model described in the next section. A description and justification of the proposed FIR method using this model is presented in Section 3, and some representative simulation results are found in Section 4.

2. MODELING ASSUMPTIONS

Let us consider that an arbitrary m -element array asynchronously receives the DS-SS signal transmitted by a given GNSS satellite together with $d < m$ multipath reflections. The n -th sample of the signal received by the array is modeled as:

$$\mathbf{x}[n] = \sum_{k=0}^d \sum_{l=-\infty}^{\infty} \mathbf{a}_k \alpha_k b[l] c[n - \tau_k - lN] + \mathbf{u}[n] \quad (1)$$

where $\mathbf{a}_k \in \mathbb{C}^m$ is the spatial signature of the k -th component, $\alpha_k \in \mathbb{C}$ is its complex amplitude, and $\tau_k \in \mathbb{R}$ stands for its time-delay divided by the sampling period $T_s \in \mathbb{R}$. The index $k = 0$ is reserved for the LOSS, so τ_0 and the phase of α_0 are the unknown *code-phase* and *carrier-phase* respectively, and \mathbf{a}_0 is assumed to be known up to a scaling factor. The sequence of symbols $b[l]$ forms the navigation message of the satellite, and it is assumed to be a stationary process. For its part, $c[n] := c(nT_s)$ of length $N \in \mathbb{N}$ is the sampled version of the spreading code $c(t)$ of duration $T \in \mathbb{R}$, which is composed of a sequence of $P \in \mathbb{N}$ chips of duration $T_c \in \mathbb{R}$. Note that τ_k is not necessarily an integer number, but we use the notation $c[n - \tau_k]$ to denote the sampled version of $c(t - \tau_k T_s)$. Finally, $\mathbf{u}[n] \in \mathbb{C}^m$ contains the received noise at each element of the array, which is assumed to be spatially and temporarily white, and with identical noise power σ_u^2 at each sensor.

The signal obtained after despreading is a correlated version of the received signal (1) with a local discrete replica of the code $c(t)$,

and it can be written as:

$$\mathbf{y}[n] = \sum_{k=0}^d \sum_{l=-\infty}^{\infty} \mathbf{a}_k \alpha_k b[l] r_{cc}[n - \tau_k - lN] + \mathbf{r}_{uc}[n] \quad (2)$$

where:

$$r_{cc}[n] := \sum_{l=0}^{N-1} c[l+n] c[l] \quad \mathbf{r}_{uc}[n] := \sum_{l=0}^{N-1} \mathbf{u}[l+n] c[l] \quad (3)$$

are the cross-correlation of $c[n]$ and $\mathbf{u}[n]$ with $c[n]$ respectively, and the output noise term, $\mathbf{r}_{uc}[n]$, is no longer temporarily white, but only spatially white.

Generally, the post-despreading spatial correlation matrix $\mathbf{R}_{\mathbf{y}\mathbf{y}}[n] = \mathbb{E}\{\mathbf{y}[n]\mathbf{y}[n]^H\}$ is used to calculate the beamforming weights, but only one estimate $\hat{\mathbf{R}}_{\mathbf{y}\mathbf{y}}$ is calculated from all available samples. This is a problem since the information of the LOSS and multipath are mixed and cannot be distinguished properly. However, the output signal $\mathbf{y}[n]$ may be treated as a cyclostationary process, and hence $\mathbf{R}_{\mathbf{y}\mathbf{y}}[n]$ cannot be considered constant but N -periodic. The MLE estimate of $\mathbf{R}_{\mathbf{y}\mathbf{y}}[n]$ can be obtained as:

$$\hat{\mathbf{R}}_{\mathbf{y}\mathbf{y}}[n] = \frac{1}{L} \sum_{l=0}^{L-1} \mathbf{y}[n-lN] \mathbf{y}[n-lN]^H \quad (4)$$

where L out of LN available samples are used.

In this work we calculate all possible correlation matrices in a period N through (4). Then, their structure is exploited through the signal model presented in (2) to estimate the subspace spanned by the multipath spatial signatures $\mathbf{a}_1, \dots, \mathbf{a}_d$ or *multipath subspace*. Once this is done, a beamformer that uses this subspace to mitigate the multipath is presented.

3. GNSS MULTIPATH MITIGATION

In this section we present and justify the proposed beamforming technique for multipath mitigation.

3.1. Post-despreading Correlation Matrix

For a given set of samples in a period N , let us say $n \in \{lN, lN+1, \dots, lN+N-1\}$ for some $l \in \mathbb{N}$, the output signal (2) can be approximately reduced to:

$$\mathbf{y}[n] \approx \sum_{k=0}^d \mathbf{a}_k b[l] \phi_{k,n} + \mathbf{e}_n \quad (5)$$

where $\tau_k < N \forall k$ is assumed for simplicity, $\phi_{k,n} := \alpha_k r_{cc}[n - \tau_k - lN]$ and $\mathbf{e}_n := \mathbf{r}_{uc}[n]$. This approximation just neglects the contribution of $r_{cc}[n - \tau_k - lN]$ for those samples located far away from its peak. The notation $\phi_{k,n}$ is used to emphasize that the autocorrelation values are $r_{cc}[-\tau_k], r_{cc}[1 - \tau_k], \dots, r_{cc}[N-1 - \tau_k]$ regardless of the value of l .

With this new formulation, $\mathbf{R}_{\mathbf{y}\mathbf{y}}[n]$ can be written as:

$$\mathbf{R}_{\mathbf{y}\mathbf{y}}[n] = P_b \mathbf{A} \phi_n \phi_n^H \mathbf{A}^H + \sigma_e^2 \mathbf{I} \quad (6)$$

where $P_b = \mathbb{E}\{b[l]b[l]^*\}$, $\phi_n = [\phi_{0,n} \phi_{1,n} \dots \phi_{d,n}]^T$, $\mathbf{A} = [\mathbf{a}_0 \mathbf{a}_1 \dots \mathbf{a}_d]$, \mathbf{I} denotes the identity matrix, and σ_e^2 is the power of \mathbf{e}_n , which does not depend on n . As a result we have that $\mathbf{R}_{\mathbf{y}\mathbf{y}}[n]$ is the sum of a rank 1 positive definite signal matrix $\mathbf{A} \phi_n \phi_n^H \mathbf{A}^H$

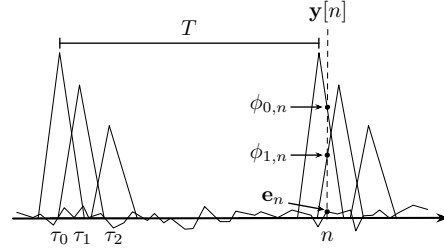


Fig. 1. Example of the underlying analog signal $\mathbf{y}(t)$ corresponding to $\mathbf{y}[n]$ as the sum of a signal term and a noise term, assuming $d = 2$.

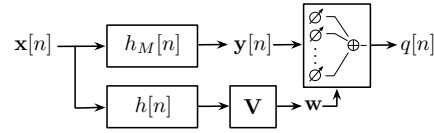


Fig. 2. Proposed processing with a new filter $h[n]$ parallel to the traditional matched filter $h_M[n]$ and followed by an estimation stage of \mathbf{V} , which finally produces the weights \mathbf{w} to apply to $\mathbf{y}[n]$.

and a full-rank positive definite noise matrix $\sigma_e^2 \mathbf{I}$. Thus, the eigendecomposition of $\mathbf{R}_{\mathbf{y}\mathbf{y}}[n]$ has the particular property that its eigenvalues are $\lambda_{n,1} > \lambda_{n,2} = \dots = \lambda_{n,m} = \sigma_e^2$ and the eigenvector associated with $\lambda_{n,1}$ is a scaled version of $\mathbf{A} \phi_n$.

Now assume that we estimate $\mathbf{R}_{\mathbf{y}\mathbf{y}}[n]$ for a given sample times n_1, \dots, n_S within a period N through (4). Then the eigenvectors $\mathbf{v}_1, \dots, \mathbf{v}_S$ corresponding to the maximum eigenvalues of $\mathbf{R}_{\mathbf{y}\mathbf{y}}[n_1], \dots, \mathbf{R}_{\mathbf{y}\mathbf{y}}[n_S]$ can be obtained via an eigendecomposition. As they are a scaled version of the vectors $\mathbf{A} \phi_{n_1}, \dots, \mathbf{A} \phi_{n_S}$, then the image space of the matrix $\mathbf{V} = [\mathbf{v}_1 \dots \mathbf{v}_S] \in \mathbb{C}^{m \times S}$ is:

$$\text{Im}[\mathbf{v}_1 \dots \mathbf{v}_S] = \text{Im}[\mathbf{A} \phi_{n_1} \dots \mathbf{A} \phi_{n_S}] = \text{Im} \mathbf{A} \Phi \quad (7)$$

where $\Phi = [\phi_{n_1} \dots \phi_{n_S}]$ and Im denotes the image space. Finally, if the set $\{\phi_{n_1}, \dots, \phi_{n_S}\}$ contains $d+1$ linearly independent vectors, then Φ will be full row rank. As a consequence, $\text{Im} \mathbf{V}$ will be $\text{Im} \mathbf{A} \Phi = \text{Im} \mathbf{A}$, which is the space spanned by all the spatial signatures. However, if the previous condition is not fulfilled, then $\text{Im} \mathbf{A} \Phi \subsetneq \text{Im} \mathbf{A}$, and we do not obtain as much information as in the previous case.

As defined in (5), the coefficients $\phi_{k,n}$ are mainly the correlation contributions of the received signals after despreading. Hence, the shape of $r_{cc}[n]$ plays a decisive role in the linear independence among $\phi_{n_1}, \dots, \phi_{n_S}$. Fig. 1 illustrates this observation and that samples close to τ_0 will produce nearly linearly dependent vectors if the multipath signals are close enough to the LOSS, i.e. $\tau_k - \tau_0$ small enough for some $k \neq 0$, which results in a rank deficient matrix Φ . A natural question is then if there exists an approach different than despreading that provides a different Φ with some structure that allows us to extract information about the multipath subspace from \mathbf{V} . As despreading can be modeled as a discrete matched filter with impulse response $h_M[n] = c^*[-n]$, using another FIR filter $h[n]$ seems a reasonable decision. As tracking cannot be properly achieved without $h_M[n]$, then $h[n]$ should be only used to calculate the multipath subspace and hence, the beamforming weights. Fig. 2 shows the proposed processing scheme in the case of applying \mathbf{w} to $\mathbf{y}[n]$, which results in the signal $q[n] := \mathbf{w}^H \mathbf{y}[n]$.

3.2. Inverse FIR Filtering

As Fig. 1 shows, a filter $h[n]$ that gives a narrower response to $c[n]$ than $h_M[n]$ should greatly improve the structure of Φ . The narrowest possible response corresponds to:

$$c[n] * h[n] = \delta[n] \quad (8)$$

where $\delta[n]$ is the dirac impulse and $*$ denotes convolution. This obviously gives linearly independent vectors in Φ . However, the zeros in the spectrum of $c[n]$ produce a very high response in the spectrum of $h[n]$, which amplifies the input noise too much. Furthermore, a solution to (8) may not exist.

To avoid the first limitation, we introduce white noise $z[n]$ with power $\epsilon \in \mathbb{R}^+$ together with $c[n]$ to the input of the filter to design. The idea behind this is that, in order for the output to be as close as possible to $\delta[n]$, the filter $h[n]$ should also mitigate the noise $z[n]$ since it is uncorrelated with $c[n]$. To address the second limitation, we find the filter that minimizes the error between the reference $\delta[n]$ and the real output as:

$$\underset{\mathbf{h}}{\operatorname{argmin}} E\{\|\mathbf{d} - (\mathbf{c} + \mathbf{z}) * \mathbf{h}\|^2\} \quad (9)$$

where $\mathbf{d} \in \mathbb{R}^{2N-1}$, $\mathbf{c} \in \mathbb{C}^N$, $\mathbf{z} \in \mathbb{C}^N$ and $\mathbf{h} \in \mathbb{C}^N$ are the column vectors that contain the samples of $\delta[n]$, $c[n]$, $z[n]$ and $h[n]$ respectively, and $\|\cdot\|$ is the 2-norm. Note that $h[n]$ is chosen to have the same length as the matched filter $h_M[n]$. After some manipulations, the solution to (9) becomes:

$$\tilde{\mathbf{h}} = [\mathbf{R}_{cc} + N\epsilon\mathbf{I}]^{-1} \mathbf{h}_M \quad \epsilon \in \mathbb{R}^+ \quad (10)$$

where $\mathbf{h}_M \in \mathbb{C}^N$ corresponds to $h_M[n]$ and $\mathbf{R}_{cc} \in \mathbb{C}^{N \times N}$ is defined as $\mathbf{R}_{cc}(k, l) = r_{cc}[k - l]$.

The filter described by (10) has a degree of freedom given by ϵ . This parameter allows us to vary the behaviour of the filter depending on the scenario of interest. However, note that $\tilde{\mathbf{h}}$ verifies $\lim_{\epsilon \rightarrow \infty} \tilde{\mathbf{h}} / \|\tilde{\mathbf{h}}\| = \mathbf{h}_M / \|\mathbf{h}_M\|$, and hence it only attains a scaled version of \mathbf{h}_M for very large ϵ . In order to overcome this limitation and obtain a more practical filter, we finally propose:

$$\mathbf{h} = [(1 - \rho)\mathbf{R}_{cc} + \rho\mathbf{I}]^{-1} \mathbf{h}_M \quad \rho \in [0, 1] \quad (11)$$

which let the designer to obtain \mathbf{h}_M and the same possible filters as in (10) up to a scaling factor using $\rho = N\epsilon/(1 + N\epsilon)$. With this notation we have that $\rho = 0$ corresponds to $\epsilon = 0$, and hence we refer to the solution as the inverse filter or \mathbf{h}_I . In contrast, $\rho = 1$ corresponds to $\epsilon \rightarrow \infty$, and we obtain \mathbf{h}_M . For $\rho \in (0, 1)$ we obtain an intermediate behavior between \mathbf{h}_I and \mathbf{h}_M . The lower ρ is, the narrower the response to $c[n]$ is, but the lower the Signal-to-Noise Ratio (SNR) is, which gives us a trade-off between resolution and SNR. More precisely, the SNR at the output of the filter \mathbf{h} , which is defined as the ratio between the signal power and noise power at one of the peak samples, can be written as:

$$\text{SNR} = \text{SNR}_{\text{in}} \frac{\mathbf{c}^H [(1 - \rho)\mathbf{R}_{cc} + \rho\mathbf{I}]^{-1} \mathbf{c}}{\mathbf{c}^H [(1 - \rho)\mathbf{R}_{cc} + \rho\mathbf{I}]^{-2} \mathbf{c}} \quad (12)$$

where SNR_{in} is the input SNR. Fig. 3 shows the SNR versus ρ for different values of the sampling frequency f_s .

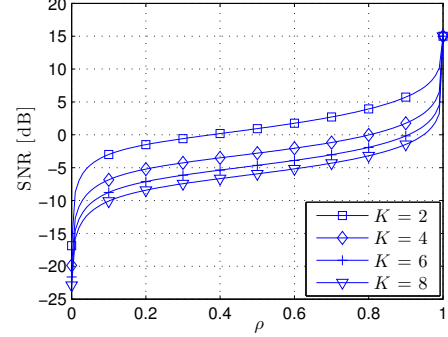


Fig. 3. SNR versus ρ for f_s equal to K samples per chip. The SNR_{in} is computed assuming $\text{CN}_0 = 45\text{dB-Hz}$ and the corresponding f_s .

3.3. Multipath Subspace Estimation and Robust Beamforming

The proposed method for estimating the multipath subspace starts by obtaining the matrix \mathbf{V} from the output of the filter (11) only for those samples that contain signal contribution, since the other eigenvectors do not give information about the multipath subspace. Assuming that (8) holds, each signal contribution is only present in one sample and the maximum eigenvalue of $\mathbf{R}_{yy}[n_i]$ is:

$$\lambda_{i,1} = \begin{cases} \sigma_e^2 & \text{if } \nexists k : n_i = \tau_k \\ \sigma_e^2 + mP_k \frac{(\mathbf{c}^H \mathbf{R}_{cc})^2}{\|\mathbf{R}_{cc}\|^2} & \text{if } \exists k : n_i = \tau_k \end{cases} \quad (13)$$

where $P_k := |\alpha_k|^2 P_b$ and $\mathbf{R} := [(1 - \rho)\mathbf{R}_{cc} + \rho\mathbf{I}]^{-1}$.

From (13), a threshold λ_1 must be defined to determine whether a sample contains signal contribution or not. As \mathbf{h}_I is an approximate solution of (8), each signal contribution may be present in more than one sample. Furthermore, in practice some estimation errors occur when calculating the eigenvalues. These two facts imply that the property (13) will hold only approximately, and hence λ_1 must not be as restrictive as $\sigma_e^2 + mP_k (\mathbf{c}^H \mathbf{R}_{cc})^2 / \|\mathbf{R}_{cc}\|^2$, but instead, an intermediate value should be chosen between the two possible values presented in (13). As the values of P_k are unknown, a reasonable choice is to always use a rough estimate of P_0 divided by some factor in order to also take the multipath into account. Those weak multipaths that do not exceed λ_1 will not be detected, but their impact can be neglected.

Once \mathbf{V} is obtained, the LOSS contribution must be removed. Assuming that we use a sufficiently small sampling period (e.g. $T_s \leq \tau_k - \tau_0 \forall k \neq 0$ when $\rho = 0$), an eigenvector that only has a contribution from \mathbf{a}_0 exists, and the remaining ones only have multipath contributions. As a result, the entire LOSS contribution can be found by the following search:

$$\underset{\mathbf{v}_i}{\operatorname{argmax}} |\mathbf{v}_i^H \mathbf{a}_0| \quad (14)$$

Then, removing this vector from \mathbf{V} results in a matrix $\bar{\mathbf{V}}$ that spans the multipath subspace. If the sampling period is not sufficiently small, equation (14) just allows us to remove a portion of the LOSS contribution, which worsens the estimation of the multipath subspace from $\bar{\mathbf{V}}$. However, the fact that $\bar{\mathbf{V}}$ contains a small contribution of \mathbf{a}_0 does not necessarily prevent the successful application of the method, as it will be shown in the numerical results.

Once $\bar{\mathbf{V}}$ is estimated, designing the beamforming weights $\mathbf{w} \in \mathbb{C}^m$ that mitigate the multipath is not an issue. We propose a distortionless beamformer, i.e. $\mathbf{w}^H \mathbf{a}_0 = 1$, that lies in the subspace orthogonal to $\text{Im } \bar{\mathbf{V}}$, i.e. $\mathbf{w} \perp \text{Im } \bar{\mathbf{V}}$. Among all possible solutions, a very straightforward one is:

$$\mathbf{w} = \frac{\mathbf{P}_{\bar{\mathbf{V}}}^\perp \mathbf{a}_0}{\mathbf{a}_0^H \mathbf{P}_{\bar{\mathbf{V}}}^\perp \mathbf{a}_0} \quad (15)$$

where $\mathbf{P}_{\bar{\mathbf{V}}}^\perp = \mathbf{I} - \bar{\mathbf{V}}(\bar{\mathbf{V}}^H \bar{\mathbf{V}})^{-1} \bar{\mathbf{V}}^H$.

3.4. Discussion

The SNR at the output of our filter \mathbf{h} is notably degraded for $\rho < 1$, which renders the output signal useless for time-delay estimation by current single-antenna techniques. The impact of this low SNR behavior on the multipath estimation technique manifests itself in producing higher noise eigenvalues for $\hat{\mathbf{R}}_{\mathbf{y}\mathbf{y}}$. However, as $\hat{\mathbf{R}}_{\mathbf{y}\mathbf{y}}$ is used in practice and the estimation errors increase if the SNR decreases, increasing the averaging time L becomes indispensable. As a result, the lower the ρ , the higher the time devoted to multipath estimation must be, which yields a trade-off between resolution and computing time. A different way to improve resolution is to increase the sampling frequency $f_s := 1/T_s$, since for $\rho = 0$ the proposed method is able to mitigate those multipath reflections with $\tau_k - \tau_0 \geq T_s$. But Fig. 3 shows that increasing f_s gives lower SNR, so a similar trade-off is also present.

Finally, note that there exist some issues in a real system that have not been considered in our results and deserve special attention for future work. First, \mathbf{h} will not be perfectly matched to the input, as the sampling of the input and reference signals are not necessarily the same. Second, the delay of each signal is not necessarily an integer number. As a result, when a signal or multipath is received, the corresponding output contribution may be distributed among two samples. This means that $\bar{\mathbf{V}}$ can still have a contribution from the LOSS after using (14), which worsens the performance of \mathbf{w} .

4. NUMERICAL RESULTS

This section presents some numerical examples of the proposed multipath mitigation technique in a scenario with $\text{CN}_0 = 45\text{dB-Hz}$. We assumed that a Global Positioning System (GPS) LOSS signal and two multipaths are received by a 5-element antenna array with delays τ_1 and τ_2 so that $\tau_1 - \tau_0 = T_c/4$ and $\tau_2 - \tau_0 = 5T_c/4$. The GPS signal consists of several navigation data bits at a rate of 50bps. Each bit contains 20 copies of a coarse acquisition (C/A) code of 1023 chips, so $T = 1\text{ms}$ and $T_c \approx 1\mu\text{s}$, and a rectangular pulse shaping is assumed for simplicity.

In order to contrast the resolution offered by the matched filter and the inverse filter, Figure 4 plots the corresponding noiseless outputs for a sampling frequency $f_s = 8.184\text{ MHz}$. It is very clear that \mathbf{h}_I allows us to distinguish the 3 received signals. In contrast, \mathbf{h}_M has such low resolution that the contribution of the 3 signals basically becomes one wide peak.

Figure 5 shows the performance obtained by the weights of (15) with $f_s = 4.092\text{ MHz}$. This value is chosen to prove that $T_s = \min\{\tau_k - \tau_0 : k = 1, 2\}$ is small enough for the method to work satisfactorily. The figure plots the spatial attenuation $|\mathbf{w}^H \mathbf{a}_0|^2 / (0.5|\mathbf{w}^H \mathbf{a}_1|^2 + 0.5|\mathbf{w}^H \mathbf{a}_2|^2)$ versus the value of ρ . For low ρ , the filter \mathbf{h} gives very narrow peaks but the SNR is so low that the eigenvalue estimates are very noisy. Then, when ρ is

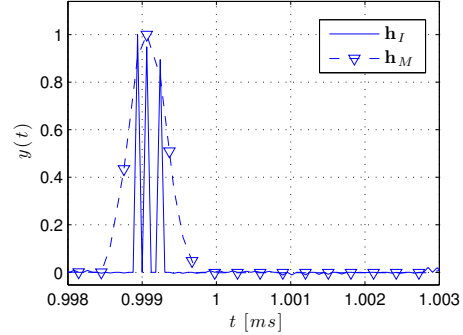


Fig. 4. Normalized noiseless output signal $y(t)$ from \mathbf{h}_M and \mathbf{h}_I versus time t . Scenario with sampling frequency $f_s = 8.184\text{ MHz}$, $\alpha_1/\alpha_0 = 0.9$, $\alpha_2/\alpha_0 = 0.8$, $\tau_1 - \tau_0 = T_c/4$ and $\tau_2 - \tau_0 = 5T_c/8$.

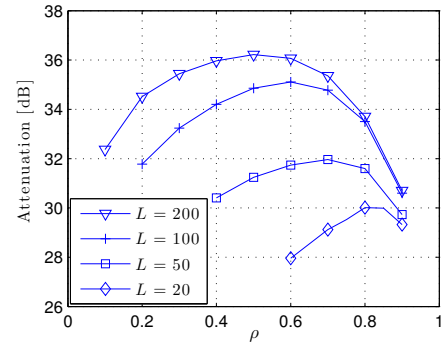


Fig. 5. Attenuation versus ρ . Scenario with sampling frequency $f_s = 4.092\text{ MHz}$, $\alpha_1/\alpha_0 = 0.9$, $\alpha_2/\alpha_0 = 0.8$, $\tau_1 - \tau_0 = T_c/4$ and $\tau_2 - \tau_0 = 5T_c/4$. The directions of arrival are $\theta_0 = 40^\circ$, $\theta_1 = 90^\circ$ and $\theta_2 = 140^\circ$.

increased, \mathbf{h} gives wide peaks but the SNR increases and the performance improves. This happens until a certain point, where the peaks are so wide that $\bar{\mathbf{V}}$ has some contribution from \mathbf{a}_0 . Then $\mathbf{w} \perp \bar{\mathbf{V}}$ also deletes the LOSS and the performance decreases. This explains why all curves show a maximum for $\rho \in (0, 1)$. Finally note that when the averaging time L increases, the low SNR consequences are mitigated and hence a lower ρ can be used, so the position of the maximum is closer to $\rho = 0$.

5. CONCLUSION

In this work we have proposed a novel technique to estimate the subspace spanned by the spatial signatures of the GNSS multipath signals received by an antenna array. In order to do so, a tunable FIR filter that offers a trade-off between resolution and SNR has been used. Then, a beamformer that lies on the subspace orthogonal to the estimated multipath subspace can be obtained. Our simulation results have shown that the proposed beamformer effectively attenuates the multipath signals for several values of the FIR filter design parameter, and that this parameter can be adjusted in order to obtain the balance between resolution and SNR that maximizes the multipath attenuation.

6. REFERENCES

- [1] B. Hofmann-Wellenhof, H. Lichtenegger, and J. Collins, *Global Positioning System, Theory and Practice*. Springer-Verlag Wien New York, 2001.
- [2] M. Z. H. Bhuiyan and E. S. Lohan, "Advanced multipath mitigation techniques for satellite-based positioning applications," *Int. Journal of Navig. and Obs.*, 2012.
- [3] H. L. Van Trees, *Optimum Array Processing (Detection, Estimation, and Modulation Theory, Part IV)*, 1st ed. Wiley-Interscience, Mar. 2002.
- [4] B. Widrow, K. Duvall, R. Gooch, and W. Newman, "Signal cancellation phenomena in adaptive antennas: causes and cures," *IEEE Trans. Antennas Propag.*, vol. 30, no. 3, pp. 469–478, May 1982.
- [5] M. D. Zoltowski and F. Haber, "A Vector Space Approach to Direction Finding in a Coherent Multipath Environment," *IEEE Trans. on Antennas and Propag.*, vol. 34, no. 9, pp. 1069–1078, Sept. 1986.
- [6] Y. Bresler, V. Reddy, and T. Kailath, "Optimum beamforming for coherent signal and interferences," *IEEE Trans. ASSP*, vol. 36, no. 6, pp. 833–843, Jun. 1988.
- [7] S. Pillai and B. Kwon, "Forward/backward spatial smoothing techniques for coherent signal identification," *IEEE Trans. ASSP*, vol. 37, no. 1, pp. 8–15, Jan. 1989.
- [8] I. Ziskind and M. Wax, "Maximum Likelihood Localization of Multiple Sources by Alternating Projection," *IEEE Trans. ASSP*, vol. ASSP-36, no. 10, pp. 1553–1560, Oct. 1988.
- [9] F. Qian and B. D. V. Veen, "Quadratically constrained adaptive beamforming for coherent signals and interference," *Trans. on Signal Process.*, vol. 43, no. 8, pp. 1890–1900, 1995.
- [10] T.-S. Lee and T.-T. Lin, "Reception of coherent signals with steering vector restoral beamformer," *Signal Processing*, vol. 72, no. 3, pp. 141–145, 1999.
- [11] Y. Jiang, P. Stoica, Z. Wang, and J. Li, "Capon beamforming in the presence of steering vector errors and coherent signals," in *Proc. ASAP Workshop*, Lexington, MA, Jun. 2007.
- [12] K. Ichige, H. Li, and H. Arai, "SURE: Simultaneous DOA and polarization estimation for arbitrary array configurations," in *7th IEEE Conf. on Sensor Array and Multichannel Signal Process.*, Yokohama, Japan, Jun. 2012, pp. 293–296.
- [13] A. Naguib and A. Paulraj, "Performance of CDMA cellular networks with base-station antenna arrays," in *Mobile Commun. Advan. Syst. and Components*, ser. Lect. Notes in Comp. Science. Springer Berlin / Heidelberg, 1994, vol. 783, pp. 87–100.
- [14] J. Miller and S. Miller, "An adaptive antenna array for multiple received signals in direct-sequence code-division multiple-access communication systems," in *Proc. IEEE MILCOM*, Fort Monmouth, NJ, Oct. 1994, pp. 733–737.
- [15] J. Ramos, M. Zoltowski, and M. Urgos, "Robust blind adaptive array. A prototype for GPS," in *Proc. IEEE Int. Symp. on Phased Array Syst. and Tech.*, Boston, Massachusetts, Oct. 1996, pp. 406–410.
- [16] D.-J. Moelker and Y. Bar-Ness, "An optimal array processor for GPS interference cancellation," in *Proc. AIAA/IEEE Digital Avionics Syst. Conf.*, Atlanta, GA, Oct. 1996, pp. 285–291.
- [17] G. Seco and J. A. Fernández, "Multipath and Interference Errors Reduction in GNSS by Joint Pseudorange Measurement and Array Beamforming," in *Proc. Europ. Sym. on GNSS*, Munich, Germany, Apr. 1997, pp. 605–614.
- [18] W. Myrick, M. Zoltowski, and J. Goldstein, "Anti-jam space-time preprocessor for GPS based on multistage nested Wiener filter," in *Proc. IEEE MILCOM*, vol. 1, 1999, pp. 675–681.
- [19] M. Amin, L. Zhao, and A. R. Lindsey, "Subspace array processing for the suppression of FM jamming in GPS receivers," *IEEE Trans. on Aerospace and Electr. Syst.*, vol. 40, no. 1, pp. 80–92, Jan. 2000.
- [20] R. L. Fante and J. J. Vaccaro, "Wideband cancellation of interference in a GPS receive array," *IEEE Trans. on Aerospace and Electronic Syst.*, vol. 36, no. 2, pp. 549–564, Apr. 2000.
- [21] R. G. Lorenz and S. P. Boyd, "Robust beamforming in GPS arrays," in *Proc. ION Nation. Technic. Meeting*, San Diego, CA, Jan. 2002.
- [22] S.-J. Kim and R. A. Iltis, "GPS C/A code tracking with adaptive beamforming and jamming," in *Proc. Asilomar Conf. on Signals, Syst. and Comput.*, vol. 2, Pacific Grove, CA, Nov. 2002, pp. 975–979.
- [23] —, "STAP for GPS receiver synchronization," *IEEE Trans. Aerosp. and Electr. Syst.*, vol. 40, no. 1, pp. 132–144, Jan. 2004.
- [24] S. seung Hwang and J. J. Shynk, "An adaptive array based on composite and null despanders for multiple GPS signals," in *Proc. Asilomar Conf. on Signals, Syst. and Comput.*, Pacific Grove, CA, Nov. 2005, pp. 807–810.
- [25] G. Seco-Granados, J. A. Fernandez-Rubio, and C. Fernandez-Prades, "ML estimator and hybrid beamformer for multipath and interference mitigation in GNSS receivers," *IEEE Trans. on Signal Process.*, vol. 53, no. 3, pp. 1194–1208, Mar. 2005.
- [26] M. Amin and W. Sun, "A novel interference suppression scheme for global navigation satellite systems using antenna array," *IEEE Journal on Selected Areas in Commun.*, vol. 23, no. 5, pp. 999–1012, May 2005.
- [27] W. Sun and M. Amin, "Maximum signal-to-noise ratio GPS anti-jam receiver with subspace tracking," in *Proc. IEEE ICASSP*, vol. 4, Philadelphia, PA, Mar. 2005, pp. 1085–1088.
- [28] M. Sahmoudi and M. Amin, "Optimal robust beamforming for interference and multipath mitigation in GNSS arrays," in *Proc. IEEE ICASSP*, vol. 3, Honolulu, Hawaii, Apr. 2007.
- [29] D. Lu, R. Wu, P. Li, and Z. Su, "GPS smart jammer suppressin algorithm based on spatial APES," in *Proc. Int. Symp. on Intellig. Signal Process. and Commun. Syst.*, Xiamen, China, Dec. 2007, pp. 88–91.
- [30] J. L. Vicario, F. Antreich, M. Barcelo, N. Basta, J. Cebrian, M. Cuntz, O. Gago, L. Gonzales, V. Heckler, C. Lavin, M. Manosas-Caballu, J. Picanyol, G. Seco-Granados, M. Sgammini, and F. Amarillo, "ADIBEAM: Adaptive digital beamforming for Galileo reference ground stations," in *Proc. ION GNSS*, Portland, OR, Sep. 2010, pp. 172–184.
- [31] S. Backén, "On dynamic array processing for GNSS software receivers," Ph.D. dissertation, Lulea Univ. of Techn., 2011.
- [32] D. de Lorenzo, F. Antreich, H. Denks, A. Hornbostel, C. Weber, and P. Enge, "Testing of adaptive beamsteering for interference rejection in GNSS receivers," in *Proc. Europ. Navig. Conf. - GNSS*, 2007.

Paper E

Robust Time-Slotted Round-Trip Carrier and Timing Synchronization for Distributed Beamforming

© 2011 EURASIP. Reprinted with permission from M. Mañosas-Caballú and G. Seco-Granados, Proc. EUSIPCO (Aug. 2011), pp. 1190-1194.

ROBUST TIME-SLOTTED ROUND-TRIP CARRIER AND TIMING SYNCHRONIZATION FOR DISTRIBUTED BEAMFORMING

Martí Mañosas-Caballú, Gonzalo Seco-Granados

Telecommunications and Systems Engineering Department, Universitat Autònoma de Barcelona
Edifici Q - Campus de la UAB, 08193, Bellaterra (Barcelona), Spain
phone: (+34) 93 581 40 30, fax: (+34) 93 581 40 31, email: {marti.manosas, gonzalo.seco}@uab.cat
web: spcomnav.uab.es

ABSTRACT

Distributed beamforming has arisen as a significant approach in multi-user wireless communication systems. It allows several transmitters with common information to emulate an antenna array and focus their transmissions towards an intended destination. However, carrier and timing synchronization among the transmitters is necessary to ensure that the information is aimed in the desired direction. In this work we present a robust time-slotted round-trip carrier and timing synchronization protocol that is valid in dynamic environments in the sense that sensors can disappear from the network without affecting the performance severely. The protocol is based on the execution of simple rules at each sensor and leaves freedom to choose those signals that provide better timing synchronization. Numerical results show that a large fraction of the maximum beamforming gain can be maintained for death ratios as high as 50%.

1. INTRODUCTION

A fundamental problem in ad-hoc wireless networks such as wireless sensor networks (WSN) is the use of energy-efficient communication techniques. Lately, much of the research in this area has focused on cooperative approaches. The term “cooperative communication” typically refers to a system where users share and coordinate their resources in order to improve the quality of their transmissions [1]. The idea is particularly attractive in wireless scenarios due to both the large variety of channel qualities for different transmitter-receiver pairs and the limited energy and bandwidth resources.

Conventional transmit beamforming is a communication technique that allows a transmitter with several antennas to focus its bandpass signal in an intended direction. The advantages of conventional transmit beamforming are numerous and well-documented in the literature [2]. For instance, by focusing the transmission towards the intended destination, less transmit power is needed to achieve a desired signal-to-noise ratio (SNR) target, which is known as *beamforming gain*. This feature is particularly appealing in wireless communication systems with energy constrained nodes such as sensor networks. However, in this type of systems nodes are typically too small to allow for the use of conventional antenna arrays.

Recently, the idea of transmit beamforming has been extended to distributed networks of single-antenna transmitters. By means of cooperation, transmitters can emulate a conventional beamformer and behave as a “distributed beamformer”. The idea is that individual sources with common information transmit with phase and time aligned carriers such

that their bandpass transmissions combine constructively at the intended destination. Nevertheless, unlike conventional beamforming, in distributed networks each transmitter has an independent and imperfect oscillator. For this reason, it is necessary to synchronize the signals of the transmitters.

In this work we distinguish three types of synchronization procedures that complement each other for the pursued goal: *carrier frequency synchronization* lets each user work with the same carrier frequency; *carrier phase synchronization* makes each carrier arrive with the same phase at the destination; finally *timing synchronization* is necessary in order to achieve simultaneity of the signals at the receiver. Although there exist several papers that investigate the practical problem of multi-user carrier synchronization for distributed beamforming, most of them are still very preliminary because they either do not solve all types of synchronization or consider ideal scenarios. Some of these methods are [3–7].

One of the latest techniques can be found in [8], and it solves the three commented synchronization procedures while avoids the communication from sensors to destination. The other methods only focus on achieving frequency and phase synchronization, what implies that it can exist a mismatch in the symbols alignment at the receiver and hence an imperfect addition of the information is likely to occur. The impact of this phenomenon worsens for high data-rate transmissions. For this reason those methods that do not provide timing synchronization present limitations in many scenarios. In addition, it is also important to bear in mind that sensors in a WSN can leave the network without previous warning. An example of this happens when a sensor breaks down, hence being unable to send any type of notification prior to its disappearance. To the best of our knowledge, it does not exist any work that presents a distributed beamforming scheme suitable for this kind of dynamic environments.

In this paper we present a new synchronization protocol based on the work of [8]. The two main contributions of the paper are: i) the protocol is robust in dynamic environments in the sense that sensor disappearances can occur without affecting the performance of the system severely; ii) synchronization procedures are separated in such a manner that they allow the use of specific signals for high accuracy timing synchronization. The robustness of the protocol is achieved thanks to the execution of simple rules at each sensor.

We also analyse the performance of the proposed algorithm in terms of the beamforming gain and its dependency on estimation errors. We show that a large fraction of the maximum beamforming gain can be sustained, even when 50% of the existing nodes disappear during the synchronization procedure (i.e. when the death ratio is equal to 50%).

2. SYSTEM MODEL

Let us consider a system of N sensors S_j for $j = 1, \dots, N$ arbitrarily distributed over some region and with a limited maximum transmit power. The index j represents only a logical position used to apply the different steps of the protocol described in Section 3.

Consider also a distant base station which acts as a destination (D_0) and is not power constrained. The nodes want to send a common message $m(t)$ modulated on a carrier frequency f_c to D_0 , as shown in Fig. 1. In order to assure correct transmission of the information from the N sensors to the base station, a distributed beamforming protocol is applied. Note that the proposed model is not related to any specific network topology. In fact, it can represent one link of a larger network that includes many-to-one transmissions. For instance, S_1, \dots, S_N could be a group of relay nodes used to transmit from a distant source to the destination.

We suppose the transmitted carrier signal by node S_j is:

$$x_j(t) = \cos(2\pi f_j(t - t_j^*) + \phi_j) \quad t \geq t_j^* \quad (1)$$

where t refers to the time, f_j is the carrier frequency, ϕ_j is the initial phase and t_j^* is the transmission starting instant.

The channel from node S_i to node S_j (including D_0 with the index 0) is assumed to be *flat fading* and invariant with impulse response $h_{i,j}$ during the transmission of a message. Therefore, the channel can be characterized by an attenuation $\alpha_{i,j}$, a propagation delay $\tau_{i,j}$, and a phase $\phi_{i,j}$ on the top of the one caused by the propagation delay. In this situation the signals will combine constructively at the destination whenever the carriers are fully synchronized. Thus we can simplify the problem by omitting each baseband signal and considering only the corresponding carrier. Finally, we also assume channel reciprocity such that $h_{i,j} = h_{j,i}$.

With these assumptions, the received signal at destination D_0 produced by the transmission of the signal (1) is:

$$y_{j,0}(t) = \alpha_{j,0} \cos(2\pi f_j t + \phi_{j,0}^{eq}) + n_0(t) \quad (2)$$

where $\phi_{j,0}^{eq} = \phi_j + \phi_{j,0} - 2\pi f_j t_j^* - 2\pi f_j \tau_{j,0}$ is the equivalent phase of the signal at time $t = 0$ and $n_0(t)$ denotes the additive white Gaussian noise (AWGN). Note that the expression of (2) is only valid for $t \geq t_j^* + \tau_{j,0}$. This formulation will help us to explain our new round-trip protocol in section 3.

Next we describe the key aspects that make distributed beamforming more challenging than the conventional case. First of all we remark that each source keeps its local time using its own local oscillator, which implies the following:

- The nodes do not possess a common time scale due to the use of imperfect oscillators.
- The nodes do not possess a common time reference due to the use of independent oscillators.

Because of this, none of the nodes in the system know the “true” time and then they do not know the “true” frequency or phase of their local oscillator either. This means that nodes cannot generate absolute phase or frequency estimates with respect to the “true” time. We model this phenomenon by relating the “true” time t and the j -th sensor time $t^{(j)}$ through a multiplicative factor ε_j and an offset δ_j :

$$t^{(j)} = \varepsilon_j \cdot t + \delta_j \quad (3)$$

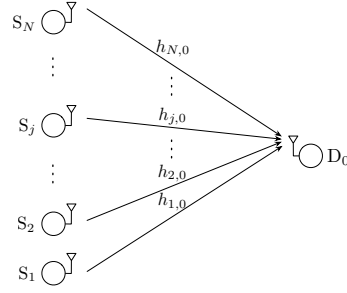


Figure 1: System model for a network of N sensors and a base station D_0 .

In addition to the aforementioned two points, positions of the nodes are completely unknown either absolutely or relatively, which renders the delays $\tau_{j,0}$ between each sensor node and the base station unknown. The lack of a common time scale makes only coherence (i.e. carrier phase alignment) difficult and can be solved by means of frequency synchronization. However, the uncertainty of the positions and the lack of a common time reference make it difficult to obtain both simultaneity and coherence at the destination. This can be solved through phase and timing synchronization.

Finally note that the coherent transmission cannot last an unlimited period of time due to synchronization errors. The beamforming protocol will need to resynchronize periodically in order to avoid unacceptable phase drift during beamforming. As a consequence, we distinguish two separate procedures: the beamforming stage T_{beam} and the synchronization stage T_{syn} .

3. ROBUST ROUND-TRIP SYNCHRONIZATION PROTOCOL

In this section we present the proposed robust time-slotted round-trip carrier synchronization protocol. The main goal of the protocol is to achieve frequency, phase and timing synchronization even if several sensors disappear at any time without previous warning.

3.1 Protocol overview

Our key proposal lies in splitting the whole problem in three independent requirements at the destination and provide a specific solution to each of them. This let us make synchronization procedures simple and somehow independent.

The first requirement is that all carriers arrive simultaneously at destination. The second requirement is that all carriers arrive with the same initial phase at destination (phase of (2) at $t = t_j^* + \tau_{j,0}$). Finally, the third requirement is that all carriers arrive with the same frequency at destination. Note that the fulfilment of the first two requirements implies that carriers arrive at destination coherently at the start of the beamforming. On the other hand, the third requirement lets each user maintain coherence over time.

The synchronization protocol begins with a calibration step in which the destination broadcasts at t_c a sinusoidal tone $x_0(t)$ of duration T_c and frequency f_c to all sensors:

$$x_0(t) = \cos(2\pi f_c(t - t_c) + \phi_c) \quad t \in [t_c, t_c + T_c]$$

Then, each sensor locally estimates the phase and frequency of the received tone as detailed in subsections 3.3 and 3.4.

Afterwards a total of $2N - 1$ consecutive timeslots TS_k for $k = 0, \dots, 2N - 2$ are used for the key part of the synchronization protocol, each of them starting at time t_k . Finally, an additional time T_{beam} is dedicated to beamforming. The activity in each timeslot is summarized here:

1. TS_0 : the destination broadcasts a temporal reference signal $r_0(t)$ of duration T_0 to all sensors.
2. TS_k for $k = 1, \dots, N - 1$: S_k broadcasts a temporal reference signal $r_k(t)$ of duration T_k to all sensors. The transmitted signal is sent just after the reception of the signal corresponding to the timeslot TS_{k-1} . We denote this set of slots as *up-cycle*.
3. TS_k for $k = N, \dots, 2N - 2$: S_{2N-k} broadcasts a temporal reference signal $r_{2N-k}(t)$ of duration T_{2N-k} to all sensors. The transmitted signal is sent just after the reception of the signal corresponding to the timeslot TS_{k-1} . We denote this set of slots as *down-cycle*.
4. $TS_{2N-1} = T_{beam}$: all sensors transmit to the destination as a distributed beamformer. This interval starts at t_{2N-1} , just after node S_1 receives the temporal reference signal from S_2 , at the end of the down-cycle.

In addition to these basic rules, each node has to count the time that elapses since the reception of each temporal reference signal. When this time exceeds the value of $(2T_p)m$ for some $m \in \mathbb{N}$, each node must deduce that m consecutive nodes have disappeared. Here T_p is an upper bound on the propagation delay between any two nodes of the network, and it should be known by all sensors. The value of $2T_p$ guarantees that there is enough time for a sensor to receive the temporal reference signal that is sent at a given timeslot TS_k since the reception of the temporal reference signal that is sent at TS_{k-1} .

Thanks to the simple exchange of reference signals, each sensor can readily deduce which nodes have disappeared by means of a counter and update its network view. Specifically a given sensor S_j is supposed to update the total number of nodes to $N - m$ and its position to $j - m$ when m consecutive nodes with a logical position below j die. When m nodes with a logical position above the given sensor die, only the variable N should be updated. The node following the last dead one is the responsible for sending the next temporal reference signal. This simple procedure prevents the nodes from being blocked by waiting for the reception of signals from missing sensors. In the following we describe in more detail how each type of synchronization is achieved in our protocol.

3.2 Timing synchronization

Our timing synchronization proposal makes use of the whole set of $2N - 1$ first timeslots. The rules are focused on letting each user know the precise moment it has to send the information towards the destination for achieving simultaneity during T_{beam} . In a general form each user S_j will send (at time t_j^*) after waiting a delay of τ_j seconds since the end of the emission of its temporal reference signal during the down-cycle:

$$t_j^* = t_{2N-j} + T_j + \tau_j \quad \forall j \in \{1, \dots, N\} \quad (4)$$

Although the first node is not supposed to send any temporal reference signal in the down-cycle, it also has to send towards destination according to (4), at time $t_1^* = t_{2N-1} + T_1 + \tau_1$.

The key point here is the way each sensor deduces its own delay τ_j . Similar to [8], the calculation of τ_j results

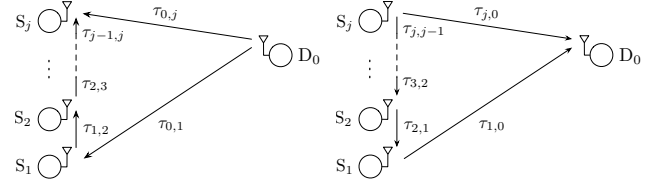


Figure 2: Path delays used for the deduction of τ_j .

from forcing that each signal $x_j(t)$ for $j = 2, \dots, N$ arrives at destination simultaneously with $x_1(t)$. A solution would be to use a value of τ_j equal to the difference between the arrival times at D_0 of both signals $x_j(t)$ and $x_1(t)$ when considering $\tau_j = 0$ in (4). After assuming reciprocity at each channel, it is easy to prove that this difference time can be estimated from the elapsed time between the end of the observation times at S_j of the signal coming from S_{j-1} during the up-cycle and the signal coming from D_0 :

$$\tau_j = (t_{j-1} + \tau_{j-1,j} + T_{j-1}) - (t_0 + \tau_{0,j} + T_0) \quad (5)$$

Fig. 2 depicts this idea. First, it shows the delays used by sensor S_j to calculate τ_j , and second the delays that S_j actually wants to emulate in order to achieve simultaneity.

However, in order to take into account possible disappearances supplementary rules must be applied. A node having m consecutive deaths below its logical position during the up-cycle, has an additional error in the calculus of τ_j corresponding to the performed waiting $(2T_p)m$ of the first alive sensor, which we denote by S_d . This waiting becomes an error because it is not performed again during the down-cycle.

In order to counteract this error, we propose that each affected node subtracts the known quantity $(2T_p)m$. Note that the generated time of a given sensor S_j will be affected by ϵ_j due to its imperfect clock (see (3)). Hence with this rule each node will produce $\bar{\tau}_j$ instead of (5) and use it in (4):

$$\bar{\tau}_j = \tau_j - \frac{(2T_p)m}{\epsilon_j}$$

where the error in the correction is:

$$e_j = (2T_p)m \left(\frac{1}{\epsilon_d} - \frac{1}{\epsilon_j} \right) \quad (6)$$

In case that m deaths occur during the down-cycle, there is no way to correct τ_j , and it is appropriate that those nodes that are positioned below the dead ones cancel beamforming.

Algorithm 1 shows the commented rules in an algorithmic form. We emphasize that it corresponds to a reduced version of our implemented code and that a realistic algorithm must consider that nodes may face some critical situations.

3.3 Frequency synchronization

Let us consider that the sinusoidal tone received at sensor S_j in the absence of noise produced by the emission of $x_0(t)$ during the calibration step can be written as:

$$y_{0,j}(t) = \alpha_{0,j} \cos(2\pi f_c(t - t_c - \tau_{0,j}) + \phi_c + \phi_{0,j}) \quad (7)$$

which is only valid for $t \in [t_c + \tau_{0,j}, t_c + \tau_{0,j} + T_c]$. As in (2), $\alpha_{0,j}$ and $\phi_{0,j}$ account for the channel effects, including multipath.

Algorithm 1 Network updating for timing synchronization

```

if  $m$  deaths below then
  if up-cycle then
     $N \leftarrow N - m, j \leftarrow j - m, \bar{\tau}_j = \tau_j - \frac{(2T_p)m}{\varepsilon_j}$ 
  else {down-cycle}
     $N \leftarrow N - m, j \leftarrow j - m$ 
  end if
else if  $m$  deaths above then
  if up-cycle then
     $N \leftarrow N - m$ 
  else {down-cycle}
     $N \leftarrow N - m$ , cancel beamforming
  end if
end if

```

Then we propose that each sensor generates its local estimate $\hat{f}_{c,j}$ of the frequency f_c from the received signal $y_{0,j}(t)$, and uses this estimation as the carrier frequency f_j of the signal (1) that has to be sent to the base station. Note that the frequency reading will be slightly modified by the time scale of each sensor, but the error will be counteracted by the same time scale when f_j is generated during T_{beam} .

3.4 Phase synchronization

In order to perform phase synchronization we must achieve that $\phi_{j,0}^{eq} = \phi_{i,0}^{eq} \forall j, i \in \{1, \dots, N\}$. Assuming that simultaneity is fulfilled at the destination, it is verified that $t_j^* + \tau_{j,0} = t_i^* + \tau_{i,0} \forall j, i \in \{1, \dots, N\}$. Hence, the previous condition reduces to:

$$\phi_j + \phi_{j,0} = \phi_i + \phi_{i,0} \quad \forall j, i \in \{1, \dots, N\} \quad (8)$$

which is equivalent to what is explained at the beginning of section 3: force all carriers to arrive with the same initial phase at destination. Note that we have assumed in (8) that $f_j = f_i \forall j, i \in \{1, \dots, N\}$, which is reasonable as sensors will be frequency synchronized before sending towards D_0 .

From (8) the only degrees of freedom are the initial phases of the transmitting carrier signals: ϕ_j for $j = 1, \dots, N$. Thus the optimal solution is that each sensor S_j uses a value for its initial carrier phase equal to $-\phi_{j,0}$ when transmitting towards the destination. In the following we show how each sensor can get a good alternative to this value from the calibration step.

Denoting the initial phase of $y_{0,j}(t)$ as $\phi_{0,j}$, that corresponds to the phase of (7) at time $t = t_c + \tau_{0,j}$, we see that:

$$\phi_{0,j} = \phi_c + \phi_{0,j}$$

Assuming reciprocity in all channels we can apply $\phi_{j,0} = \phi_{0,j} \forall j \in \{1, \dots, N\}$, from where we deduce that $-\phi_{0,j}$ is a good choice for the initial phase ϕ_j . For this reason we propose that each user S_j performs an estimate $\hat{\phi}_{0,j}$ of the initial phase of $y_{0,j}(t)$ and use it as $-\phi_j$. Note that this estimate will be generated from the same data as the frequency estimate.

3.5 Discussion

Unlike the current existing works, this protocol avoids the realization of a high number of frequency and phase estimations. However a considerable number of time-delay estimations is needed, whose errors affect the simultaneity and

hence can penalize the resulting beamforming. In order to overcome this limitation, reference signals should allow high accuracy delay estimation, such as Ultra-Wideband signals [9]. Note that, unlike in [8], we have not imposed any constraint on the nature of the reference signals, which leaves freedom to choose those signals that provide better simultaneity at destination, and this facilitates the use of future high data-rate transmissions.

We want to stand out that if $r_0(t)$ and the calibration signal $x_0(t)$ could be sent together, then the calibration procedure could be done in the timeslot TS_0 , which would reduce the synchronization time. Note that it is not vital to calibrate before each timing synchronization stage, though.

Regarding to the negative consequences of the sensors disappearances, we remark that the worst cases correspond to situations where deaths occur during the down-cycle, because it would imply that some alive sensors cancel beamforming until the end of the next synchronization stage. Fortunately, the probability that a sensor is alive during the up-cycle and dies during the down-cycle is very low given the short duration of these cycles compared to the beamforming time T_{beam} . For this reason we only need to consider the consequences of sensor disappearances during the up-cycle.

A good measure of the overhead is the ratio R between the wasted time due to deaths, i.e. $(2T_p)m$, and the total synchronization time. Assuming that the total synchronization time when no deaths occur follows an uniform distribution between 0 and $(2N-1)T_p$, the expected value of R for large networks ($N \rightarrow +\infty$) is:

$$\lim_{N \rightarrow +\infty} E\{R\} = r \log \left(\frac{r+1}{r} \right) \quad r \in (0, 1]$$

where r is the death ratio. For $r = 0$, R equals 0. This asymptotic value approximates $E\{R\}$ very accurately (the error in the approximation is less than 0.01 for $N \geq 15$).

4. SIMULATION RESULTS

This section presents numerical examples of the robust time-slotted round-trip carrier synchronization protocol. We assumed that $x_0(t)$ is sent at a frequency of 900 MHz and has a duration of $T_c = 5 \mu s$, where T_c can be large because the base station is not power constrained and the calibration step needs not be carried out very often. We also considered that all signals are received at a SNR of 20 dB.

Monte Carlo simulations with 5000 iterations were executed for all the examples, and at each iteration different estimations of the frequency, phase and time-delay were performed. The errors in the phase, frequency and time-delay estimates were modelled as Gaussian, with zero mean and standard deviation given by the corresponding Cramér-Rao bound. For those cases where we considered sensor disappearances, we selected different nodes to die at each iteration by following an uniform distribution. The error in the correction of τ_j was computed as in (6) and each sensor oscillator deviation factor ε_j was modelled as a Gaussian random variable with unitary mean and standard deviation $\sigma_\varepsilon = 10^{-6}$, which corresponds to a clock with 1 ppm precision.

The example of Fig. 3 shows the probability that the beamforming gain is greater than αN versus the elapsed time since the start of T_{beam} , where $\alpha \in [0, 1]$ and N is the maximum achievable gain. All time-delay estimations include errors with standard deviation $\sigma_\tau = 1 ps$. In order to show the

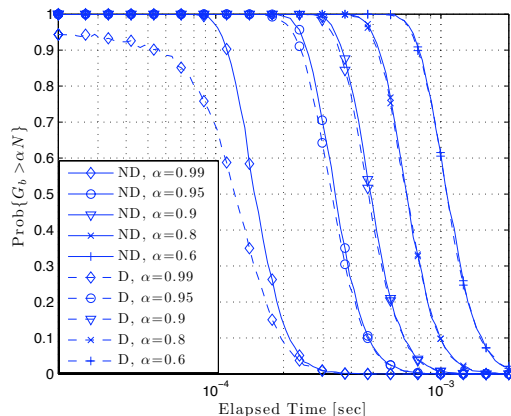


Figure 3: Probability that the beamforming gain (G_b) is greater than a fraction of the number of alive sensors ($N = 10$) versus elapsed time. The label “D” corresponds to deaths with $r = 0.5$. The label “ND” corresponds to no deaths.

robustness of our protocol we simulated cases where 50% of the sensors disappear during the up-cycle ($r = 0.5$). Higher ratios were considered and the results did not deteriorate up to 70%. We see how the carrier phases are efficiently aligned at the destination up to $600\mu\text{s}$, where a 60% quality beamforming no longer can be achieved with high probability.

We want to stand out that simulations of Fig. 3 were done for the same number of alive sensors in order to do a fair comparison. It means that the cases with deaths correspond to an scenario with N alive sensors when initially there were $2N$. On the other hand, the cases with no deaths correspond to an scenario with N sensors and no deaths.

The second example shows the performance of the protocol versus the delay estimation quality σ_τ . Concretely, Fig. 4 plots the achieved beamforming gain after $100\mu\text{s}$ for different number of sensors. The results for $r = 0$ and $r = 0.5$ were indistinguishable, so we only represent the first case. We can see that errors with $\sigma_\tau < 50\text{ps}$ are not deleterious for this protocol. For higher values, the imperfect simultaneity reduces the beamforming gain at the start of the beamforming stage, hence decreasing the beamforming time. In the case that reference signals let $\sigma_\tau = 1\text{ps}$, errors can be neglected.

We remark that we also corroborated the behaviour of our algorithm using an event-based implementation of the protocol in MATLAB[®], and results were satisfactory.

5. CONCLUSION

In this paper, we have proposed a robust time-slotted round-trip carrier and timing synchronization protocol for distributed beamforming in WSNs. We have described how the protocol prevents the nodes from being blocked and how it avoids cancelling beamforming when some sensors disappear. It has been shown that our proposal is based on a simple exchange of reference signals and a calibration signal.

We have analysed the performance of the protocol and its dependency on time-delay estimation errors. Our numerical results have shown that a good beamforming time can be achieved, even for cases where nodes disappear with death ratios as high as 50%. The effect of the quality of the delay estimations on the final beamforming time has shown that it is necessary to obtain accuracies as good as 50ps . However

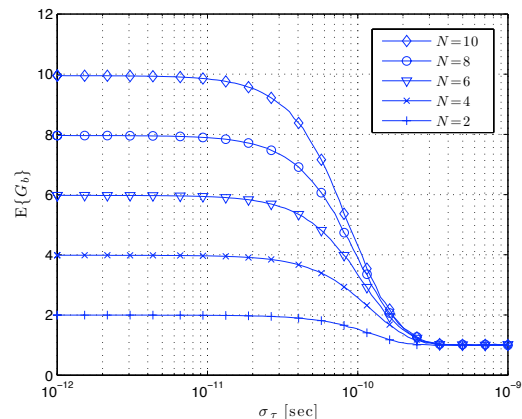


Figure 4: Expected beamforming gain versus delay estimation standard deviation σ_τ for several number of sensors N .

we leave freedom to choose those signals that provide better simultaneity at destination, which also makes possible the use of future high data-rate systems.

REFERENCES

- [1] Y. Hong, W. Huang, F. Chiu, and C. Kuo, “Cooperative Communications in Resource-Constrained Wireless Networks,” *IEEE Signal Process. Magazine*, vol. 24, pp. 47–57, May 2007.
- [2] H. L. Van Trees, *Optimum Array Processing (Detection, Estimation, and Modulation Theory, Part IV)*, 1st ed. Wiley-Interscience, March 2002.
- [3] Y.-S. Tu and G. Pottie, “Coherent cooperative transmission from multiple adjacent antennas to a distant stationary antenna through awgn channels,” in *Proc. IEEE Veh. Technol. Conf.*, vol. 1, Birmingham, AL, May 2002, pp. 130–134.
- [4] G. Barriac, R. Mudumbai, and U. Madhow, “Distributed beamforming for information transfer in sensor networks,” in *Proc. IEEE/ACM Int. Conf. on Inf. Process. in Sens. Net.*, Berkeley, CA, Apr. 2004, pp. 81–88.
- [5] R. Mudumbai, J. Hespanha, U. Madhow, and G. Barriac, “Scalable feedback control for distributed beamforming in sensor networks,” in *Proc. IEEE Int. Symp. Inf. Theory*, Adelaide, Australia, Sep 2005, pp. 137–141.
- [6] R. Mudumbai, G. Barriac, and U. Madhow, “On the feasibility of distributed beamforming in wireless networks,” *IEEE Trans. Wireless Commun.*, vol. 6, no. 5, pp. 1754–1763, May 2007.
- [7] Q. Wang and K. Ren, “Time-slotted round-trip carrier synchronization in large-scale wireless networks,” in *Proc. IEEE Int. Conf. on Commun.*, Beijing, China, May 2008, pp. 5087–5091.
- [8] D. Brown and H. Poor, “Time-slotted round-trip carrier synchronization for distributed beamforming,” *IEEE Trans. on Signal Process.*, vol. 56, no. 11, pp. 5630–5643, Nov. 2008.
- [9] S. Gezici, H. Celebi, H. Arslan, and H. Poor, “Theoretical limits on time delay estimation for ultra-wideband cognitive radios,” in *Proc. IEEE Int. Conf. on Ultra-Wideband*, Hannover, Germany, Sep. 2008, pp. 177–180.

Paper F

A Method and a Portable Rescue Device for Locating Avalanche Victims

Reprinted from M. Mañosas-Caballú and G. Seco-Granados,
WIPO Publications (Mar. 2015), WO/2015/040156.

A method and a portable rescue device for locating avalanche victims

Field of the Art

The present invention generally relates, in a first aspect, to a method for locating
5 avalanche victims, based on measurements of electromagnetic signals emitted from a
transmitter carried by a victim, and more particularly to a method comprising performing
a final approach step that exploits the spatial diversity provided by an array of magnetic
vector sensors.

A second aspect of the invention relates to a portable rescue device for locating
10 avalanche victims adapted to implement the method of the first aspect of the invention.

Prior State of the Art

A fundamental problem in the rescue of avalanche victims is the little time that an
injured person may remain alive when buried by snow after being struck by an
15 avalanche. Several studies agree that the chance of survival drops sharply after 15
minutes of being buried. That is why the rescues organized by outside groups are not
effective in saving the lives of the injured, and therefore the rescue has to be done by
those in the group who have not been buried by the avalanche, what is known as self-
rescue.

20 Given the time it takes to dig up an avalanche victim, the location of a victim has
to be resolved in a maximum of only 5 minutes. For this reason, one of the main
objectives in designing victim localization devices is that the search method
implemented by the device is as efficient as possible in terms of speed of localization.
Another important objective is to reduce as much as possible the complexity of its use,
25 so that factors such as panic, fatigue, adverse conditions or inexperience, cannot
prevent the rapid location of the victim.

Currently these self-rescue devices are known as Avalanche Victim Detector
(AVD) or Avalanche Transceiver (AT), and consist of an electromagnetic transmitter-
receiver equipped with three (or less) orthogonal coils acting like antennas, and are
30 governed by the rules laid down in the standard ETSI EN 300 718. By default, the
device operates in transmit mode, radiating a magnetic vector field $\mathbf{B}(t) = (B_x(t), B_y(t), B_z(t))$
through one of the coils that can be modelled as the field generated by a
magnetic dipole. The device uses a modulation A1A (carrier on/off) at the frequency
450KHz.

35 In case of an avalanche, the group members who have not been buried activate
the receive mode of the device, and start to search from the receiver measures at the

three coils. These three mutually orthogonal coils behave like a single antenna capable of obtaining the three vector components of $\mathbf{B}(t)$, that is, they behave like a single magnetic vector sensor. Since the vector $\mathbf{B}(t)$ is tangent to the field line of the emitted field, simply by following the direction of $\mathbf{B}(t)$ as its measure is being updated is enough to trace a path that coincides with said field line, which leads to the emitter. If there are L victims, then $L-1$ received signals are blocked to follow only the field line of one of them. By performing this protocol in an iterative manner the different victims are being encountered.

Two drawbacks affect this search method directly increasing the search time. First, the followed path is not straight. This makes the ride a little longer, and it does not allow the user to get an idea of the area where the victim can be until it is very close, because the directions change, although slightly, unpredictably for the user. Second, the direction of $\mathbf{B}(t)$ can vary greatly near the receiver, which can make the rescuer be easily confused, especially without proper training and a familiarization with the device. This second current limitation makes the known search method for the last few meters not to be based on the tracking of the field lines, but on power measurements only, which is known as fine search. As the fine search is still quite inaccurate, it leads to a time-consuming subsequent step known as pinpointing that consists on probing systematically starting from the estimated location until the victim is located. Left view of Fig. 1 illustrates the trajectories followed by a rescue user according to this conventional method, and will be described in more detail posteriorly.

There are several patent documents disclosing different rescue portable rescue devices and associated search methods, based on the detection of RF signals emitted by a transmitter of the avalanche victim, some of which emit a magnetic field pattern, acting as a magnetic dipole. Some of said patent documents based on the detection of said magnetic field patterns are cited next and their relevant background is briefly described.

US7116272B2 discloses a system and method for locating an avalanche victim based on the RF reception of the transmitted field as emitted by a distress beacon carried by the victim, during a search and rescue operation. It provides point to point directional data as to the direction of the RF field source based on flux field characteristics, and also an estimated distance between the searcher's receiver and the victim's transmitter field source using path loss slope and/or triangulation, where the estimation of distance is based upon field signal strength transmitted by the victim's transmitter avalanche or field strength changes in a certain direction with regard to the field lines and/or over a certain distance. Neither a direct estimation/calculation of the

magnetic dipole source position is disclosed in US7116272B2 nor the use of an array of magnetic vector sensors.

US6246863B1 discloses another rescue device for locating persons buried by avalanches also based on signal strength, which operates in either a transmit mode or a receive mode, and has a case and a harness constructed from belts for securing the case to the individual, where the rescue device switches on or off and changes its operating mode, between a transmission mode and a receiving mode, based on the locking or unlocking of the belts to the case. The device includes a display which provides graphic information to expedite searching, including graphical information related to when a coarse search or a pin-point search should be conducted, when the stage of a multistage amplifier should be changed, when the rescue device needs to be reoriented to obtain maximum signal strength, the signal strength as a bar graph and an estimated distance to the buried transmitter. Neither an array of magnetic vector sensors for providing spatial diversity nor a direct calculation of the transmitter position is disclosed in US6246863B1.

US2005151662 discloses an avalanche transceiver comprising a receiver including three mutually orthogonal receiving antennas each capable of receiving a radio signal at a predetermined frequency which are somewhat mutually orthogonal, and a processor that is capable of: selecting one or more of the said antennas, controlling the sensitivity of an antenna, and digitally processing received signals to measure signal strength and/or relative polarity for providing indications of the received flux field regarding proximity, horizontal alignment and vertical alignment. The provision of such three antennas is for always receiving the emitted signal in close proximity to a burial regardless of the orientation of the buried transmitter. Neither an array of magnetic vector sensors for providing spatial diversity nor a direct estimation/calculation of the transmitter position is disclosed in US2005151662.

US6167249 and US6484021 both disclose a rescue transceiver apparatus for transmitting a signal to and receiving a signal from another rescue transceiver apparatus is provided. The apparatus comprises a housing and a radio signal transmitter for the transmission of a radio signal in a transmitting mode with a first predetermined frequency with the radio signal transmitter being mounted within the housing. The receiver comprises first and second antennae arranged substantially perpendicular to each other, and a virtual third antenna being derived from phase information generated by the first antenna and the second antenna. The first antenna, the second antenna, and the third virtual third antenna provide three-dimensional vector analysis by the receiver of a predetermined frequency received from the radio transmitter. Neither an array of

magnetic vector sensors for providing spatial diversity nor a direct calculation of the transmitter position is disclosed in US6167249 nor in US6484021.

Description of the Invention

5 It is an object of the present invention to provide an alternative to the prior state of the art, which the purpose of achieving a faster and easier rescue of an avalanche victim than those provided by the devices and methods of the state of the art.

To that end, the present invention relates, in a first aspect, to a method for locating avalanche victims, comprising performing sequentially the next steps, in a
10 known manner:

a) an initial step comprising, a user carrying a portable electromagnetic signal receiver, performing an electromagnetic signal search by moving around a first area, away from the victim, in order to detect, by its reception with the portable electromagnetic signal receiver, an electromagnetic signal (generally the magnetic field
15 included therein) emitted by a portable electromagnetic signal transmitter carried by an avalanche victim and acting as a magnetic dipole;

b) a first tracking step, started after said electromagnetic signal has been detected and comprising measuring, with said portable electromagnetic signal receiver, the magnetic field emitted by said portable electromagnetic signal transmitter, and
20 moving, said user carrying said portable electromagnetic signal receiver, following a curve path coincident with the magnetic field line of said emitted magnetic field approaching to the victim through a second area closer thereto; and

c) a second tracking step performed after said first tracking step, comprising moving the user carrying the portable electromagnetic signal receiver through a third
25 area, even closer to the victim, for finally locating the victim.

Contrary to the known methods, the method of the first aspect of the invention comprises, in a characteristic manner, providing and using, as said portable electromagnetic signal receiver, a portable electromagnetic signal receiver with an array of magnetic vector sensors arranged for receiving said electromagnetic signal with
30 spatial diversity, and said step c) comprises, based on the measurement of said magnetic field performed with part or preferably all of said magnetic vector sensors, determining the location of said portable electromagnetic signal transmitter by estimating the spatial position of said magnetic dipole from output signals provided by said magnetic vector sensors of said array, exploiting their spatial diversity through one or
35 more array signal processing techniques.

The method comprises arranging said magnetic vector sensors of said array physically separated one from another by a minimum distance to provide said spatial diversity when they are at or below a predetermined distance from the portable electromagnetic signal transmitter.

5 The method of the first aspect of the invention comprises performing said step a) by using the output signal of one of said magnetic vector sensors, and if no signal is detected with only said magnetic vector sensor (or detected poorly), performing a detection by adding to each other the output signals provided by, preferably, each of the magnetic vector sensors when receiving said electromagnetic signal emitted by the
10 portable electromagnetic signal transmitter, thus achieving a signal-to-noise ratio much higher than the one achieved in the state of the art methods which perform said step a) with only one output signal, therefore reducing the time taken for performing step a), in comparison with the conventional search methods. For this step a), only detecting the electromagnetic signal is of interest. Moreover, in most cases there exists a long
15 distance to the avalanche victim and hence the spatial diversity provided by the magnetic vector sensors is not high. As a result, spatial diversity is not exploited in step a).

For another embodiment, step a) is performed, from the start to the end thereof, by performing said detection using array processing different than addition with the
20 output signals provided by each of the magnetic vector sensors (or at least by two or more of them).

The method of the first aspect of the invention comprises performing said step b) based on the measurement of said magnetic field performed with at least one of the magnetic vector sensors and/or based on the measurement of said magnetic field
25 performed by adding to each other the output signals provided by each of said magnetic vector sensors when measuring said magnetic field.

Particularly, for an embodiment, the method comprises starting performing step b) based on the measurement of the magnetic field performed by adding to each other the output signals provided by each of the magnetic vector sensors when measuring the
30 magnetic field and, once the output signal of one of the magnetic vector sensors so allows it, continuing performing step b) based on the measurement of the magnetic field performed with only said one of said magnetic vector sensors.

For an embodiment, the method of the first aspect of the invention comprises automatically stopping step b) and starting step c) upon considering, based on their
35 analysis, that the output signals of said magnetic vector sensors provide a degree of spatial diversity above a certain threshold and/or that the magnetic field lines information

calculated by said portable electromagnetic signal receiver does not allow performing the first tracking step with a certain amount of reliability.

The trajectory followed by the user at step c) can be a straight line (if possible due to geographical obstacles), hence providing a quicker approach to the victim than the curve trajectory of step b). Therefore, the sooner said spatial diversity is considered as allowing to start step c), the sooner step b) is stopped and step c) is started, thus reducing the time the user is arriving to the avalanche victim. Although the method of the first aspect of the invention has been described as including said step b), ideally it could work doing without it, i.e. passing directly from step a) to step c) if, when the electromagnetic signal has been received at step a) by the magnetic vector sensors, the spatial diversity provided thereby already allows the start of step c) that could happen, for example, if the victim is near the rescue user, or if the separation between the magnetic vector sensors is very high).

The trigger for activating step c) is preferably implemented automatically, based on the analysis of one or several parameters of the output signals of the magnetic vector sensors, such as their magnetic powers and directions.

A second aspect of the invention relates to a portable rescue device for locating avalanche victims, comprising:

- electromagnetic receiving means for receiving an electromagnetic signal emitted by a portable electromagnetic signal transmitter carried by an avalanche victim and acting as a magnetic dipole, and measuring the magnetic vector field emitted by said portable electromagnetic signal transmitter, and
- processing means connected to said electromagnetic receiving means for receiving and analysing electrical output signals provided thereby and providing to a user of the portable rescue device, through indication means thereof, indications regarding the result of said reception and analysis to allow him to perform said moving of the user through said first, second and third areas towards the victim of steps a), b) and c) of the method of the first aspect of the invention.

Depending on the embodiment, said indication means comprise at least one of a display (for displaying graphical information including, for example, a three-dimensional map of the search and rescue areas and the updating estimated locations of the victim) and acoustic means (for emitting acoustic signals differing in, for example frequency, volume or pitch, for indicating the different situations of the search).

Contrary to the known portable rescue devices for locating avalanche victims, in the one of the second aspect of the invention, in a characteristic manner, its receiving means comprise an array of magnetic vector sensors arranged for receiving said

electromagnetic signal with spatial diversity, and said processing means implement the method of the first aspect of the invention for performing at least said estimation of the spatial position of said magnetic dipole exploiting the spatial diversity of the output signals of the magnetic vector sensors.

5 For a preferred embodiment, each of said magnetic vector sensors is capable of performing a three-axes magnetic vector measurement.

Depending on the embodiment, each of said magnetic vector sensors is a magnetoresistive sensor, such as an Anisotropic Magnetoresistive Sensor (ARM), or an antenna comprising three orthogonally arranged magnetic coils.

10 Said magnetic vector sensors of said array are physically separated one from another by a minimum distance to provide said spatial diversity when they are at or below a predetermined distance from the portable electromagnetic signal transmitter. The higher said minimum distance is the further from the avalanche victim the exploitation of spatial diversity of the output signals of the magnetic vector sensors can
15 be used, thus reducing the time for locating the victim.

Depending on the embodiment, said array include magnetic sensors arranged occupying at least one line (linear array), one plane (planar array), or any other general geometry such a surface (conformal array).

20 Optionally, for an embodiment, the portable rescue device of the second aspect of the invention comprises adjusting means for adjusting different operating parameters of the device regarding the implementation of each of steps a), b) and c), such as predetermined and adjustable threshold values for automatically triggering the start of step c).

25 For an embodiment, the portable rescue device of the second aspect of the invention comprises a main casing housing at least said processing means and part of said receiving means, and a support onto which said magnetic vector sensors are attached, such that they adopt the physical separation with each other which provides said spatial diversity.

30 Said elongated support is, for an embodiment, at least one deployable and/or extensible arm connected to said main casing and onto which at least part of said magnetic vector sensors are attached such that they adopt the physical separation with each other which provides said spatial diversity when said at least one arm is at the deployed and/or extended position.

35 For another embodiment, said elongated support is a flexible band to be worn by said user in an extended position, such as diagonally crossing his chest.

The portable rescue device of the second aspect of the invention further comprises, for a preferred embodiment, electromagnetic transmission means and selection means, the latter for alternately:

5 - activating said electromagnetic receiving means for receiving said electromagnetic signal emitted by a portable electromagnetic signal transmitter carried by an avalanche victim, for allowing the user of the portable rescue device act as an avalanche victim locator by activating the device in a receiving mode; or

10 - activating said electromagnetic transmission means for transmitting said electromagnetic signal, for allowing the user of the portable rescue device act as a potential avalanche victim to be located by activating the device in a transmitting mode.

In other words, for the above indicated embodiment, a plurality of portable rescue devices according to the second aspect of the invention can be used by a group of users which, before an avalanche, activate its transmitting mode (as they are potential avalanche victims), and after an avalanche has occurred, those users which are not 15 victims of said avalanche activate their portable rescue devices in their receiving modes in order to locate the victim or victims of said avalanche which are carrying respective portable rescue devices still activated in their transmitting modes.

The method and the rescue device of the present invention allow the estimation of the positions of multiple avalanche victims simultaneously.

20 Particularly, for an embodiment of the method of the first aspect of the invention, step c) comprises simultaneously estimating the spatial positions of multiple magnetic dipoles, associated to multiple avalanche victims, from output signals provided by the magnetic vector sensors of the array, exploiting their spatial diversity through one or more array signal processing techniques.

25

Brief Description of the Drawings

The previous and other advantages and features will be better understood from the following detailed description of embodiments, with reference to the attached drawings, which must be considered in an illustrative and non-limiting manner, in which:

30 Fig. 1 shows the trajectories followed by a rescue user to locate an avalanche victim, according to a conventional method (left view) and according to the method of the first aspect of the invention (right view);

35 Fig. 2 shows the architecture of the portable rescue device of the second aspect of the invention for another embodiment, being carried by a user, where the sensors of the array of magnetic vector sensors are attached to a band worn by the user;

Fig. 3 schematically shows the portable rescue device of the second aspect of the invention, including its internal elements, for an embodiment for which most of the sensors of the array of magnetic vector sensors are attached to two deployable arms; and

5 Fig. 4 shows a processing scheme of the receiving means of the portable rescue device of the second aspect of the invention.

Detailed Description of Several Embodiments

Left view of Fig. 1 shows the trajectories followed by a rescue user to locate an avalanche victim, according to a conventional method, and includes the next stages, indicated in Fig. 1, left view as 1, 2, 3 and 4:

10 Stage 1 – Signal search: With the current sensitivity of the antenna used, the conventional device is able to detect signal at about 50 meters approximately. Until the signal is not detected a search for said signal is performed by the user walking through the searching area according to the meandered path depicted in Fig. 1 left view, to pick up the trail, i.e. to detect the signal. This stage is inevitable but undesirable because it wastes time. In order to reduce the lasting of this stage and hence not wasting time, the sensitivity of the receiver must be as high as possible.

20 Stage 2 – Coarse search: Once the signal has been detected, the magnetic field vector is calculated and its direction is followed by the rescuer. The rescuer must walk in the two directions of the field line to see if the field power decreases or increases, and choose the direction where the field increases, otherwise he moves away from the victim. As the path is not straight, but curved, it causes wasting some time.

25 Stage 3 – Fine search: This stage starts when following the field lines of the magnetic field is no longer reliable, and consists in searching for the maximum power above the surface crossways and in straight lines, and mark the point with crossed poles. This stage is time-consuming and inaccurate.

30 Stage 4 – Pinpointing: The rescuer pinpoints the ground with a probe starting from the marked crossed poles in order to accurately locate the victim. Time is wasted for this manual stage.

For comparison with said conventional search method, right view of Fig. 1 shows the trajectories followed by a rescue user to locate an avalanche victim according to the method of the first aspect of the invention, which includes the next stages, indicated in Fig. 1, right view as 1, 2 and 3:

Stage 1 (referred above as step a)) – Signal search: The outputs of the M magnetic vector sensors of the array are directly added up due to the low spatial diversity, which improves the signal-to-noise ratio by a factor M . Thus the sensitivity is improved, and therefore the signal is detected earlier than in the conventional method.

5 As a result, the meandered path that the rescuer must follow is shorter than the one of left view of Fig. 1, and the time wasted in this stage is thus reduced. The comparison with the conventional method has been done assuming that each of the magnetic vector sensors of the array has the same sensitivity as the coil used in the conventional search method.

10 Stage 2 (referred above as step b)) – Coarse search: Being away from the victim, spatial diversity is still not good enough and it is preferable to use the output of the M magnetic vector sensors just to calculate the magnetic field vector therefrom and follow its direction. This stage is only applied until the rescue user is close enough to the victim so that there exists enough spatial diversity. An adequate value for this distance is
 15 about 10 meters with the current technology and the standard being used. In the conventional method, in contrast, this stage has to be applied until the rescue user is about 2 meters away of the victim.

Stage 3 (referred above as step c)) – Fine search: Once the user is close enough to exploit spatial diversity, the position of the magnetic dipole (i.e. of the transmitter) is
 20 calculated and the rescuer follows a straight path to find it. It is faster than following a curve and there is no need of a probing stage.

The change between phase 2 and 3 of the proposed method is transparent to the user and is performed automatically by the portable rescue device. This is a very important advantage because it simplifies the location in essentially two phases, the
 25 signal search (1) and to follow a given direction by, for example, a display (2 and 3).

Fig. 2 depicts the device of the second aspect of the invention, for an embodiment for which it contains a loop (or more if desired) which is used as a transmitting antenna A of the transmitter Tx, and an array of M magnetic sensors S1-S5
 30 arranged in a specific and known manner for reception and connected to the receiver Rx. Each of these sensors S1-S5 is capable of calculating the field vector received thereby. Thus, three mutually orthogonal coils would correspond to a single sensor. Another interesting option for its size and weight are magnetoresistive sensors, such as Anisotropic Magnetoresistive (AMR) sensors.

35 With this new architecture, spatial diversity existing in the M measures $\mathbf{B}_1(t)$, ..., $\mathbf{B}_M(t)$ of the field $\mathbf{B}(t)$ (see fig. 4) in the same receiver can be exploited and estimate the

position \mathbf{p} for the magnetic dipole generating the measured magnetic field. The positions $\mathbf{p}_1, \dots, \mathbf{p}_L$ (see fig. 4) of L victims can also be estimated simultaneously.

Fig. 2 only illustrates an example of a possible architecture of the portable rescue device D of the second aspect of the invention, for an embodiment where its receiving means Rx include a linear array of five magnetic vector sensors S1-S5. In this case, optionally and to obtain a higher spatial diversity, the portable rescue device of the second aspect of the invention has two side extendable arms Ta, Tb where part of the magnetic vector sensors of the array are placed, particularly sensors S1, S2, S4 and S5. The sensor S3 is attached to the main casing H which houses the rest of elements of the device, including the processing means connected to the transmitter Tx and to the receiver Rx, in order to process the output signals coming therefrom. The block indicated as UP is used for illustrating, not only the processing means, but also control means for controlling the operation of the transmitter Tx and of the receiver Rx, and selection means for selecting if operating the device in the transmitting or in the receiving mode.

These arms Ta, Tb, which in Fig. 2 are shown deployed (their rest positions indicated by means of dotted lines in the side edges of main casing H), can be, for an embodiment, extendable (for example telescopically) to provide even more spatial diversity. Also, two more arms can be added to obtain an array on a two-dimensional surface, or even eight arms can be used for a three-dimensional array geometry. However, an armless device is also a right solution, for a less preferred embodiment, in which case the linear array could be distributed along one side of the main casing H, and a rectangular array could be distributed along all four sides of the main casing H.

Fig. 3 shows another embodiment, where the portable rescue device D comprises, attached to the main casing H, a flexible band T to be worn by the user (in the illustrated embodiment diagonally across his chest) such that the magnetic vector sensors of the linear array, in this case four sensors S1-S4, keep separated so as to provide the mentioned spatial diversity.

Fig. 4 shows the processing scheme of the receiver Rx. It will vary slightly depending on the type of magnetic vector sensor used in the array. In case the sensors measure the instantaneous field $\mathbf{B}_1(t)$, $\mathbf{B}_2(t)$, ..., $\mathbf{B}_M(t)$, a down-conversion stage (I/Q decomposition) has to be performed together with a processing from the baseband signals $\mathbf{b}_1(t)$, $\mathbf{b}_2(t)$, ..., $\mathbf{b}_M(t)$, by means of the processing means UP, as shown in Fig. 4. In this case, the baseband signals $\mathbf{b}_1(t)$, $\mathbf{b}_2(t)$, ..., $\mathbf{b}_M(t)$ are complex. Although Fig. 4 only shows the I/Q decomposition of $\mathbf{B}_{1x}(t)$, for the rest of components of $\mathbf{B}_1(t)$ ($\mathbf{B}_{1y}(t)$, $\mathbf{B}_{1z}(t)$) and also of $\mathbf{B}_2(t)$ and $\mathbf{B}_3(t)$, a respective I/Q decomposition is also performed.

In case the magnetic sensors calculate the envelope of the received field, or even directly the received power, such as some magnetic sensors integrated into a digital chip, the processing is directly applied to the measured signal, because it is already a baseband signal. In this case the baseband signal is a real signal.

- 5 A person skilled in the art could introduce changes and modifications in the embodiments described without departing from the scope of the invention as it is defined in the attached claims.

Claims

1.- A method for locating avalanche victims, comprising performing sequentially the next steps:

5 a) an initial step comprising, a user carrying a portable electromagnetic signal receiver (Rx), performing an electromagnetic signal search by moving around a first area, away from the victim, in order to detect, by its reception with the portable electromagnetic signal receiver (Rx), an electromagnetic signal emitted by a portable electromagnetic signal transmitter carried by an avalanche victim and acting as a magnetic dipole;

10 b) a first tracking step, started after said electromagnetic signal has been detected and comprising measuring, with said portable electromagnetic signal receiver (Rx), the magnetic field emitted by said portable electromagnetic signal transmitter, and moving, said user carrying said portable electromagnetic signal receiver (Rx), following a curve path coincident with the magnetic field line of said emitted magnetic field
15 approaching to the victim through a second area closer thereto; and

c) a second tracking step performed after said first tracking step, comprising moving the user carrying the portable electromagnetic signal receiver (Rx) through a third area, even closer to the victim, for finally locating the victim;
wherein the method is **characterised** in that it comprises providing and using, as said
20 portable electromagnetic signal receiver (Rx), a portable electromagnetic signal receiver with an array of magnetic vector sensors (S1-SM) arranged for receiving said electromagnetic signal with spatial diversity, and in that said step c) comprises determining the location of said portable electromagnetic signal transmitter by estimating the spatial position of said magnetic dipole from output signals provided by said
25 magnetic vector sensors (S1-SM) of said array, exploiting their spatial diversity through at least one array signal processing technique.

2.- The method of claim 1, comprising performing, at said step c), a three-axes magnetic vector measurement with each of said magnetic vector sensors (S1-SM).

3.- The method of claim 1 or 2, comprising arranging said magnetic vector
30 sensors (S1-SM) of said array physically separated one from another by a minimum distance to provide said spatial diversity when they are at or below a predetermined distance from the portable electromagnetic signal transmitter.

4.- The method of any of the previous claims, comprising performing said step a)
by using the output signal of one of said magnetic vector sensors (S1-SM) and if no
35 signal is detected with only said magnetic vector sensor, or detected poorly, performing

a detection using array processing with the output signals provided by each of said magnetic vector sensors (S1-SM) when receiving said electromagnetic signal emitted by the portable electromagnetic signal transmitter.

5 5.- The method of any of the previous claims, comprising performing said step b) based on the measurement of said magnetic field performed with at least one of said magnetic vector sensors (S1-SM) and/or based on the measurement of said magnetic field performed by adding to each other the output signals provided by each of said magnetic vector sensors (S1-SM) when measuring said magnetic field.

10 6.- The method of claim 5, comprising starting performing said step b) based on the measurement of said magnetic field performed by adding to each other the output signals provided by each of said magnetic vector sensors (S1-SM) when measuring said magnetic field and, once the output signal of one of said magnetic vector sensors (S1-SM) so allows it, continuing performing step b) based on the measurement of the magnetic field performed with said one of said magnetic vector sensors (S1-SM).

15 7.- The method of any of the previous claims, comprising automatically stopping said step b) and starting said step c) upon considering, based on their analysis, that the output signals of said magnetic vector sensors (S1-SM) provide a degree of spatial diversity above a certain threshold and/or that the magnetic field lines information calculated by said portable electromagnetic signal receiver (Rx) does not allow
20 performing the first tracking step with a certain amount of reliability.

8.- The method of any of the previous claims, wherein said step c) comprises simultaneously estimating the spatial positions of multiple magnetic dipoles, associated to multiple avalanche victims, from output signals provided by the magnetic vector sensors (S1-SM) of the array, exploiting their spatial diversity through said at least one
25 array signal processing technique.

9.- A portable rescue device for locating avalanche victims, comprising:

- electromagnetic receiving means (Rx) for receiving an electromagnetic signal emitted by a portable electromagnetic signal transmitter carried by an avalanche victim and acting as a magnetic dipole, and measuring the magnetic vector field emitted by
30 said portable electromagnetic signal transmitter, and

- processing means (UP) connected to said electromagnetic receiving means (Rx) for receiving and analysing electrical output signals provided thereby and providing to a user of the portable rescue device (D), through indication means thereof, indications regarding the result of said reception and analysis to allow him to perform said moving
35 of the user through said first, second and third areas towards the victim of steps a), b) and c) of the method of any of the previous claims;

wherein the portable rescue device is **characterised** in that said receiving means (Rx) comprise an array of magnetic vector sensors (S1-SM) arranged for receiving said electromagnetic signal with spatial diversity, and in that said processing means (UP) implement the method of any of the previous claims for performing at least said
5 estimation of the spatial position of said magnetic dipole exploiting the spatial diversity of the output signals of the magnetic vector sensors (S1-SM).

10 10.- The portable rescue device of claim 9, wherein each of said magnetic vector sensors (S1-SM) is capable of performing a three-axes magnetic vector measurement and is a magnetoresistive sensor or an antenna comprising three orthogonally arranged magnetic coils.

11.- The portable rescue device of any of claims 9 to 10, wherein said magnetic vector sensors (S1-SM) of said array are physically separated one from another by a minimum distance to provide said spatial diversity when they are at or below a predetermined distance from the portable electromagnetic signal transmitter.

15 12.- The portable rescue device of claim 11, wherein said array of magnetic vector sensors (S1-SM) include magnetic vector sensors arranged occupying at least one line or at least one plane.

13.- The portable rescue device of claim 12, comprising a main casing (H) housing at least said processing means (UP) and part of said receiving means (Rx), and
20 a support (T; Ta-Tb) onto which at least part of said magnetic vector sensors (S1-SM) are attached, such that they adopt the physical separation with each other which provides said spatial diversity.

14.- The portable rescue device of claim 13, wherein said support is an elongated support which is one of:

25 - at least one deployable and/or extensible arm (Ta-Tb) connected to said main casing (H) and onto which said magnetic vector sensors (S1-SM) are attached such that they adopt the physical separation with each other which provides said spatial diversity when said at least one deployable and/or extensible arm (Ta-Tb) is at the deployed and/or extended position; or

30 - a flexible band (T) to be worn by said user in an extended position.

15.- The portable rescue device of any of claims 9 to 14, further comprising electromagnetic transmission means (Tx) and selection means, the latter for alternately:

35 - activating said electromagnetic receiving means (Rx) for receiving said electromagnetic signal emitted by a portable electromagnetic signal transmitter carried by an avalanche victim, for allowing the user of the portable rescue device (D) act as an avalanche victim locator; or

- activating said electromagnetic transmission means (Tx) for transmitting said electromagnetic signal, for allowing the user of the portable rescue device (D) act as a potential avalanche victim to be located.

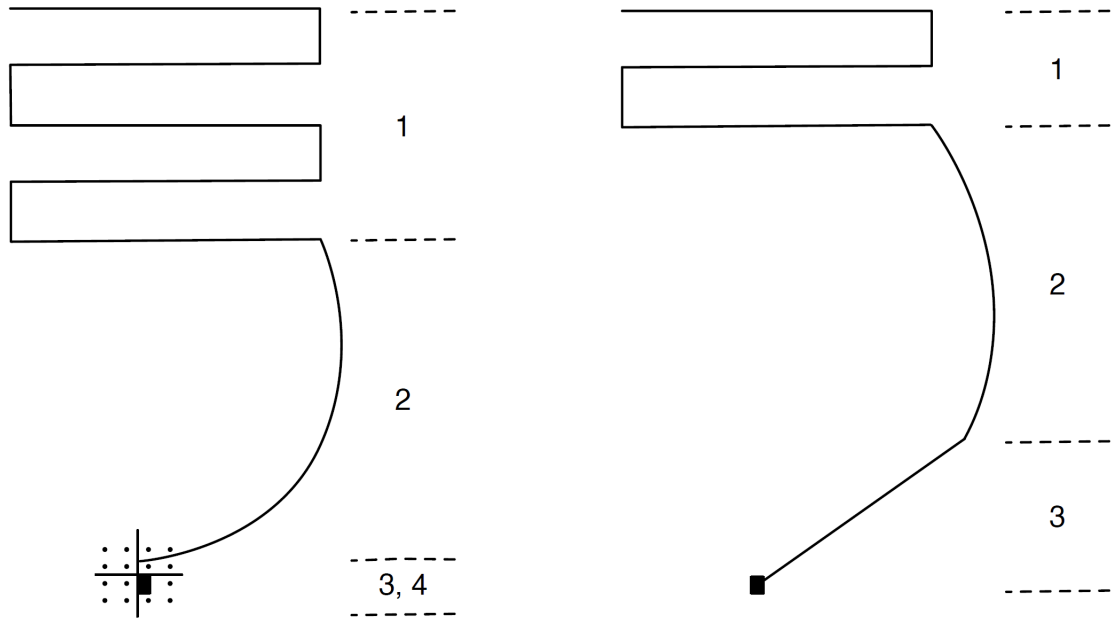


Fig. 1

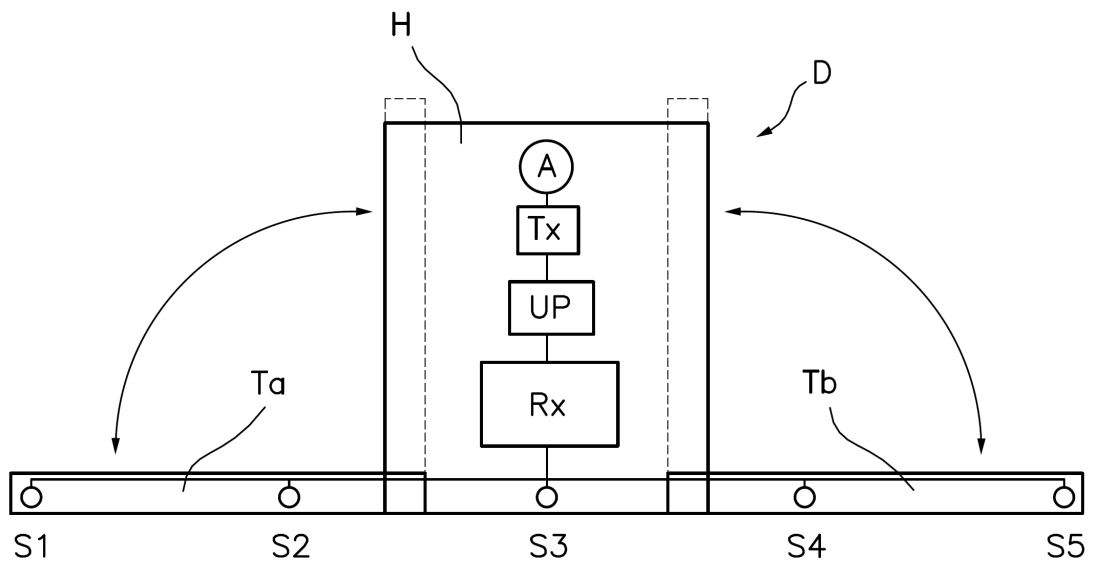


Fig.2

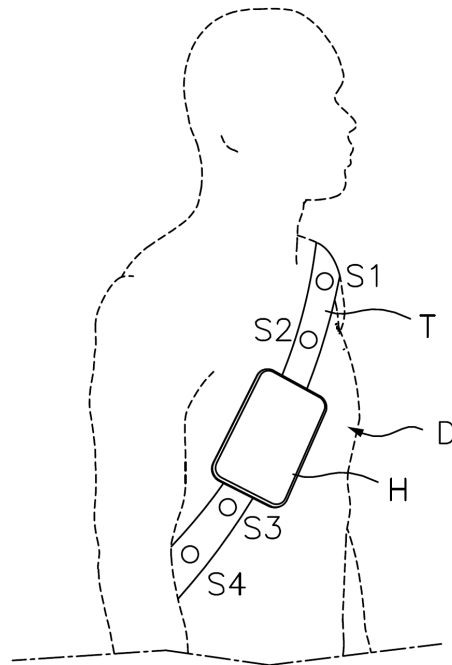


Fig.3

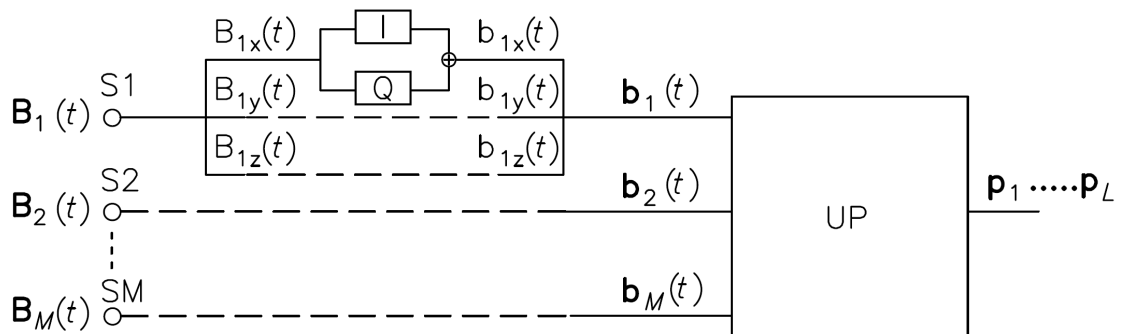


Fig.4

Abstract

A method and a portable rescue device for locating avalanche victims

The method comprises performing:

- a) searching, with a portable electromagnetic signal receiver (Rx), an electromagnetic signal emitted by a portable electromagnetic signal transmitter (Tx);
- b) a first tracking step for measuring and following the magnetic field of the electromagnetic signal emitted by the portable electromagnetic signal transmitter; and
- c) a second tracking step comprising determining the location of the portable electromagnetic signal transmitter by estimating the spatial position thereof from output signals provided by a plurality of magnetic vector sensors (S1-SM) of the portable electromagnetic signal receiver (Rx), arranged forming an array, by exploiting their spatial diversity.

The portable rescue device is adapted to implement the method of the invention.